Life, Death, and Coexistence:
Exploring and Manipulating the Respiratory Lifestyle of *Shewanella oneidensis*

A DISSERTATION
SUBMITTED TO THE FACULTY OF THE
UNIVERSITY OF MINNESOTA
BY

Eric Daniel Kees

IN PARTIAL FULFILLMENT OF THE REQUIREMENTS
FOR THE DEGREE OF
DOCTOR OF PHILOSOPHY

Advisor: Jeffrey A. Gralnick

August, 2019

Acknowledgements

No achievement is made in a vacuum, but this one especially had a lot of people who made it possible. Jeff Gralnick has been the perfect advisor, pushing me and guiding me exactly how and when I needed it. He and Daniel Bond have fostered such an amazing environment for scientific, personal, and professional growth; I feel incredibly fortunate to have been welcomed in. An extra thanks to Daniel for so freely talking shop and for being an unofficial co-advisor at times when I struggled to see the bigger picture. I could write pages on how amazing all of these people are, but here goes my attempt to be concise. Nick Kotloski, Aunica Kane, Chi Ho Chan, and Jon Badalamenti all truly set the bar for excellence and I would have drowned without their direct help. Audrey Harris, Peter Intile and Bridget Conley breathed more life to grad school, each having a preternatural ability to make the hard days easier. Ben Bonis, Brittany Bennett, and Caleb Levar, you already know how dear you are to me; to many more years of friendship. Komal Joshi is an actual wizard Building bioreactors would have been impossible without her holding my hand through it and telling me it's going to be okay, then commiserating when it's not. Every person to come through these labs has been thrilling to work with and learn from. Our culture has been kept alive thanks in no small part to Fernanda Jimenez, Rebecca Calvo, Lori Zacharoff, Abhiney Jain, Rebecca Maysonet, Anna Domenech Corts, Lizzie West, Rachel Sobel, Blake Downing, Katie Redford, Savannah Lockwood, Eric Sankary, Zac Schreiber, Maya Burroughs, Ruth Lee, Andrew Grenfell, Sol Choi, and David Hsu. Thanks to Antony Dean and the past and present members of his lab for letting us all in to use your flow cytometer and offering expertise. Most importantly, I have to extend a heartfelt thank you to Gus Pendleton for being one of the most capable and inspiring people I've ever met, and for carrying both of us at times through the hardest experiments. Seeing your growth into a brilliant scientist, scholar and teacher has been deeply rewarding.

I also have to thank so many new and old friends that have kept me going the past six years. Cody, Tyler, Evan, Devan, Ellen, Kasey, CJ, Kim, Nate, Alex, Brandon, Jamie, Kiara, thank you for memes, festivals and shows, board games and scotch, fish, ELnO, bad movies, ramen, shameless dance moves in front of James Murphy, agates, camping, fresh air, and just being great people. Thanks to my wonderful family for letting me follow my passions, even when it results in destroyed household items, constant messes, loud noises, fits of rage, forgetfulness, questionable decisions, and aloofness – through it all, somehow managing to enthusiastically welcome me home. Aubree, my partner and best friend has been with me through every step of this, supporting me, challenging me, and making me feel fully human and valid when things were especially hard. Wherever we go, whatever we do, I'm glad it's together.

Dedication

This thesis is dedicated to Dr. Edward C. Carlson. You brought me into science, taught me new ways of seeing the world, and inspired me to never stop searching. Your kindness, thoughtfulness, and generosity have meant everything.

Abstract

In their natural environment, microbes often exist in stressful, suboptimal, ever-changing conditions and have evolved innumerable and varied successful strategies for managing stresses and thriving in flux. Microbial ecosystems are defined not only by specialized members occupying defined narrow niches, but also members that move between niches and exist in a mode of constant opportunism. One such opportunistic group of organisms are those belonging to the genus *Shewanella* which are largely defined by their respiratory versatility. A particularly well-studied member of this genus, *S. oneidensis*, is the most versatile respiratory organism described to date, and is a model organism for extracellular electron transfer. This thesis explores the respiratory lifestyle of *S. oniedensis* primarily through the lens of cell physiology and competitive fitness under optimal growth conditions and those that yield catastrophic death.

The second chapter of this thesis is a study in cofactor acquisition by a key respiratory enzyme in *S. oneidensis* MR-1. The periplasmic protein FccA is both a fumarate reductase and an electron carrier protein for extracellular electron transfer, that requires a flavin cofactor for its function. Through genetic manipulation, growth experiments, and biochemical experiments, we found that for *S. oneidensis,* self-secretion of flavins comes at minimal metabolic cost and is required for periplasmic flavoprotein cofactor acquisition.

The third chapter is a probing of natural and engineered factors that enable survival under respiratory stress. *Shewanella* is considered an obligate respiring organism, and when placed under conditions in which respiration cannot normally function, it experiences massive loss in viability accompanied by cell lysis. Despite, 99-99.99% of cells undergoing death in this condition, many persist. This study leveraged synthetic proton motive force supplementation, which affords enhanced survival of *S. oneidensis,* to profile the innate strategies used to survive under respiratory stress. The key finding of this study is that the sodium motive force plays a key role in survival of *S. oneidensis* under respiratory stress, even when survival is enhanced by proton motive force supplementation.

The fourth chapter of this thesis is a series of competition experiments reframing a central paradigm of the competitive exclusion principle: that two organisms occupying

the same niche cannot coexist. This principle states that in this scenario any organism with a reproductive advantage will ultimately overtake a population. This study demonstrated that two engineered strains of *S. oneidensis* utilizing the same medium with the same food and nutrient sources, but growing a vastly different rates, can remain at stable frequencies when grown attached to an electrode as the sole sink of electrons in respiration. The primary reason for this stability is that the original parent population remains actively growing on a surface to which daughtered cells are constantly removed. While the scenario we have engineered to "break" the competitive exclusion principle could be considered a form of niche differentiation, it demonstrates an effective strategy to combat strain degeneration and contamination in industrial fermentation, by allowing a selected population of less competitively fit individuals to act indefinitely as a progenitor population.

The work in this thesis brings special attention to the adaptation towards an obligate respiratory lifestyle in *S. oneidenisis.* The systems it has evolved to secrete flavins as both respiratory cofactors and intermediates and the marked death it experiences under respiratory stress together emphasize adaptations in *Shewanella* to thrive in redox stratified environments, supported by the wide variety of respiratory nodes it can utilize. Finally, this work highlights the utility of *S. oneidensis* as a test platform for ideas, with potential benefits for biotechnological and industrial applications.

Table of Contents

List of Tables

List of Figures

Chapter 1 – *Shewanella oneidensis*: a model for an obligate respiratory lifestyle and competition among respiring microbes

1.1 The Gram-negative cell envelope

To appreciate the primary themes in this thesis centered on respiration, survival and extracellular electron transfer, special consideration should be made for the cell envelope structure in Gram-negative bacteria. Originally distinguished by their staining characteristics in a stain developed by Hans Christian Gram (1884; see Brock, 1961 for an English translation). The general cell structure of Gram-negative bacteria is of a cytoplasm surrounded by two concentric lipid bilayers, between which exists a thin layer of peptidoglycan amid a viscous periplasm (Silhavy et al., 2010).

The inner membrane, or cytoplasmic/cell membrane is conserved across all domains of life (though the specific chemistries vary), and consists of a phospholipid bilayer with integral membrane spanning proteins along with integral cytoplasmic and periplasmic-facing lipoproteins. The inner membrane forms an osmotic barrier through which solute flow is tightly regulated. A chemiosmotic gradient, or membrane potential, of protons and/or sodium ions forms across the inner membrane, driving molecular motors used in flagellar motility and synthesis of adenosine triphosphate (ATP), along with uptake and efflux of other ions and small molecules. Reactions that maintain the majority of membrane potential in most neutrophilic organisms are those that couple proton or sodium transport to reduction/oxidation (redox) reactions linked to respiratory chains, or hydrolysis of ATP. In some organisms, light-driven proton or sodium pumping can serve as a source of membrane potential (Dioumaev et al., 2002; Inoue et al., 2013)

The periplasm is a complex aqueous compartment spanning approximately 10-15 nm between the outer and inner membranes, and consists of oligosaccharides, redox-active proteins, solute-carrying proteins, and hydrolytic enzymes, salts, and peptidoglycan (Hobot et al., 1984; Silhavy et al., 2010). Some protein complexes span the entire cell envelope, including type III secretion system, flagellar motors (Masiá Canuto and Gutiérrez Rodero, 2002), multidrug efflux pumps (Koronakis et al., 2000), and the cell-division-associated Tol-Pal complex (Gerding et al., 2007)

The outer membrane of Gram-negative bacteria is a lipid bilayer of both phospholipid and lipopolysaccharide (LPS), with LPS concentrated to the surface exposed outer leaflet to form a “gel-like” permeability barrier with decreased fluidity compared to phospholipid (Nikaido, 2003). The LPS typically consists of lipid A, a core

oligosaccharide, and an outer polysaccharide layer often referred to as O-antigen or O-specific polysaccharide, the structure – and at times existence – of which is highly variable between taxa (Rietschel et al., 1994; Silhavy et al., 2010). Proteins present in the outer membrane include porins though which molecules diffuse depending on size, and lipoproteins, including the murein lipoprotein, Lpp, which serves to covalently bond to peptidoglycan and anchor the outer membrane to it (Braun, 1975; Silhavy et al., 2010).

1.2 Overview of respiration

At the center of the chemiosmotic theory originally proposed by Peter Mitchell (1961), is the exergonic transport of electrons down a redox gradient which is tied to proton translocation across the cytoplasmic membrane. In any electron transport chain, electrons are carried by proteinaceous complexes with specialized flavin, heme or Fe-S-containing domains, and/or a redox-active pool of lipids in the inner membrane called quinones. The quinone pool can have varying chemical makeup depending on the species and respiratory context, but generally takes the form of ubiquinone or menaquinone in aerobic and anaerobic respiration, respectively. Electrons are supplied to the electron transport chain from catabolism of an electron donor (often a sugar or organic acid), typically via reduced nicotinamide adenine dinucleotide (NADH), or by direct reduction of the quinone pool. Terminal electron acceptors are the final physiological destination of electrons in respiration, and can consist of oxygen (aerobic respiration) or other compounds (anaerobic respiration). Anaerobic terminal electron acceptors can consist of inorganic compounds such as nitrate, sulfate, metal oxides, or organic compounds such as trimethylamine-*N*-oxide (TMAO), dimethyl sulfoxide (DMSO) or fumarate. Electron carriers utilized in respiration depend on the redox potentials of both the electron donor and electron acceptor, where the redox potential of electron carriers must typically fall between that of the electron donor and acceptor. Membrane potential is generated from electron transport either through proton or sodium pumping, or by coupled reduction/oxidation of quinones at the respective inner or outer surface of the cytoplasmic membrane.

1.3 The genus *Shewanella*

Organisms within the genus *Shewanella* are Gram-negative gamma-proteobacteria that occupy a wide variety of marine and aquatic niches, from water and sediment columns at a wide range of depths, to fish and mammalian hosts (Fredrickson et al., 2008; Hau and Gralnick, 2007; Nealson and Scott, 2006). Much of this niche diversity is owed to the diversity of compounds shewanellae are equipped to respire from organic terminal electron acceptors such as fumarate, DMSO, TMAO, and histidine degradation product urocanate, to inorganic terminal electron acceptors such as oxygen, sulfite, nitrate and various metal oxides (Bogachev et al., 2012; Lovley et al., 2004; Myers and Nealson, 1988; Nealson and Scott, 2006). The range of solid and dissolved metal oxides respired by *Shewanella* is vast and includes iron, manganese, cobalt, nickel, chromium, uranium, mercury, technetium, and vanadium oxides (Fredrickson et al., 2008).

The carbon sources that shewanellae can utilize are much less varied and are generally limited to fermentation end products such as lactate, acetate, and pyruvate, along with *N*-acetylglucosamine. Due to the wide respiratory diversity but limited carbon source utilization, *Shewanella* are often found in redox stratified environments where carbon input is high (Nealson and Scott, 2006). Shewanellae were originally isolated from putrefied butter (Derby and Hammer, 1931), are often found in association with fish, and they are sometimes opportunistic pathogens (Hau and Gralnick, 2007). The ability to respire iron and manganese oxides, along with both nitrate and nitrite implicates *Shewanella* in biogeochemical cycling of nitrogen, iron and manganese (Aigle et al., 2017; Nealson and Scott, 2006).The machinery used to respire metals allows *Shewanella* to interface with electrodes, and as a result they have been used as models and test platforms for biosensors and unbalanced cathodic fermentation applications (Bursac et al., 2017; Flynn et al., 2010; Kim et al., 1999; Tefft and TerAvest, 2019; Webster et al., 2014).

1.4 Extracellular electron transfer in *Shewanella*

In most respiring organisms, terminal electron acceptors are soluble compounds and are reduced at the cytoplasmic surface of the inner membrane or within the periplasm. This trait extends to *Shewanella* for aerobic, nitrate, nitrite sulfite, TMAO and fumarate respiration (Chen and Wang, 2015). However, a problem is presented when respiring insoluble extracellular compounds, in that they can only be accessed outside the cell. As a solution, *Shewanella* and similar organisms have evolved pathways for transporting electrons through both membranes and the periplasm, a process termed extracellular electron transfer (EET). The basic parts of the EET pathway in *Shewanella* include an inner membrane quinone-linked tetraheme cytochrome CymA, periplamic **s**mall **t**etraheme **c**ytochrome (STC) encoded by gene *cctA,* periplasmic flavocytochrome *c* FccA, and the outer membrane **m**e**t**al **r**eduction (Mtr) complex consisting of two decaheme cytochromes MtrA and MtrC and a specialized outer membrane porin MtrB. What is known to date about electron flow in this system indicates that electrons in the reduced quinone pool are coupled to CymA, which transfers them to MtrA via periplasmic components STC and FccA. Electrons then travel up the MtrA conduit within MtrB by hopping between tightly-spaced hemes onto MtrC, which can pass electrons directly onto a solid or soluble terminal electron acceptor, or indirectly through soluble flavin electron shuttles (Fig 1.1)

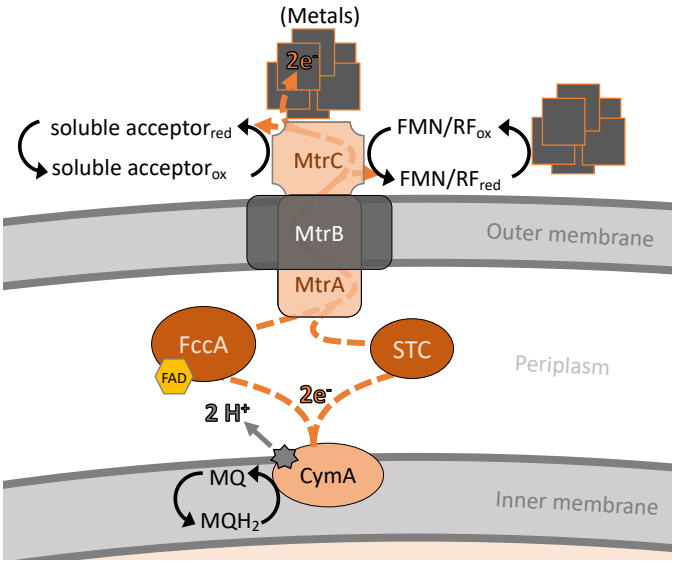

Fig 1.1 Schematic representation of extracellular electron transfer in *Shewanella oneidensis.* MtrABC: metal reduction complex decaheme cytochromes A and C, along with porin MtrB; FccA – flavocytochrome c; STC – small tetraheme cytochrome; FAD – Flavin adenine dinucleotide; FMN – flavin mononucleotide; RF – riboflavin: MQ – oxidized menaquinone; MQH – reduced menaquinone; ox – oxidized; red – reduced.

Although FccA is considered primarily a fumarate reductase, as shown above it can also participate in EET. As the most abundant protein in the periplasm, it is thought

to act in concert with STC as a transient sink of electrons from CymA, potentially affording *Shewanella* with the ability to temporarily move away from solid electron acceptors or across redox strata while continuing to metabolize (Schuetz et al., 2009; Sturm et al., 2015). In this sense, the pool of FccA and STC act as a capacitor to intermittently charge and discharge electrons. Interestingly, while STC can transfer electrons to a number of other CymA-dependent respiration pathways, FccA appears to only interact with MtrA in this function (Alves et al., 2015).

Another outer membrane cytochrome encoded on the genome next to *mtrCAB*, OmcA, is homologous to, shares similar structure and heme orientation as, and can functionally overlap with MtrC (Coursolle and Gralnick, 2010; Edwards et al., 2015, 2014), but may play different roles depending on the terminal electron acceptor. For instance, MtrC is necessary for reduction of hematite, with OmcA playing a more supportive role, possibly in attachment (Coursolle & Gralnick, 2010; Mitchell et al., 2012), while hexavalent chromium reduction is carried out predominantly by OmcA (Belchik et al., 2011).

A second complex for electron transfer through the outer membrane, MtrDEF, is homologous to MtrABC, and can partially complement MtrABC loss of function mutants for Fe(III) citrate reduction (Coursolle & Gralnick, 2010; Wang et al., 2019) but its physiological role in wild-type *S. oneidensis* is unclear. While *mtrCAB* expression is increased under conditions of electron acceptor limitation, *mtrD* and *mtrF* expression, which appears to be regulated by a different promoter, is either unaffected or downregulated under this condition (Barchinger et al., 2016; Fredrickson et al., 2008). One published case where *mtrDEF* expression is upregulated is during aerobic auto-aggregation of cells in mM CaCl concentrations, coinciding with upregulation of other anaerobic respiration genes (McLean et al., 2008). While, both FccA and STC overlap in function concerning electron transfer between CymA and MtrA, neither bind to MtrD with appreciable affinity (Alves et al., 2015), leaving the path of electrons between CymA and MtrD unclear.

1.5 Flavins as cofactors and electron shuttles

As introduced in section 1.2 flavins are common electron carriers, and they are also integral to *Shewanella* physiology at multiple levels. These molecules are characterized by an isoalloxazine ring, which can be in oxidized form (quinone), partially reduced to a semiquinone state with one electron, or fully reduced to a hydroquinone state with two electrons (Abbas and Sibirny, 2011). As with inner membrane quinones, and unlike heme and Fe-S clusters, flavins can be hydrogen carriers. Most microorganisms synthesize their own flavins to satisfy nutritional and cofactor requirements, and synthesis is carried out in the cytoplasm by a specialized riboflavin biosynthetic pathway. In bacteria, riboflavin is synthesized in multiple steps from precursors ribulose-5-P and guanosine triphosphate, then converted to FMN and FAD in two successive ATP-consuming reactions by a bifunctional riboflavin kinase/FMN adenylyltransferase.

Most flavoproteins (~75%) use FAD as a cofactor, with nearly all others using FMN (MacHeroux et al., 2011). Riboflavin has only been noted as a redox cofactor in one case – for the *Vibrio cholerae* Na^+-pumping NADH:quinone oxidoreductase (Na^+-NQR), which also contains two covalent FMN cofactors and a noncovalent FAD (Bogachev et al., 2018; Juárez et al., 2008). For both FAD and FMN, noncovalent binding is the most common linkage to flavoproteins, with only 10% of flavoproteins containing at least one covalent flavin (MacHeroux et al., 2011). Typically, covalent FAD/FMN bonds are formed between the isoalloxazine ring and a cysteine, histidine or tyrosine, with maturation generally assumed to be carried out in an autocatalytic manner (Bogachev et al., 2018). However, an unusual covalent FMN transferase was discovered in *Shewanella*, which uses FAD as a donor substrate to form a covalent FMN:threonine phosphodiester bond (Bertsova et al., 2013). The gene for this enzyme, *apbE*, was first discovered to be essential for thiamine biosynthesis in *Salmonella* enterica (Beck and Downs, 1998), but during later attempts to express and purify the *V. harveyi* Na^+-NQR in *E. coli,* it was found that only the apoenzyme could be purified, until *S. oneidensis* MR-1 *apbE* was heterologously expressed, yielding a flavinylated holoenzyme (Bertsova et al., 2013). ApbE was then characterized as a flavin transferase, with predicted homologues encoded on the genomes of a number of other organisms (Bogachev et al., 2018).

In *Shewanella,* flavins have been shown to be actively secreted and used as soluble electron shuttles to mediate respiration of insoluble substrates (Kotloski and Gralnick, 2013; Marsili et al., 2008; von Canstein et al., 2008). This behavior isn't entirely unusual in bacteria; humic substances and anthraquinone-2,6-disulfonate (AQDS) are previously characterized electron shuttling mechanisms in bacteria (Lovley et al., 2004). Endogenously produced compounds, such as phenazines in *Pseudomonas*, can serve as redox mediators (Brutinel and Gralnick, 2012a; Pham et al., 2008). The unusual aspect of flavins as endogenously produced electron shuttles, especially FMN and FAD, is that they are presumably metabolically costly to make, requiring both ATP and central metabolic precursors to synthesize, and energy to export. Flavin secretion in *S. oneidensis* MR-1 begins with FAD export by Bfe, a predicted Na^+-driven multidrug and toxin efflux (MATE) family pump (Kotloski and Gralnick, 2013). Although FAD is the primary flavin exported through Bfe, and can be used as an electron shuttle, only FMN and riboflavin are detected in the medium, as FAD is hydrolysed to FMN and AMP by the actions of UDP-sugar/AMP hydrolase UshA (Covington et al., 2010; Kotloski and Gralnick, 2013; von Canstein et al., 2008).

1.6 The competitive exclusion principle and exceptions to the rule

While much has been learned about *Shewanella* through pure-culture methods, its evolution has ostensibly been driven by competition and cooperation among mixed populations. Although often directly linked to growth rate, experiments measuring fitness in direct competition allow a researcher to more closely examine cell physiology through an ecological and evolutionary lens. In a homogenous environment supplying conditions for constant growth and where a single resource is shared, a relatively fast growing subpopulation will exclude its competitor (Gause, 1932; Hardin, 1960). As succinctly stated by Hardin (1960), *"*Complete competitors cannot coexist." The competitive exclusion principle is easily demonstrated using microbial competition assays in which relative fitness of two microorganisms can be determined (Lenski, Rose, Simpson, & Tadler, 1991; Wiser & Lenski, 2015). Exceptions to this principle do exist in homogeneous environments, such as those in which resources are temporally variable (Stewart and Levin, 1973), or when an inhibitor or predator of one competitor is present

(Davison & Stephanopoulos, 1986; Lenski & Hattingh, 1986; Levin, Stewart, & Chao, 1977), or in those environments where heterogeneity is introduced such as a single-resource chemostat at equilibrium where one population develops a wall attachment phenotype (Baltzis and Fredrickson, 1983; Dykhuizen and Hartl, 1983). For each of these exceptions, either niches are differentiated or temporal fluctuations in relative growth rate are introduced. For example, frequent enough temporal growth rate fluctuations, accumulation of inhibitory growth byproducts, or a specific predation can provide conditions in which an inferior competitor can either successfully persist during periods of starvation or actively grow alongside an inhibited but otherwise superior competitor, thereby never reaching an extinction threshold. When wall attachment is introduced as a parameter in an otherwise planktonic community, a second niche is created and coexistence is possible in theory due to environmental heterogeneity (Baltzis and Fredrickson, 1983). Wall growth in a chemostat also provides a condition in which washout does not occur even at dilution rates beyond the specific growth rate of the organism (Herbert et al., 1956; Pilyugin and Waltman, 1999).

1.7 Thesis Summary

The goal of this thesis is to illuminate key physiological factors behind respiratory lifestyle of *Shewanella oneidensis* and leverage them into a broader understanding of ecological dynamics and evolution. Chapter 2 is a study of cofactor acquisition by the periplasmic flavoproteins FccA and UrdA. This chapter primarily affords an understanding of the necessity of FAD secretion in *Shewanella,* along with the associated metabolic burdens. Furthermore, this chapter highlights the careful balance *Shewanella* must maintain between periplasmic FAD cofactor secretion, and the enzymatic cleavage of FAD by the periplasmic hydrolase UshA.

Chapter 3 is a probing of genetic factors used to survive under electron acceptor starvation. The lifestyle of *S. oneidensis* as an obligate respiratory organism reliant upon the versatility of its respiratory nodes is emphasized by uncovering a very limited set of evolved strategies for coping with respiratory stress, while characterizing a potential synthetic strategy for respiratory stress survival.

Chapter 4 questions a central paradigm in evolution and ecology, that organisms occupying the same niche cannot coexist. Through the use of engineered mutants of *S. oneidensis* and a flow-through three-electrode bioreactor system as an experimental platform, it is demonstrated that two strains of the same species possessing differential growth rates and utilizing the same carbon source, nutrients, and electron acceptor can remain at stable relative frequencies when grown as a surface-attached community.

Finally chapter 5 is a set of overarching conclusions from this work, along with a discussion on unanswered questions and future research.

Chapter 2 – Secreted flavin cofactors for anaerobic respiration of fumarate and urocanate by *Shewanella oneidensis*: cost and role

This chapter is a reprint of a published article, with minor alterations.

Kees ED, Pendleton AR, Paquete CM, Arriola MB, Kane AL, Kotloski NJ, Intile PJ, Gralnick JA. 2019. Secreted flavin cofactors for anaerobic respiration of fumarate and urocanate by *Shewanella oneidensis*: cost and role. Appl Environ Microbiol 85:e00852-19. https://doi.org/10.1128/AEM.00852-19.

2.1 Summary

Shewanella oneidensis strain MR-1, a facultative anaerobe and model organism for dissimilatory metal reduction, uses a periplasmic flavocytochrome, FccA, as both a terminal fumarate reductase and as a periplasmic electron transfer hub for extracellular respiration of a variety of substrates. It is currently unclear how maturation of FccA and other periplasmic flavoproteins is achieved, specifically in the context of flavin cofactor loading, nor has the fitness cost of flavin secretion been quantified. We demonstrate that deletion of the inner membrane flavin adenine dinucleotide (FAD) exporter Bfe results in a 23% slower growth rate than wild-type during fumarate respiration, and an 80-90% loss in fumarate reductase activity. Exogenous flavin supplementation does not restore FccA activity in a Δ*bfe* mutant unless the gene encoding the periplasmic FAD hydrolase UshA is also deleted. We demonstrate that the small Bfe-independent pool of FccA is sufficient for anaerobic growth with fumarate. Strains lacking Bfe were unable to grow using urocanate as the sole electron acceptor, which relies on the periplasmic flavoprotein UrdA. We show that periplasmic flavoprotein maturation occurs in careful balance with periplasmic FAD hydrolysis, and that the current model for periplasmic flavin cofactor loading must account for a Bfe-independent mechanism for flavin transport. Finally, we determine that the metabolic burden of flavin secretion is not significant during growth with flavin-independent anaerobic electron acceptors. Our work helps frame the physiological motivations to that drove evolution of flavin secretion by *Shewanella*.

2.2 Introduction

Shewanella oneidensis strain MR-1 is a Gamma proteobacterium found in a variety of aquatic and marine environments, ranging from sediments to aquatic multicellular organisms (Hau and Gralnick, 2007; Nealson and Scott, 2006). As a model organism for dissimilatory metal-reducing bacteria, *S. oneidensis* is capable of respiring a wide variety of organic and inorganic compounds, including nitrate, sulfate, trimethylamine N-oxide (TMAO), dimethyl sulfoxide (DMSO), urocanate, fumarate, and both solid and dissolved metal oxides (Bogachev et al., 2012; Lovley et al., 2004; Myers and Nealson, 1988; Nealson and Scott, 2006). Central in the reduction of many of these terminal electron acceptors, including nitrate, DMSO, and metals, are two periplasmic proteins: a flavocytochrome and fumarate reductase, FccA (SO_0970) and a small tetraheme cytochrome (STC) encoded by the gene *cctA* (SO_2727). Both STC and FccA receive electrons from the inner membrane tetraheme cytochrome CymA and donate electrons to the MtrABC metal respiration complex in the outer membrane, forming a periplasmic electron transfer hub (Schuetz et al., 2009; Sturm et al., 2015). FccA, shares 59% amino acid sequence identity with the well-characterized flavocytochrome *c* fumarate reductase (Fcc_3) of *S. frigidimarina* NCIMB400, and is highly abundant in the periplasm of both organisms (Leys et al., 1999; Maier et al., 2003; Schuetz et al., 2009; Taylor et al., 1999). FccA requires a noncovalent flavin adenine dinucleotide (FAD) cofactor to function (Leys et al., 1999; Pealing et al., 1992; Taylor et al., 1999), which is produced intracellularly and transported through the inner membrane by an exporter Bfe (Kotloski and Gralnick, 2013). It is unclear whether FccA acquires its cofactor due to Bfe-driven FAD transport, or if other processes lead to its flavin cofactor acquisition.

While FAD is the primary flavin secreted by *S. oneidensis* (Covington et al., 2010), flavin mononucleotide (FMN) and riboflavin are predominantly found in the extracellular space of *Shewanella* cultures, ranging in concentrations between 250 nM and 1 μM (Coursolle et al., 2010; Marsili et al., 2008; von Canstein et al., 2008). At these concentrations, extracellular flavins act as electron shuttles to mediate reduction of solid substrates such as metal oxides and electrodes, and additional supplementation enhances reduction rates (Baron et al., 2009; Brutinel and Gralnick, 2012a; Coursolle et al., 2010; Kotloski and Gralnick, 2013; Marsili et al., 2008; Ross et al., 2009; von Canstein et al.,

2008). Additionally, extracellular flavins have potential to play a role as cofactors for outer-membrane cytochromes OmcA and MtrC, accelerating reduction of mineral surfaces via direct interaction (Edwards et al., 2015; Okamoto et al., 2013; Okamoto et al., 2014; Z. Wang et al., 2015; White et al., 2016). Although FAD can also function as an electron shuttle, it is efficiently cleaved in the periplasm to FMN and adenosine monophosphate (AMP) by the metallophosphoesterase, UshA, which further enables growth of *S. oneidensis* with AMP as its sole carbon source through hydrolysis of AMP to adenosine and inorganic phosphate (Covington et al., 2010). Periplasmic UshA activity presents a potential problem for cofactor binding to FccA, which as a CxxCH motif-bearing flavocytochrome (Pealing et al., 1992) enters the periplasm in an unfolded state through the Sec system and is processed by the CcmABCDEFGH complex (Thöny-Meyer, 2002), presumably before acquiring noncovalently bound FAD. Another periplasmic flavoprotein, the urocanate reductase UrdA, is homologous to FccA in its FAD-binding domain (Bogachev et al., 2012). UrdA is predicted to be Sec secreted (Arkhipova et al., 2015), indicating it enters the periplasm in an unfolded state as with FccA. Unlike FccA however, UrdA does not bind heme, and contains a covalent FMN-binding motif in addition to its noncovalent FAD-binding domain (Bogachev et al., 2012).

At present, the processes behind cofactor loading and maturation of either FccA or UrdA – especially the factors that balance flavinylation with UshA activity– are not well understood. Here we lay a basis for the metabolic costs of flavin secretion and the cellular conditions required for free acquisition by FccA and UrdA. We probe flavin secretion requirements for both growth and enzymatic activity in fumarate and urocanate respiration. Finally, we provide insights for further elucidation of specific mechanisms behind periplasmic flavoprotein maturation in *S. oneidensis*.

2.3 Results and discussion

Metabolic burden of FAD secretion

To determine the metabolic cost of flavin secretion in *S. oneidensis* we performed competition assays for fitness of a flavin-nonsecreting Δ*bfe* (ΔSO_0702) deletion mutant (see ref 12). When grown in co-culture with a genomic GFP-bearing strain of *S. oneidensis* (MR-1+*gfp*), using lactate as the carbon source and fumarate as the sole terminal electron acceptor, the Δ*bfe* mutant was outcompeted (Fig 2.1A), with a fitness cost near 14% relative to wild-type (WT) MR-1 (Table 2.1). The cost to fitness associated with *bfe* deletion under fumarate respiring conditions was slightly higher in an inverse experiment in which Δ*bfe* engineered to produce GFP (Δ*bfe*+*gfp*) was competed against wild-type (WT) MR-1 (Fig 2.1B). GFP production itself manifests a fitness cost as in the WT background under fumarate-respiring conditions (Table 2.1; Fig 2.2A).

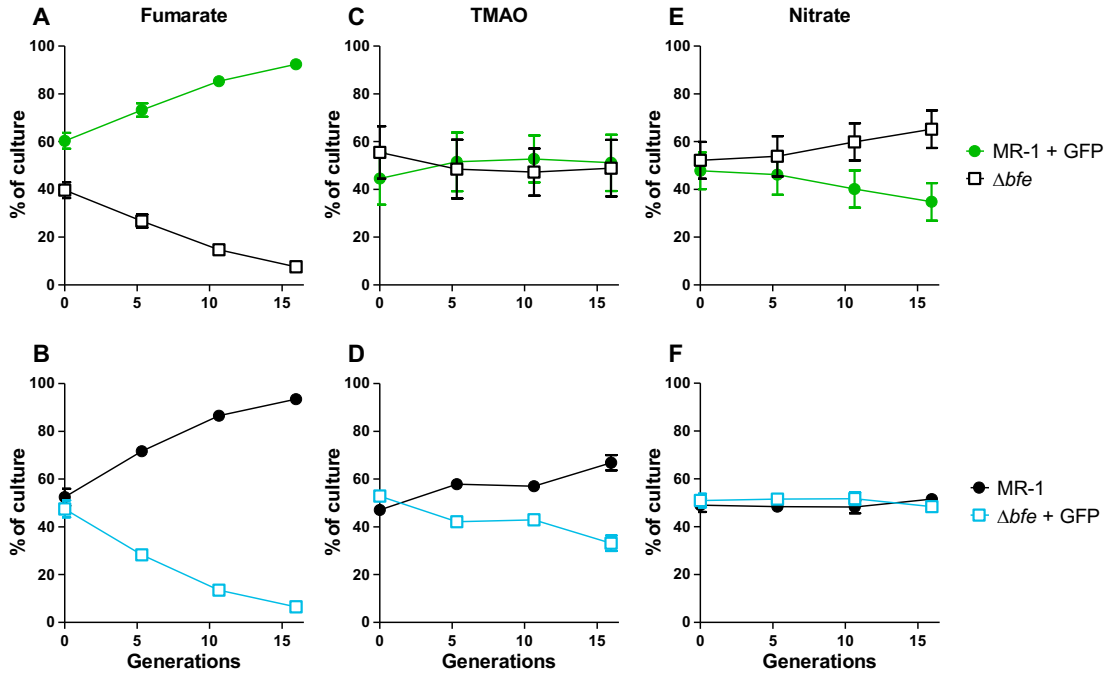

Fig 2.1 Anaerobic competition assays. Assays containing 20 mM D,L-lactate as the carbon source with *S. oneidensis* MR-1 expressing GFP (strain MR-1+*gfp*) competed against the Δ*bfe* mutant (A, C, and E) or WT MR-1 competed against the Δ*bfe*+*gfp* mutant (B, D, and F) on 40 mM fumarate (A and B), 20 mM TMAO (C and D), or 40 mM nitrate (E and F). Symbols and error bars indicate averages and standard errors of the means (SEM) for measured ratios; data are from $n = 3$ replicate cultures, except for panels A and E, where $n = 6$.

When grown with TMAO as the sole terminal electron acceptor, the Δ*bfe* mutant displayed near-WT fitness (Fig 2.1C), while *gfp* expression in Δ*bfe* led to an expected fitness cost compared to WT (Fig 2.1D), likely due to GFP production. Finally, when grown in competition under nitrate respiring conditions, Δ*bfe* had an apparent fitness benefit (Fig 2.1E) while Δ*bfe*+*gfp* had a near neutral relative fitness (Fig 2.1F). While at first glance this may appear to suggest that FAD secretion has a slight metabolic burden under nitrate respiration, we are unable to conclude whether this is the case, as the difference in fitness between Δ*bfe* and MR-1+*gfp* is no greater than the fitness cost associated with *gfp* expression under nitrate-respiring conditions (Table 2.1; Fig 2.2B).

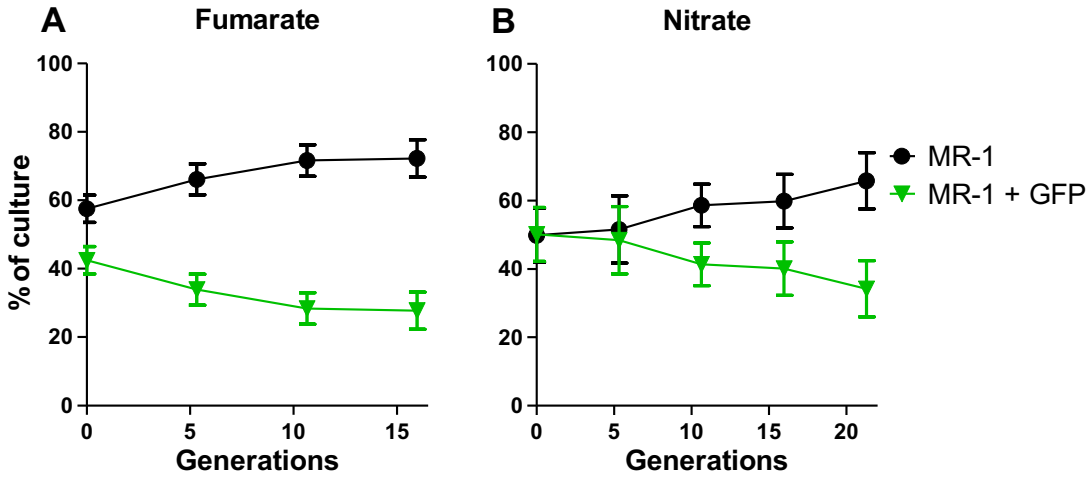

Fig 2.2 Metabolic burden of GFP production. Anaerobic competition assays containing 20 mM D,L-Lactate as carbon source with *S. oneidensis* MR-1 expressing GFP (▼) competed against WT MR-1 (●) 40 mM Fumarate (A), or 40 mM Nitrate (B). Error bars indicate standard error mean (SEM) of measured ratios.

Table 2.1 Relative fitness (*w*) of Δ*bfe,* *gfp*-expressing Δ*bfe,* and *gfp*-expressing MR-1 vs WT strains

	Relative fitness (*w*)[a]		
Strain	Fumarate	TMAO	Nitrate
Δ*bfe* (vs MR-1+*gfp*)	0.858 ± 0.011[b]	0.990 ± 0.016	1.039 ± 0.008[b]
Δ*bfe* +*gfp* (vs MR-1)	0.839 ± 0.008	0.948 ± 0.016	0.994 ± 0.005
MR-1+*gfp* (MR-1)	0.954 ± 0.021	-	0.967 ± 0.011

[a] Values are averages ± SEM; All data represent *n* = 3 replicate cultures, except where noted otherwise.
[b] Values are from *n* = 6 replicate cultures.

These results show that the benefits afforded by FAD secretion under fumarate respiration greatly outweigh the potential metabolic costs. Furthermore, TMAO and nitrate competition assay results suggest that the cost of flavin secretion is minimal for *S. oneidensis* even under anaerobic conditions in which FAD does not perform a role as a cofactor. Similarly, there was not a clear cost or benefit to flavin secretion under aerobic conditions (Fig 2.3). Altogether these results led us to the hypothesis that active secretion of FAD into the periplasm is required for maximal function of FccA.

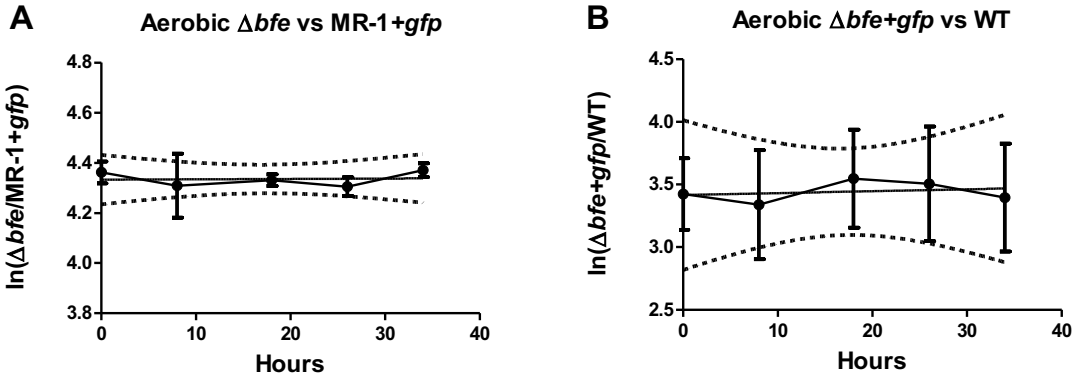

Fig 2.3 Metabolic burden of flavin secretion in aerobic cultures. Aerobic competition assays containing 20 mM D,L-Lactate as carbon source, with Δ*bfe* competed against MR-1+*gfp* (A) or Δ*bfe*+*gfp* against WT MR-1 (B). Values are the natural logarithm of the ratio of Δ*bfe* to WT in each sample time point, lines and dashed indicate linear regression of the ln ratios; n=3

FAD secretion by Bfe is required for peak FccA activity

To quantify the contribution of Bfe-exported FAD to enzymatic function of FccA, methyl viologen oxidation assays (Fig 2.4) were performed using Δ*bfe,* Δ*ushA* (ΔSO_2001)*,* and Δ*bfe*Δ*ushA* deletion mutant strains of *S. oneidensis.* FAD was separately added to determine whether defects could be rescued by supplementation, and whether UshA activity inhibits binding of exogenous flavin by FccA. When FAD was not provided exogenously, both Δ*bfe* and Δ*bfe*Δ*ushA* mutant strains had strong defects for bulk FccA activity (Fig 2.4A), with an unsupplemented Δ*bfe* strain displaying only ~18% FccA activity as WT (Table 2.2). Growth with 1 μM or higher FAD fully restores FccA activity in a Δ*bfe*Δ*ushA* mutant (Fig 2.4B), but a Δ*bfe* mutant is only slightly rescued by exogenous FAD at 10 μM (Fig 2.4C), a concentration 5-50x greater than total flavin

secretion by *Shewanella* species under aerobic and anaerobic growth conditions(Coursolle et al., 2010; Marsili et al., 2008; von Canstein et al., 2008).

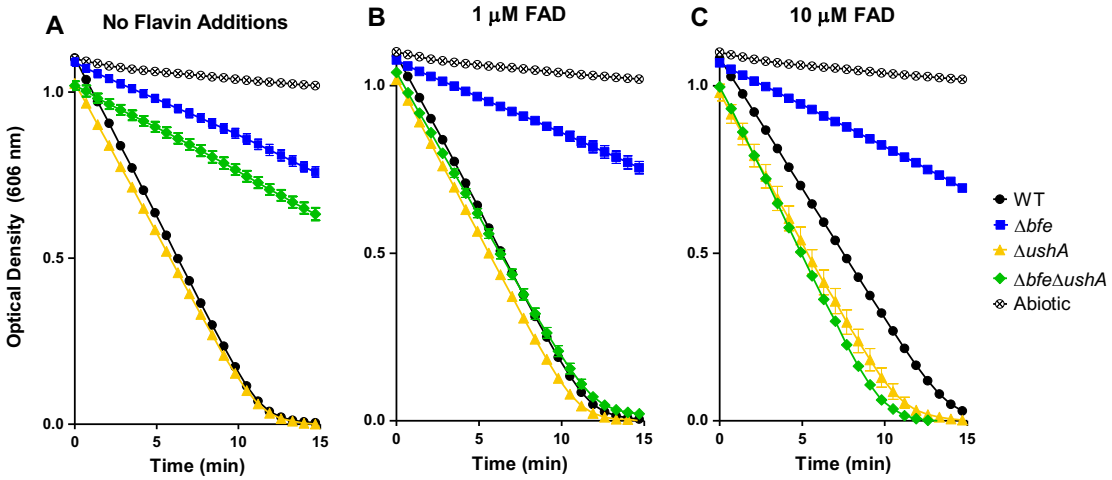

Fig 2.4 Methyl viologen assay for fumarate reductase (FccA) activity. Methyl viologen oxidation coupled to fumarate reduction via FccA in whole cells was measured for WT, Δ*bfe*, Δ*ushA*, and Δ*bfe* Δ*ushA* strains and abiotic controls with no flavin supplementation (A), 1 µM FAD supplementation (B), and 10 µM FAD supplementation (C). Symbols and error bars represent averages and SEM for n = 3 technical replicate assays.

These results indicate a greater effect of Bfe-driven FAD secretion on total fumarate reductase activity (82% reduction in FccA activity in Δ*bfe*) than we anticipated from fitness scores under fumarate respiration (~15% cost to fitness for Δ*bfe*). Furthermore, the finding that exogenous FAD does not fully restore FccA function in a Δ*bfe* background unless *ushA* is also deleted suggests that FAD must be derived intracellularly to be used as a periplasmic cofactor, pointing to uncharacterized FAD chaperone activity, which may facilitate binding of Bfe-derived FAD to periplasmic proteins and preempts UshA cleavage.

Table 2.2 Methyl viologen oxidation / fumarate reduction rate per OD cells for Δ*bfe* strains; Values are means and standard error means from *n*=3 technical replicate assays.

	$(OD_{MV+,\ 606nm})(min)^{-1}(OD_{cells,\ 600nm})^{-1}$		
	No exogenous FAD	1 µM FAD	10 µM FAD
WT	-71.94 ± 0.98	-69.78 ± 1.06	-58.38 ± 1.57
Δ*bfe*	-16.58 ± 0.70	-16.14 ± 0.84	-18.90 ± 0.20
Δ*ushA*	-67.79 ± 1.24	-69.43 ± 0.92	-66.60 ± 1.75
Δ*bfe*Δ*ushA*	-19.74 ± 0.31	-64.09 ± 1.35	-75.67 ± 1.25
Abiotic	-3.97 ± 0.18	-4.48 ± 0.36	-3.64 ± 0.04

Bfe is not essential for growth with fumarate

While Δ*bfe* mutants had a measurable fitness defect, and displayed severely diminished FccA activity, Δ*bfe* and Δ*bfe*Δ*ushA* mutants showed relatively minor defects in growth with fumarate as sole terminal electron acceptor even when no exogenous flavins were added (Fig 2.5A; Table 2.3). Subsequent transfers of strains into fresh medium in an attempt to eliminate carryover of cofactor-loaded FccA did not impact growth (Fig 2.6). As with biochemical assays, growth defects were rescued by exogenous FAD supplementation in Δ*bfe*Δ*ushA* but not Δ*bfe* (Fig 2.5B and Fig 2.5C; Table 2.3). While observed growth rate differences between Δ*bfe* and WT MR-1 (specific growth, $k_{\Delta bfe}$ / $k_{WT} \approx 0.77$) align well with the observed fitness defect of Δ*bfe* under fumarate respiration ($w_{\Delta bfe} = 0.86$ vs MR-1+*gfp*), they do not match FccA activity by methyl viologen assay. These results suggest that far more FccA is produced in *S. oneidensis* than is strictly required to respire fumarate, a notion supported by the proposed function of FccA as a transient periplasmic electron transfer hub (Schicklberger et al., 2013; Schuetz et al., 2009; Sturm et al., 2015) in addition to its role as a terminal fumarate reductase. Together with biochemical assays, the ability of Δ*bfe* to grow on fumarate implies that the FccA produced by Δ*bfe* strains retains its FAD cofactor and is lower in abundance than in WT.

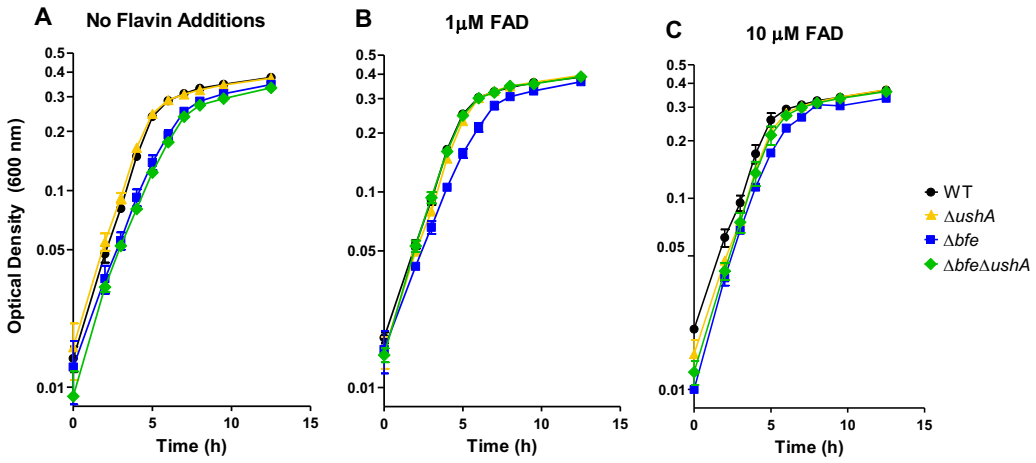

Fig 2.5 Anaerobic growth assay for phenotypic assessment of Δ*bfe* strains during fumarate respiration with flavin additions. Growth of WT, Δ*bfe*, Δ*ushA*, and Δ*bfe* Δ*ushA* strains was measured in anaerobic minimal medium containing 20 mM D,L-lactate and 40 mM fumarate without exogenous flavin supplementation (A) and with 1 μM FAD supplementation (B) or 10 μM FAD supplementation (C). Symbols and error bars represent averages and SEM for $n = 3$ replicate cultures. See Table 3 for growth rate measurements.

Table 2.3 Specific growth rates (*k,* h^{-1}) of bfe mutants during fumarate respiration (Fig 3). Values are averages and standard error means; n=3.

	No exogenous FAD	1 μM FAD	10 μM FAD
WT	0.586 ± 0.024	0.570 ± 0.009	0.529 ± 0.016
Δ*bfe*	0.451 ± 0.018	0.440 ± 0.010	0.483 ± 0.008
Δ*ushA*	0.568 ± 0.032	0.572 ± 0.033	0.565 ± 0.027
Δ*bfe*Δ*ushA*	0.438 ± 0.013	0.562 ± 0.007	0.583 ± 0.038

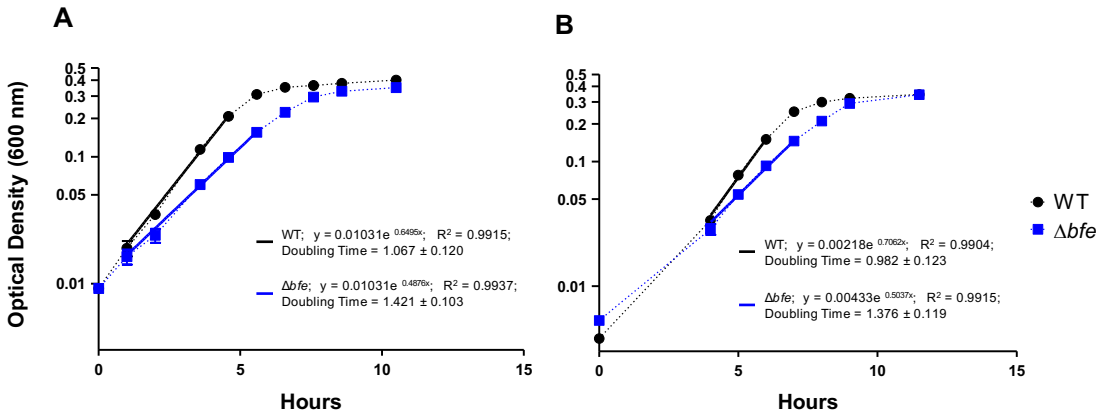

Fig 2.6 Cofactor carryover analysis. Anaerobic growth of WT (●) and Δ*bfe* (■) in minimal medium with 20 mM lactate and 40 mM fumarate at 30°C, transferred from an initial anaerobic overnight (A), and transferred serially to fresh medium from culture A via syringe (B). Specific growth rates of WT and Δ*bfe* were significantly different from each other within each culture and did not significantly change after transfer. Dashed lines connect averaged data points, solid lines indicate curve fit of exponential growth equation across selected data points; n=3.

FccA production and fccA expression in Δbfe

To address questions of FccA production and FAD cofactor retention in Δbfe, we purified FccA from Δbfe and WT backgrounds and characterized it by NMR spectroscopy. We observed decreased abundance of FccA in Δ*bfe* compared to WT by heme-stain (Fig 2.7A, Table 2.4, Fig 2.8A), and FccA purified from a Δ*bfe* background (Fig 2.8B) is similar to WT-derived FccA as determined by NMR spectroscopy (Fig 2.7B), suggesting that Δ*bfe*-derived FccA retains its cofactor. However, a small percentage has a different conformation, given by the small peaks that appear in the NMR spectrum (shown with grey squares), suggesting that a small fraction of the protein

is unfolded or has a different conformation state than the wild-type protein.

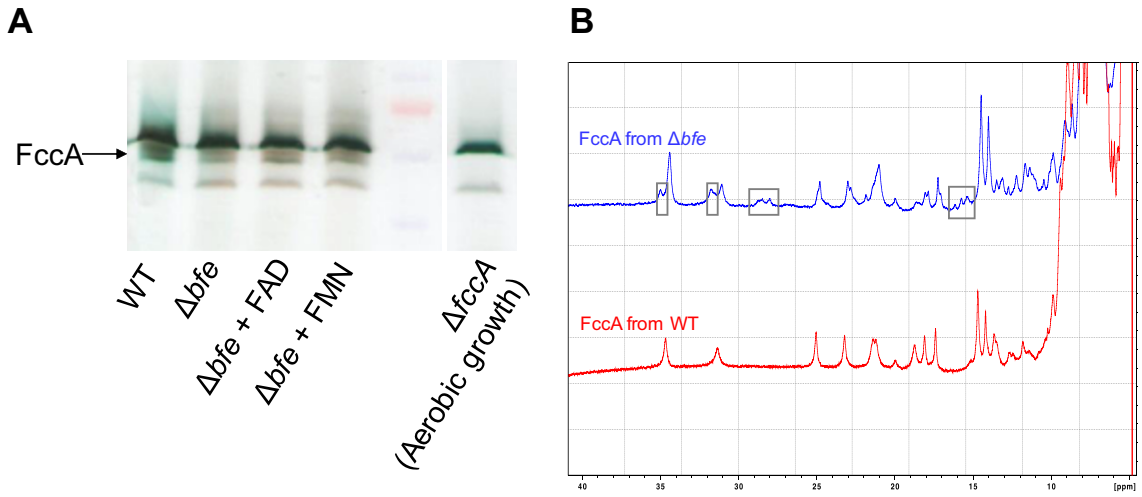

Fig 2.7 FccA protein characterization in Δ*bfe strain.* A) Protein gel comparison of Δ*bfe* with WT. SDS-PAGE (12%) heme-stained gel loaded with 1mL each of anaerobic (SBM) cultures of WT, Δ*bfe,* and Δ*bfe* grown with 10 µM FAD or 10 µM FMN, lysed with Bacterial Cell Lysis Buffer (nzytech). Heme stain from Δ*fccA* cells grown aerobically in LB medium at 30 °C displays lack of FccA. B) 1D ^{1}H NMR spectrum of FccA isolated from Δ*bfe* (blue trace) and wild-type (red trace).

Table 2.4 Densitometry results of heme-stained SDS-PAGE gel; n=1.

	Density	Relative Density
WT	14337.761	100.00%
Δ*bfe*	5397.033	37.64%
Δ*bfe*+FAD	6666.497	46.50%
Δ*bfe*+FMN	6304.983	43.97%

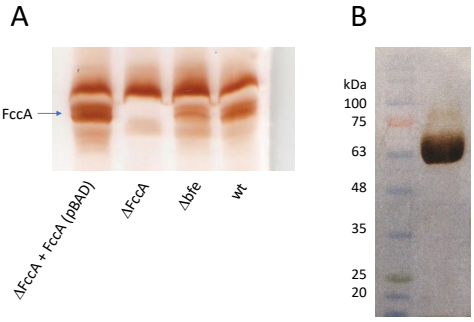

Fig 2.8 Purification of FccA from Δbfe following aerobic growth. A) Heme stain from cells grown aerobically in LB medium at 30 °C. B) Heme stain of FccA purified from Δbfe.

One hypothetical explanation for the decreased fitness, growth rate, and fumarate reduction rates observed in Δ*bfe* compared to WT, is that *bfe* deletion decreases expression of *fccA*. Similarly, rescue of Δ*bfe*Δ*ushA* by exogenous FAD could be explained by positive regulation of *fccA* by a hypothetical flavin sensing mechanism. While we observed decreased abundance of FccA protein in a Δ*bfe* mutant, there were no significant differences from WT in *fccA* expression as determined by RT-qPCR in either Δ*bfe or* Δ*bfe*Δ*ushA* strains with or without exogenous flavin addition (Table 2.5).

Table 2.5 FccA expression by RT-qPCR

	$2^{\Delta\Delta Ct}$ (*recA*, WT)[a]			
	SBM	FAD	FMN	RF
Δ*bfe*	1.03 ± 0.17	0.97 ± 0.22	0.75 ± 0.51	1.37 ± 1.02
Δ*bfe*Δ*ushA*	1.26 ± 0.62	0.79 ± 0.34	N/A	1.23 ± 0.09
WT ΔCt (*recA*)	-7.89 ± 0.37	-8.60 ± 0.50	-8.73 ± 0.47	-7.68 ± 0.69

[a] Values for Δbfe and Δbfe ΔushA strains are reported as 2-log threshold cycles (CT) relative to the WT and normalized to recA, for $n = 3$ replicate assays. WT values are reported as the threshold cycle relative to recA. Data for Δbfe ΔushA strain with FMN supplementation are not available. All flavins were at 1 µM concentration. $P > 0.05$ for all one-sample t tests against 1.0.

A likely explanation for the discrepancy between expression and protein abundance is that FccA is unstable without FAD and is thereby degraded. Notably, when the Δ*bfe*Δ*ushA* mutant was grown without FAD supplementation, its bulk biochemical activity was not rescued by exogenous flavins added to the assay (Fig 2.9; Table 2.6), altogether indicating that Δ*bfe* mutants and Δ*bfe*Δ*ushA* mutants grown without flavin supplementation have a lower total abundance of FccA than in WT cells or Δ*bfe*Δ*ushA* mutants supplemented during growth.

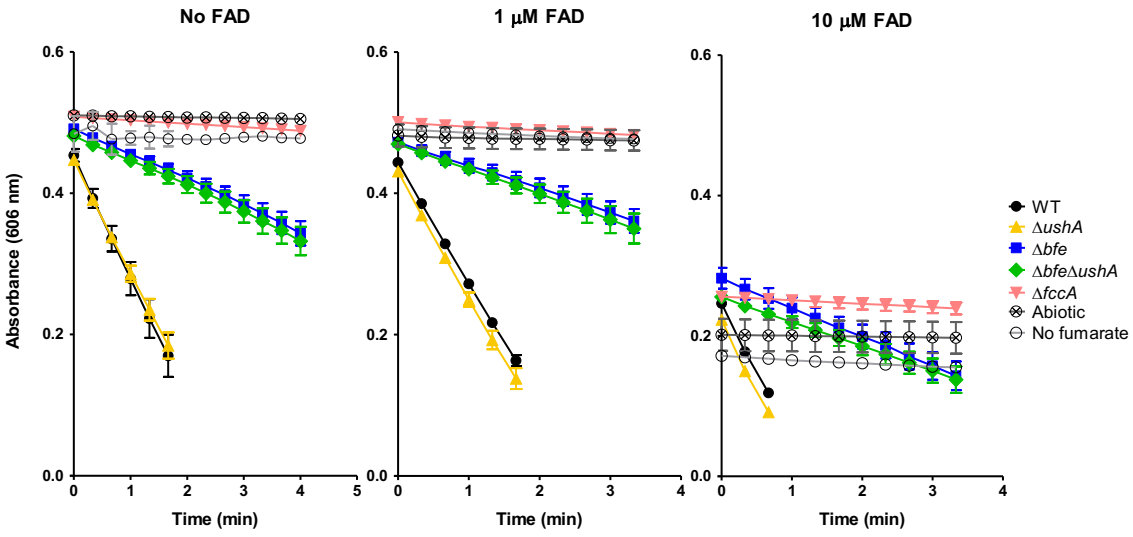

Fig 2.9 Methyl viologen reduction assay with flavin supplementation in assay only. WT (●), Δ*ushA* (▲), Δ*bfe* (■), Δ*bfe*Δ*ushA* (◆), and Δ*fccA* (▼), pregrown without flavin supplementation, and supplemented in assay with FAD. Abiotic (⊗) and no fumarate (○) controls are shown. These results suggest that Δ*bfe* and Δ*bfe*Δ*ushA* mutants grown without FAD supplementation have lower abundance of FccA enzyme. Table 2.6 contains corresponding values. n=3.

Table 2.6 Methyl viologen oxidation rates with flavin supplementation in assay only. n=3.

	$(OD_{MV+,\ 606nm})(min)^{-1}(OD_{cells,\ 600nm})^{-1}$		
	no FAD addition	1 μM FAD	10 μM FAD
WT	-59.35 ± 7.87	-58.86 ± 1.35	-69.94 ± 6.45
Δ*ushA*	-54.82 ± 7.55	-62.52 ± 6.17	-65.74 ± 6.57
Δ*bfe*	-11.84 ± 2.16	-10.67 ± 2.00	-13.49 ± 3.07
Δ*bfe*Δ*ushA*	-12.17 ± 1.92	-11.73 ± 2.63	-11.55 ± 2.08
Δ*fccA*	-2.43 ± 0.49	-2.62 ± 0.57	-2.51 ± 0.55
Abiotic	-0.43 ± 0.05	-0.60 ± 0.25	-0.45 ± 0.04
No fumarate	-0.63 ± 4.68	-1.40 ± 0.23	-1.72 ± 0.25

Bfe is required for normal growth with urocanate respiration

To determine whether phenotypes exhibited under fumarate respiration in *bfe* mutants hold for other respiratory conditions requiring Sec-secreted periplasmic flavoproteins, we tested growth phenotypes under urocanate respiration. As is the case under fumarate respiration, a Δ*bfe* mutant is able to grow with urocanate as the sole terminal electron acceptor, but unlike with fumarate respiration, Δ*bfe* exhibits a severe lag phase (Fig 2.10), along with a severe growth rate defect (Table 2.7). Without exogenous FAD supplementation, Δ*bfe*Δ*ushA* is also shows a growth defect with urocanate (Fig 2.10A), but it is partially rescued by exogenous FAD supplementation at a concentration of 10 μM (Fig 2.10B), with a distinct lag phase (approx. 8 hrs) compared to wild-type and Δ*ushA,* along with a slight growth defect. Importantly, Δ*cymA* and Δ*urdA* mutants failed to grow under these condition (Fig 2.10A and Fig 2.10B), even after approximately 30 days of continued incubation (data not shown), indicating that UrdA receives its electrons via CymA, and that growth of *bfe* mutants after extended lag was due to urocanate respiration. Altogether, these results indicate that Bfe is much more important for FAD cofactor acquisition by UrdA than by FccA.

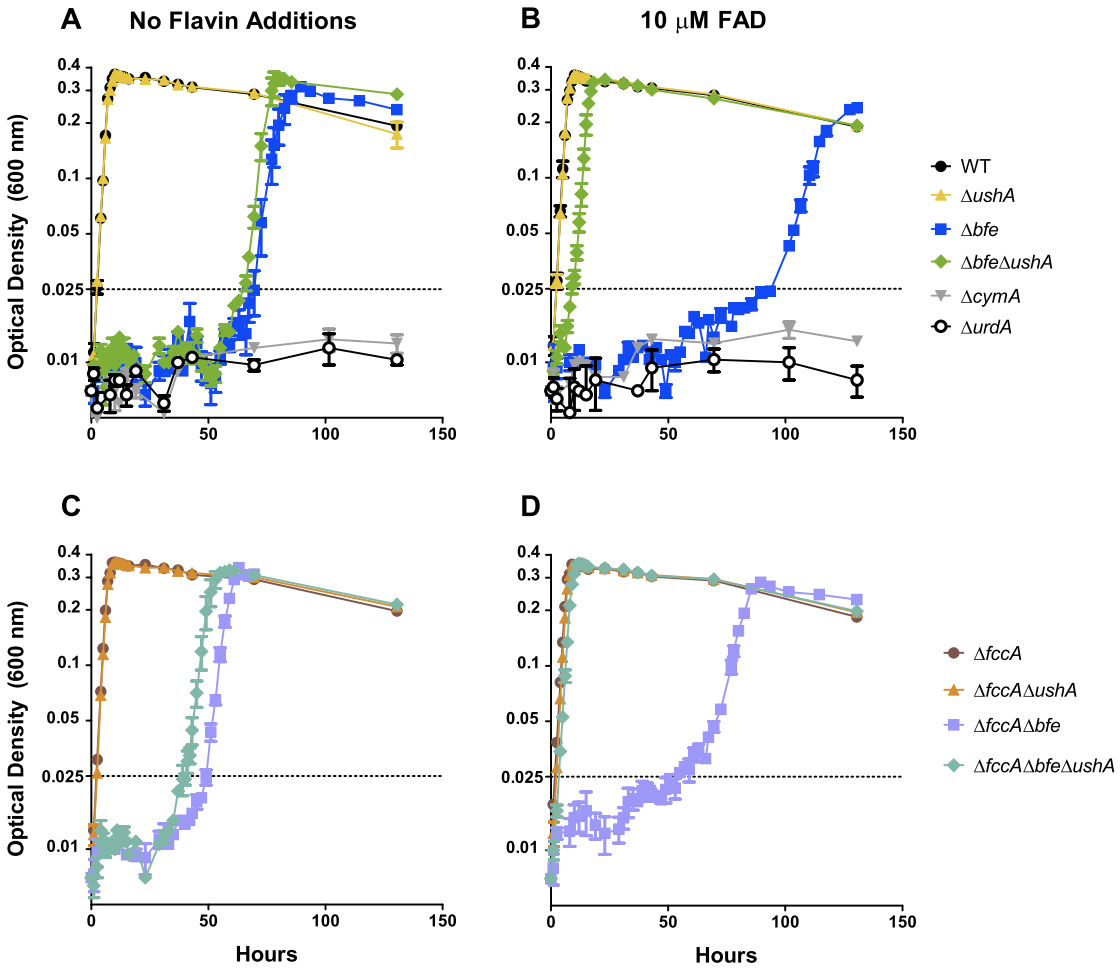

Fig 2.10 Anaerobic growth assay for phenotypic assessment of Δ*bfe*, Δ*fccA*, and Δ*cymA* strains during urocanate respiration with flavin additions. Growth of WT, Δ*bfe*, Δ*ushA*, Δ*bfe* Δ*ushA*, Δ*cymA*, and Δ*urdA* strains was measured in minimal medium containing 10 mM D,L-lactate and 20 mM urocanate without exogenous flavin supplementation (A) and with 10 μM FAD or FMN supplementation (B). Measurements were also conducted with Δ*fccA*, Δ*fccA* Δ*ushA*, Δ*fccA* Δ*bfe*, and Δ*fccA* Δ*bfe* Δ*ushA* strains without exogenous flavin supplementation (C) and with 10 μM FAD or FMN supplementation (D). Dotted lines at an OD600 of 0.025 indicate arbitrarily chosen culture density thresholds for lag-phase comparison. Symbols and error bars represent averages and SEM for $n = 3$ replicate cultures

As FccA is highly abundant in the periplasm (Schuetz et al., 2009), it is possible that its presence inhibits rescue of Δ*bfe*Δ*ushA* by exogenous FAD on urocanate by binding available FAD before it can be used to flavinylate newly synthesized UrdA. Indeed a Δ*bfe*Δ*ushA*Δ*fccA* mutant has a shorter lag phase (approx. 40h, Fig 2.10C), than Δ*bfe*Δ*ushA* (approx. 65 h, Fig 2.10A). More strikingly, when Δ*bfe*Δ*ushA*Δ*fccA* was supplied with 10 μM FAD, it did not exhibit a measurable lag (Fig 2.10D), and its growth rate was 15% faster than Δ*bfe*Δ*ushA* under the same conditions, matching that of WT (Table 2.7). Further, with

one exception (Δ*bfe*Δ*ushA* without FAD supplementation) deletion of *fccA* in mutant strains exhibiting lag on urocanate resulted in both decreased lag duration and significantly increased growth rate. These observations are consistent with FccA preferentially acquiring FAD under conditions of periplasmic flavin limitation (resulting from loss of Bfe). Considering this result, it is interesting that WT does not exhibit a measurable lag phase on urocanate and may suggest a direct role for Bfe in periplasmic flavin co-factor loading. The way in which UrdA acquires FAD, either directly from Bfe or through a chaperone, is seemingly not competitively inhibited by the presence of FccA in wild-type cells.

Table 2.7 Specific growth rates (*k,* h^{-1}) of *bfe* and *fccA* mutants during urocanate respiration (Fig. 2.9).Values are averages and standard error means; n=3.

	No exogenous FAD	10 μM FAD
WT	0.502 ± 0.013	0.477 ± 0.020
Δ*bfe*	0.157 ± 0.012	0.087 ± 0.001
Δ*ushA*	0.492 ± 0.008	0.515 ± 0.020
Δ*bfe*Δ*ushA*	0.285 ± 0.020	0.405 ± 0.002
Δ*fccA*	0.509 ± 0.004	0.471 ± 0.007
Δ*bfe*Δ*fccA*	0.226 ± 0.011	0.115 ± 0.009
Δ*ushA*Δ*fccA*	0.507 ± 0.008	0.504 ± 0.006
Δ*bfe*Δ*ushA*Δ*fccA*	0.299 ± 0.004	0.473 ± 0.015

The growth phenotype differences between fumarate and urocanate respiration of Δ*bfe* mutants are possibly due to the additional covalent FMN cofactor requirement for UrdA. Covalent attachment of FMN to UrdA has been reported to occur in the periplasm via flavin transferase ApbE (Bogachev et al., 2018). ApbE purified from *Vibrio harveyi* used FAD as the FMN donor substrate for flavinylation of Na^+-NQR, and the reaction did not proceed with FMN as the substrate (Bertsova et al., 2013), which may indicate that cofactor loading of both FAD and FMN onto UrdA in *S. oneidensis* occurs in a manner that preempts UshA activity. Since ApbE is used for covalent FMN transfer to UrdA (Bogachev et al., 2018), the extra steps involved in this process may present a higher barrier for flavin cofactor acquisition than with FccA.

Concluding remarks

The inner membrane flavin exporter Bfe is responsible for providing the FAD cofactor for FccA in *S. oneidensis* MR-1, but approximately 10-18% of FccA is able to acquire its cofactor in the absence of Bfe. Furthermore, this small pool of Bfe-independent FccA is sufficient to support robust growth with fumarate as the sole terminal electron acceptor, albeit at a 14% loss in fitness. Thus, *S. oneidensis* produces substantially more FccA than is needed strictly for fumarate respiration, supporting a proposed electron transfer hub model of FccA whereby it overlaps in function with STC as a temporary capacitive buffer for electrons generated by oxidative metabolism, primarily during extracellular metal reduction but also during nitrate and DMSO respiration (Sturm et al., 2015).

Specific mechanisms through which secreted FAD is acquired by periplasmic flavoproteins before being cleaved by UshA remain to be elucidated. Although, ApbE isolated from *Vibrio cholerae* has been shown to bind FAD with high affinity, it is not clear whether it plays a role in noncovalent FAD acquisition by flavoproteins. Interestingly, transposon insertions in *apbE* yield an apparent fitness defect in Tn-seq experiments with fumarate as the sole electron acceptor (Brutinel and Gralnick, 2012b). However, this defect could be due to several potential downstream effects of an *apbE* knockout, including NADH-dehydrogenase inactivation and additional *apbE* homologs are found in the *S. oneidensis* genome. A model in which Bfe directly interacts with a chaperone and/or flavin transferase such as ApbE is a promising prospect, but would be incomplete without accounting for the ability of Δ*bfe* to grow on fumarate without flavin supplementation. A secondary mechanism for FAD secretion and/or leakage through the inner membrane has thus far not been uncovered.

This work has implications for biotechnological applications of *Shewanella* involving respiration of solid substrates, supporting the concept that exogenous flavin supplementation to *Shewanella* cultures greatly benefits respiratory processes which utilize flavins as electron shuttles, such as metal oxide mineral and electrode surface reduction. Critically, these results show that exogenous flavin supplementation does not significantly aid in periplasmic flavin cofactor acquisition by MR-1. The requirement for *S. oneidensis* to produce its own secreted flavins as cofactors places it in stark contrast

with *Listeria monocytogenes,* which was recently discovered to have a flavin based extracellular electron transfer pathway, despite possessing no riboflavin biosynthesis pathways, making it dependent on its environment to acquire flavin cofactors (Light et al., 2018). Interestingly, *L. monocytogenes* is able to use flavins as electron shuttles for reduction of iron oxide minerals, and, as part of its extracellular electron pathway, it also possesses an FMN transferase, FmnB, with similar FAD substrate requirements as ApbE (Light et al., 2018). Finally, flavin secretion does not seem to come at a significant metabolic cost during aerobic, nitrate, or TMAO respiration, while providing a significant benefit to the reduction of fumarate and solid metal oxides such as ferrihydrite and birnessite (Kotloski and Gralnick, 2013). Ultimately this work suggests that *S. oneidensis* is evolutionarily adapted to thrive in flavin-poor environments, and that its ability to provide the communal benefit of flavin secretion is borne not just out of their utility as electron shuttles, but also out of necessity for filling its own cofactor requirements.

2.4 Materials and methods

Bacterial strains and growth conditions

S. oneidensis strain MR-1 was used as wild type control in all experiments and as parent strain for all gene deletions. Table 2.8 presents a list of strains, plasmids and primers used in this study. Strain MR-1+*gfp* was constructed by insertion of *gfpmut3** (Andersen et al., 1998), under control of the promoter $P_{A1/04/03}$ (Lanzer and Bujard, 1988), into the neutral *attTn7* insertion site downstream of gene *glmS* in MR-1 (Lambertsen et al., 2004; Teal et al., 2006). Double homologous recombination was used to target the gene insertion as well as gene deletions, and has been described previously (Saltikov and Newman, 2003). Inocula for all strains were routinely prepared for anaerobic growth experiments from frozen stock isolated on lysogeny broth (LB) 1.5% agar plates, then grown in successive aerobic overnight cultures in liquid LB and minimal medium. Inocula were transferred by syringe to anaerobic minimal medium after washing and concentrating cells to equal turbidities. Unless otherwise noted, minimal growth medium consisted of *Shewanella* basal medium (SBM) (Baron et al., 2009), containing 5 mL/L of vitamins mix excluding riboflavin (Balch et al., 1979), 5 mL/L of trace mineral mix (Marsili et al., 2008), and 0.05% casamino acids (Fisher), buffered with 10 mM HEPES and adjusted to pH 7.2

using NaOH. In all growth experiments and overnight cultures in minimal medium, D,L-lactate was supplied as the sole carbon source. In anaerobic cultures, fumarate, urocanate, TMAO, or nitrate were used as the sole terminal electron acceptor where indicated.

Competition Assays

Triplicate LB overnight cultures of two strains (GFP-labeled, and unlabeled) were centrifuged at 8000 x g, then washed and resuspended in SBM, diluting to 0.1 OD_{600}. Equal volumes of each strain were mixed, then 500 µL of the 50:50 mixture was added to 4.5 mL of minimal growth medium containing 100 mM HEPES in a butyl rubber stoppered tube to achieve a starting density of 0.01 OD_{600}. Oxygen was removed via filtered syringe using N_2/CO_2 gas mixture. Following 24 hours of culture, transfers were made into fresh anoxic medium at 0.01 OD_{600}. Ratios of each strain were determined by flow cytometry with a FACSCalibur (Becton Dickinson, Franklin Lakes, NJ) equipped with 488 nm and 640 nm lasers, using the FL1 green detection channel through a 530/30 filter. GFP-producing and non-GFP-producing cells were counted using commercial FlowJo software (Ashland, OR; see Fig. S6 for example data analysis). Relative fitness was calculated for each culture transfer as $w = 1 + \frac{ln\frac{A_f}{B_f} - ln\frac{A_i}{B_i}}{\#\ generations}$, where A is the mutant and B is *gfp*-expressing MR-1 in forward experiments, or A is the *gfp*-expressing mutant and B is MR-1 in reverse experiments. Variables *i* and *f* represent initial frequency upon inoculation and final frequency following growth, respectively. Values were represented as averages across all timepoints and replicates, using standard error mean (SEM) as the measure of variance.

Methyl viologen assay

Reduced methyl viologen was prepared by passing hydrogen gas through a 10 mM aqueous solution in the presence of a platinum wire catalyst. In a 96-well plate inside an anaerobic chamber (N_2), anaerobic cultures (20 mM lactate, 60 mM fumarate) of WT, Δ*bfe,* Δ*ushA,* and Δ*bfe*Δ*ushA* grown overnight with 0 µM, 1 µM and 10 µM FAD were diluted in SBM (pH 7.2, 100 mM HEPES) to an identical turbidity (OD_{600} = 0.2), then further diluted 1/50. Reduced methyl viologen reagent was diluted to achieve an

absorbance of 3.3 (OD_{606}). Assays were prepared by mixing 100 µL each of 10 mM fumarate in SBM, diluted methyl viologen, and diluted cells. Data was immediately collected by a 96-well plate spectrophotometer. $\Delta OD_{606\ nm}$ normalized to cellular concentration in the assay was used as a proxy for MV^+ oxidation rate by fumarate via FccA and was determined by linear regression.

RT-qPCR

WT and Δ*bfe* were grown anaerobically in minimal medium with fumarate, with and without addition of 1 mM FAD. Cell cultures were collected in mid exponential growth phase (OD_{600} = 0.260), by mixing 1:1 with RNAProtect Bacteria reagent (Qiagen), centrifugation at 4000xg for 10 min, supernatant removal, and freezing at -80°C. RNA was purified using an RNeasy Mini Kit (Qiagen), following manufacture recommended protocols for bacterial RNA isolation, including on-column DNase I treatment. Quantitative RT-PCR was performed using an iTaq Universal One-Step RT-qPCR kit (Bio-Rad), following manufacturer instructions and using 50 ng of RNA template. Data was analyzed by the $2^{\Delta\Delta Ct}$ method, normalizing to *recA* and wild-type controls.

Purification of FccA

Δ*bfe*-derived FccA was purified as previously described using Δ*bfe* grown cells under aerobic conditions (Fonseca et al., 2013). Briefly, the soluble fraction obtained from Δ*bfe* growth cells was loaded to a Q-Sepharose column previously equilibrated with 20 mM Tris buffer (pH 7.6). The fraction containing FccA eluted at approximately 150 mM NaCl was concentrated and dialyzed prior being loaded to another Q-Sepharose column, equilibrated previously with 20 mM Tris buffer (pH 7.6). FccA fraction was eluted at approximately 150 mM NaCl. This fraction was then loaded, after dialysis, to an HTP column, pre-equilibrated with 10 mM potassium phosphate buffer (pH 7.6). Pure FccA was eluted with 100 mM of potassium phosphate buffer (pH 7.6). All the chromatography fractions were analyzed by SDS-PAGE (12% gel) and UV-visible spectroscopy to select those that contain FccA. NMR experiments were performed at 25 ºC on a Bruker Avance II 500 MHz NMR spectrometer equipped with a 5 mm BBI probe.

Bacterial Cell Lysis Buffer (nzytech) was used lyse WT and Δ*bfe* trains in the presence and in the absence of flavins (FAD and FMN) to evaluate FccA production using SDS-PAGE. Toward this, anaerobic growth was performed in SBM without flavins and in the presence of 10 μM FAD or 10 μM FMN, using as pre-inoculum 1% of LB aerobically grown cells. After 24 hours of culture, 1 ml of culture was used for analysis. Densitometry measurements were determined by histogram curve areas for FccA bands within a single gel image using the FIJI package of ImageJ software (Schindelin et al., 2012).

Table 2.8 Strains, plamids and primers used in this study

Strain	Parent strain and genotype	Source
JG274	MR-1, wild-type	(Myers and Nealson, 1988)
JG686	JG274, Δ*fccA* (ΔSO_0970)	(Ross et al., 2011)
JG1079	JG274, Δ*ushA* (ΔSO_2001)	(Covington et al., 2010)
JG1637	"MR-1+gfp", JG274, +*gfpmut3** under constitutive A1/O4/O3 phage promoter expression at neutral insertion locus downstream of *glmS.*	This study
JG1758	JG274, Δ*bfe* (ΔSO_0702)	(Kotloski and Gralnick, 2013)
JG1759	JG1079, Δ*ushA*Δ*bfe*	(Kotloski and Gralnick, 2013)
JG2761	JG1637, + *gfpmut3*,* Δ*bfe*	This study
JG4278	JG1758, Δ*bfe*Δ*fccA*	This study
JG4279	JG1079, Δ*ushA*Δ*fccA*	This study
JG4280	JG274, Δ*urdA* (ΔSO_4620)	This study
JG4281	JG1759, Δ*ushA*Δ*bfe*Δ*fccA*	This study
UQ950	*E. coli* DH5α λ(pir) used for cloning; see source for genotype	(Saltikov and Newman, 2003)
WM3064	*E. coli* strain used for conjugation; see source for genotype	(Saltikov and Newman, 2003)
Plasmid	**Relevant characteristics**	**Source**
pSMV3	Deletion vector, Km^r-only version of pSMV10, *sacB*	(Saltikov and Newman, 2003)
pΔ*bfe*	pSMV3 backbone	(Kotloski and Gralnick, 2013)
pΔ*fccA*	pSMV3 backbone	(Ross et al., 2011)
pΔ*urdA*	573bp upstream and 595 bp downstream of SO_4620, including the first 8 and last 10 codons, in pSMV3 backbone at SacI and SpeI restriction sites	This study
pAK1	Homologous region targeting neutral insertion site 7 bp downstream of *glmS* cloned into pSMV3, with a SpeI recognition sequence at targeted insertion site. See primers ALK23, ALK24, ALK 25, and ALK26.	This study
pURR25	R6K derivative containing promoter $P_{A1/O4/O3}$ and *gfpmut3**	(Teal et al., 2006)
pAK2	Promoter $P_{A1/O4/O3}$ and *gfpmut3** amplified from pURR25 using primers ALK27, and ALK28, cloned into pAK1 at SpeI site.	This study
pBAD202::*fccA*$_{Strep}$	Directional TOPO expression vector containing strep-tagged *fccA*	(Schuetz et al., 2009)
pBAD202::*fccA*	pBAD202::*fccA*$_{Strep}$ modified by site directed mutagenesis kit (Nzytech) to remove strep tag, using primers Flavo_stop_forw and Flavo_stop_rev	This study

Primer	Sequence	Cut site	Source
FccAQF	ACCTGCTGCAATGACTACTG		This Study
FccAQR	CTTGAAGATGCAAGCGGTAAAG		This Study
RecAQF	AGCTATAGCCGCTGAAATCG		(Pirbadian et al., 2014)
RecAQR	CCTCGACATTGTCATCATCG		(Pirbadian et al., 2014)
Δ*urdA* UP F	ACAT GAGCTC CTGGACCCAGAACTTTATCTC	SacI	This study
Δ*urdA* UP R OE	TGCGATACG CGTAACAGCAATACCAATAATGG		This study
Δ*urdA* DN F OE	GCTGTTACG CGTATCGCAGGACAAGAAG		This study
Δ*urdA* DN R	TTAT ACTAGT GCATCACCCGCAACTTTA	SpeI	This study
ALK23	NNNN GGGCCC GGCGGCACGTTATTGGTTA	ApaI	This study
ALK24	NNNN ACTAGT ACTGGCGGTTTTTTATTGG	SpeI	This study
ALK25	NNNN ACTAGT ACCGCCAGTTAGGCGGTTT	SpeI	This study
ALK26	NNNN GAGCTC TCCTGATGTCGCGAGCTTCG	SacI	This study
ALK27	NNNN ACTAGT GTTCCGCGCACATTTCCCGA	SpeI	This study
ALK28	NNNN ACTAGT CGGCAACCGAGCGTTCTGAAC	SpeI	This study
Flavo_stop_forw	CTGCCGCTAAATTCGCTAAAGATAATTAAGCT TGGAGCCACCCGCAGTTCG		This study
Flavo_stop_rev	CGAACTGCGGGTGGCTCCAAGCTTAATTA TCTTTAGCGAATTTAGCGGCAG		This study

2.5 Acknowledgements

This work was supported by the Office of Naval Research Award (#N00014-13-10552) to JAG. EDK was partially supported by the University of Minnesota Informatics Institute and MnDRIVE. CMP was supported by Project LISBOA-01-0145-FEDER-007660 (Microbiologia Molecular, Estrutural e Celular) funded by FEDER funds through COMPETE2020 - Programa Operacional Competitividade e Internacionalização (POCI). The NMR spectrometers at CERMAX are part of the National NMR Network (PTNMR) and are partially supported by Infrastructure Project No 022161 (co-financed by FEDER through COMPETE 2020, POCI and PORL and FCT through PIDDAC).

Chapter 3 – Genetic contributors to respiratory stress induced lysis in *Shewanella*, and a synthetic strategy for respiratory stress mitigation

3.1 Summary

This study determined that electron acceptor starvation is the primary contributor to lysis and death in *Shewanella* cultures in which electron donor and acceptor are provided at stoichiometrically equivalent concentrations. By providing a synthetic supply of proton motive force (PMF) in the form of the light driven proton pump proteorhodopsin (PR), we arrested the lysis under respiratory stress phenotype and maintained cell viability despite cessation of respiration. Although PMF loss is a primary driver of lysis by lysogenic phages, deleting all three prophages in the MR-1 genome did not affect lysis phenotypes under these conditions. Finally, by leveraging high-throughput transposon screening and synthetic proton motive force maintenance, this study profiled shifts in central metabolism of *S. oneidensis* under respiratory stress, along with genes required for survival, and a limited selection of mutations that enable survival under those conditions.

3.2 Introduction

Shewanella oneidensis *MR-1*

The genus *Shewanella* includes a diverse array of marine and freshwater Gram-negative γ-proteobacteria. The ability to respire various organic and inorganic compounds, including soluble and insoluble metals is a remarkable characteristic of members of the Shewanellae (Hau and Gralnick, 2007; Nealson and Scott, 2006). *Shewanella oneidensis* is a well-studied member of this genus owing in part to its high growth rate and genetic tractability. The large number of terminal electron acceptors it can use makes *S. oneidensis* well adapted for respiration in varied and changing environments. As a model for dissimilatory metal reduction, *S. oneidensis* has generated interest for its use in a number of biotechnological applications, including removal of hexavalent uranium from contaminated water sources through bioprecipitation and/or mobilization (Jiang and Hur, 2013; Sani et al., 2008; Sheng and Fein, 2014), biosensing of hazardous materials in marine or freshwater environments (Webster et al., 2014), and electrosynthesis of valuable organic compounds (Ross et al., 2011). However, as an obligate respiratory organism, wild-type (WT) strains of *S. oneidensis* cannot grow in the

absence of a suitable terminal electron acceptor (Myers and Nealson, 1988). Strikingly, *S. oneidensis* has demonstrated a dramatic death phenotype following growth under stoichiometric equivalents of electron donor and acceptor, making it a suitable organism for studying physiological and environmental triggers of death and potentially lysis. This phenotype was noted in literature when assayed for growth using lactate and fumarate as respective electron donor and acceptor (Johnson et al., 2010), but can also be seen in published growth curves using *N*-acetylglucosamine (NAG) as a carbon source (Hunt et al., 2010), and DMSO or nitrate as electron acceptors (Sturm et al., 2015).

Proton motive force and light driven supplementation

During anaerobic growth of *S. oneidensis* with fumarate as the terminal electron acceptor, the majority of ATP synthesis occurs primarily through substrate-level phosphorylation (Hunt et al., 2010). When respiring fumarate or metals, PMF is presumably generated (though it has not been extensively studied) through the oxidation of menaquinone at inner membrane tetraheme cytochrome CymA. It has also been suggested through comparative growth experiments, that ATP synthesized by during anaerobiosis may be used in the reverse reaction catalyzed by the F_oF_1 ATP synthase (Hunt et al., 2010) to generate a portion of PMF under anerobic respiring conditions. PMF is used to drive a number of crucial processes including solute uptake and efflux, and flagellar motility (Paulick et al., 2009). The regulatory roles of PMF in autolysis and bacteriophage-driven lysis have been extensively studied in Gram-positive and Gram-negative bacteria, respectively (Rice & Bayles, 2008).

Proteorhodopsins are inner-membrane light driven proton pumps with a wide color diversity (Bamann et al., 2014) capable of supplying PMF to non-native hosts (Johnson et al., 2010; Walter et al., 2007). Highly related in structure and function to the better-studied archaeal bacteriorhodopsin (Bamann et al., 2014), they are found widespread in surface ocean bacteria, although the exact evolutionary and physiological importance is unclear (Fuhrman et al., 2008). The proton pumping capability of proteorhodopsin is dependent on a bound retinal chromophore (Bamann et al., 2014). A derivative of β-carotene, all-*trans*-retinal isomerizes to 13-*cis*-retinal upon absorption of a photon. When bound by a rhodopsin, this initial isomerization is reversed in a multistep

photocycle. Although minor differences exist in the structure and photocycles of proteorhodopsin and bacteriorhodopsin, each translocates one proton per cycle (Bamann et al., 2014). Some native proteorhodopsin-containing bacteria are conferred a light-stimulated growth advantage (Gómez-Consarnau et al., 2007; Palovaara et al., 2014), while others appear to benefit only in stationary phase under energy-stress conditions such as carbon starvation (Gómez-Consarnau et al., 2010; Steindler et al., 2011). Interestingly, engineered expression of the gene for a green-absorbing-variant of proteorhodopsin in *S. oneidensis* MR-1 results in increased rates of lactate uptake and respiration, but it does not confer an apparent growth advantage. Rather, proteorhodopsin-producing strains are enhanced for survival following exponential growth phase in anaerobic cultures containing stoichiometric equivalents of lactate and fumarate, conditions which otherwise promote lysis shortly following exponential growth (Johnson et al., 2010).

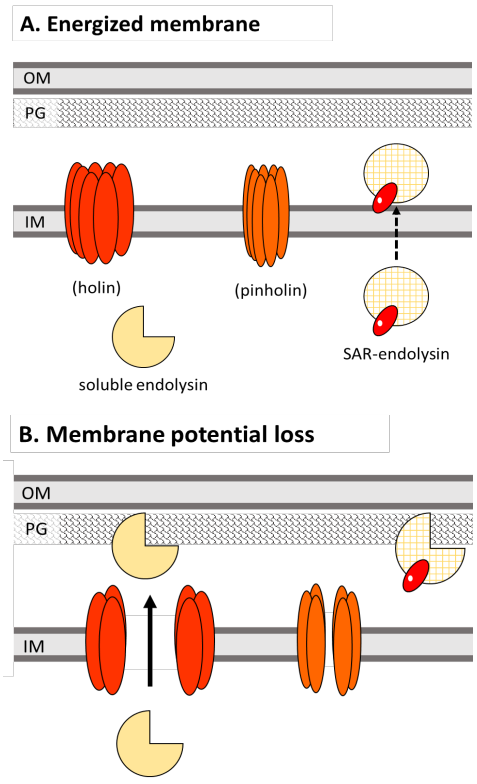

Fig 3.1 Schematic for holin/pinholin and endolysin activation. (A) Holins and endolysins are inactive when membrane potential is maintained. (B) Membrane potential loss activates holin pore formation (which further collapses membrane potential) and endolysin release.

Prophage-driven lysis in Gram negative bacteria

Most lysogenic bacteriophages lyse their hosts by muralytic enzymes known as endolysins (Young et al., 2000). Phages with Gram-negative hosts have endolysins that are either soluble/cytoplasmic, or a secreted variety characterized by an atypical uncleaved signal peptide known as a SAR (signal arrest release) domain (Catalão et al., 2013) (Fig 3.1). Soluble endolysins rely on inner membrane permeabilization by a diverse class of proteins referred to as holins, which trigger to form large holes in the inner membrane in response to PMF loss (Gründling et al., 2001). SAR-endolysins are released to the periplasm but

remain tethered to the inner membrane by the SAR domain. Under normal conditions SAR-endolysin release occurs very slowly, but is rapidly accelerated by membrane depolarization (Xu et al., 2004). Thus SAR-endolysins can be activated by PMF loss in a holin-independent manner, but they are often associated with a class of holins called pinholins. In contrast with classical holins, pinholins form much smaller lesions that do not allow passive diffusion of macromolecules, but instead act by collapsing the membrane potential (Young, 2014). Although they act to fully collapse membrane potential, pinholins themselves are triggered by an initial loss of membrane potential (Catalão et al., 2013). Finally, a third class of phage lytic protein in Gram-negative hosts, spanins, are responsible for destruction of the outer membrane as a final step in lysis. Whether, spanins are essential for this last step in lysis depends on the culturing conditions, as shear forces and osmolarity can affect outer membrane integrity following peptidoglycan degeneration (Young, 2014).

High-throughput transposon sequencing in Shewanella

The advent of high-throughput sequencing methods has enabled a suite of interrogations into the physiology of *S. oneidensis*, using a method of sequencing selected pooled transposon libraries, termed Tn-seq (van Opijnen et al., 2009). Briefly, this method requires a saturating transposon library, typically pooled and taken through selective growth conditions as a competition assay, before extracting DNA from the aggregate pool and sequencing to determine mutant abundance. As the first application of this method in *Shewanella,* utilization of genes coding for the tricarboxylis acid cycle was assayed and compared between aerobic (with lactate as carbon source) and anaerobic (with lactate and fumarate as carbon source and electron acceptor) growth conditions (Brutinel and Gralnick, 2012b). Another set of studies leveraged Tn-seq to uncover mechanisms for ferrous iron (Fe^{2+}) resistance in *S. oneidensis* (Bennett et al., 2018a, 2015), and Fe^{2+} and Co^{2+} uptake (Bennett et al., 2018b).

3.3 Results and discussion

Electron acceptor starvation is the primary determinant of S. oneidensis *lysis under fumarate respiring conditions*

Lysis of *S. oneidensis* following anaerobic growth has been noted in conditions in which stoichiometrically equivalent concentrations of electron donor and electron acceptor were provided (Hunt et al., 2010; Johnson et al., 2010; Sturm et al., 2015). To determine whether conditions of carbon starvation of terminal electron acceptor starvation elicited this death phenotype, experiments were conducted in which carbon source and electron acceptor were stoichiometrically imbalanced.

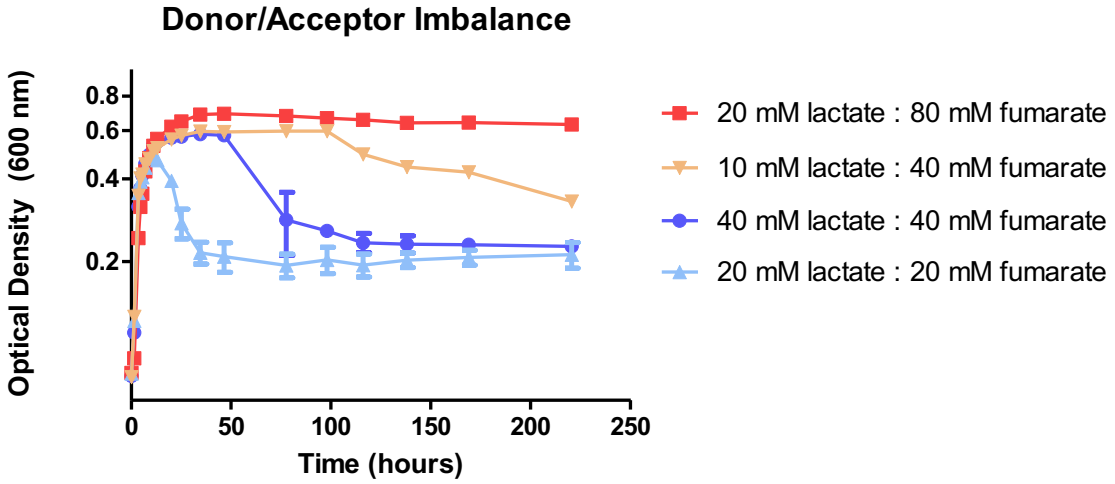

Fig 3.2 Growth/death with stoichiometric imbalance of electron donor and acceptorWT *S. oneidensis* MR-1 (JG274) cultures grown in *Shewanella* basal medium containing 10 mM HEPES, 0.05% casamino acids, and concentrations of lactate/fumarate of 20 mM / 80 mM (■), 10 mM / 40 mM (▼), 40 mM / 40 mM (●), and 20 mM / 20 mM (▲). Symbols represent mean optical density, and error bars represent standard error means across three replicates.

Generally, when lactate was limiting relative to fumarate, cultures did not exhibit an immediate death / lysis phase (Fig 3.2; 10 mM lactate and 40 mM fumarate, or 20 mM lactate and 80 mM fumarate), but survived for at least 100 hours before exhibiting marked turbidity loss. However, when fumarate was limiting relative to lactate (20 mM lactate and 20 mM fumarate; or 40 mM lactate and 40 mM fumarate), rapid lysis phenotypes were observed. Strikingly, when fumarate was provided in high concentration (80 mM) while lactate was provided at a typical concentration used for growth (20 mM), cultures remained near peak density for over 200 hours, while those with 10 mM lactate

and 40 mM fumarate, although exhibiting better survival than acceptor limited cultures, began to die around 100 hours. It is possible that 10 mM lactate and 40 mM lactate cultures continued to respire, but depleted fumarate around 100 hours. However, no HPLC was performed on these cultures to determine whether this was the case. These results suggest that carbon starvation is a condition in which *S. oneidensis* survives for prolonged periods, but acceptor starvation is not tolerated and results in catastrophic loss to cell function.

Construction and testing of candidate transposon-sequencing-amenable synthetic-proton-motive force-supplemented strains of S. oneidensis

A previous study determining the effects of proton motive force supplementation on respiratory rate (Johnson et al., 2010) used a strain, JG688, expressing the gene for proteorhodopsin on a pBBR1-MCS2 broad-range expression vector. Our goal was to determine the effects of proteorhodopsin on *Shewanella* physiology through high-throughput transposon sequencing. Since our existing pipeline for this kind of experiment relies on selection for transposon mutant via kanamycin resistance, we needed to construct an alternate proteorhodopsin expressing strain. The first strategy was to use a separate selectable marker for vector-borne proteorhodopsin, so a strain was constructed, JG2969, expressing proteorhodopsin on pBBR1-MCS a broad range expression vector containing a marker for chloramphenicol resistance. When compared to an empty vector control, JG2969 survived when grown under bright green (325 nm) light, but not when placed in the dark (Fig 3.3).

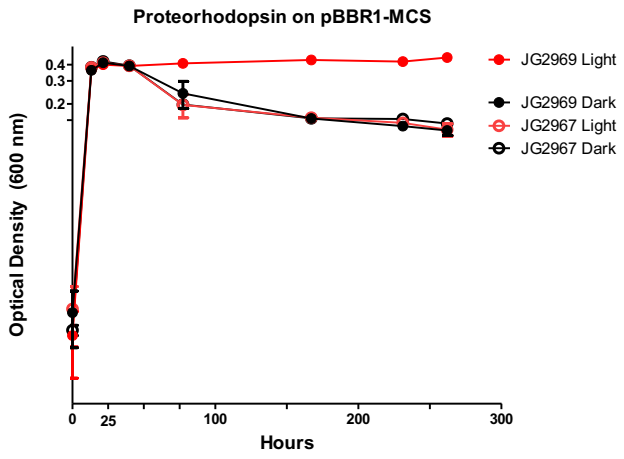

Fig 3.3 Growth/death for chloramphenicol resistant proteorhodopsin expressing *Shewanella*. *S. oneidensis* cultures expressing proteorhodopsin on expression vector pBBR1-MCS (JG2969, closed symbols) or containing empty vector (JG2967, open symbols) were grown either in the light (red symbols) or dark (black symbols) in SBM containing 10 mM HEPES, 0.05% casamino acids, 20 mM lactate and 40 mM fumarate. Symbols represent mean optical density at 600 nm, and error bars represent standard error means across three replicates.

Simultaneously, two strains were constructed to express proteorhodopsin on the genome of *S. oneidensis*. JG3000 contained proteorhodopsin at a neutral insertion site downstream of *glmS* under control of a *lac* promoter and RBS_{II} (synthetic, from vector pQE70; Andersen et al., 1998; Harris, 2014), while JG3020 contained similar insertion of proteorhodopsin, but under control of the A1/O4/O7 phage promoter (see Andersen et al., 1998) These promoter and RBS combinations were constructed to respectively provide medium and high levels of expression in *S. oneidensis* when placed on a pBBR1-MCS expression vector (Harris, 2014), but it was unknown how proteorhodopsin would be expressed on the genome when driven by these promoters, nor whether high expression of proteorhodopsin would destabilize the inner membrane. When provided with light, JG3000 survived better than dark-grown cultures under electron acceptor starvation, but not as well as JG3020 or the strain expressing proteorhodopsin on pBBR1-MCS2 (Km^r), JG688 (Fig 3.4). JG2969 survival under light (Fig 3.3) was also equivalent to JG688 and JG3020.

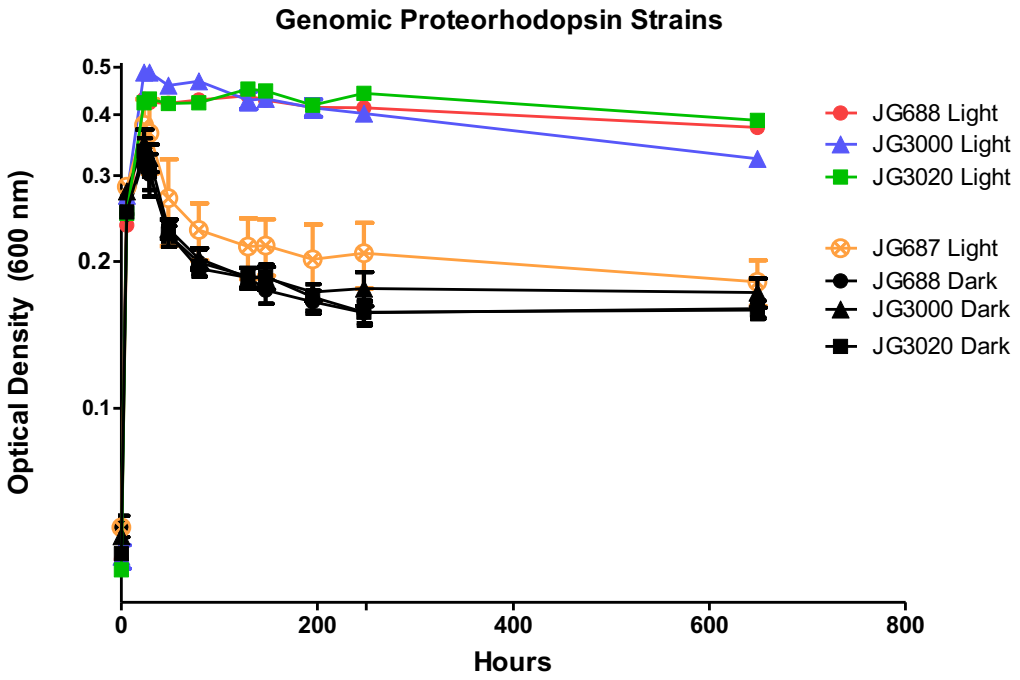

Fig 3.4 Growth/death for genomic proteorhodopsin expressing *Shewanella*. *S. oneidensis* cultures expressing proteorhodopsin on expression vector pBBR1-MCS2 (JG688, ●), expressing proteorhodopsin on the genome under *lac* promoter and RBSII (JG3000, ▲), expressing proteorhodopsin on the genome under phage promoter A1/O4/O7 (JG3020; ■), or containing empty pBBR1-MCS2 vector (JG687; ⊗) were grown either in the light (colored symbols) or dark (black symbols) in SBM containing 10 mM HEPES, 0.05% casamino acids, 20 mM lactate and 40 mM fumarate. Symbols represent mean optical density at 600 nm, and error bars represent standard error means across three replicates.

In cultures containing excess lactate to fumarate, JG3020 cells remain intact for at least 130 h following growth when under light (Fig 3.5A). However, between 37 and 130 hours after entry into stationary phase, a marked decline in viability (~65% loss) was observed (Fig 3.5B). Meanwhile, dark grown cultures dropped in viability by approximately 4 orders of magnitude from ~10^9 colony forming units(CFUs)/mL at peak growth to ~1.2x10^5 cells ~37 hours later. Intriguingly, after reaching a low point in viability, dark grown cultures grew to ~6x10^5 CFUs/mL, possibly indicating growth on lysed cell components.

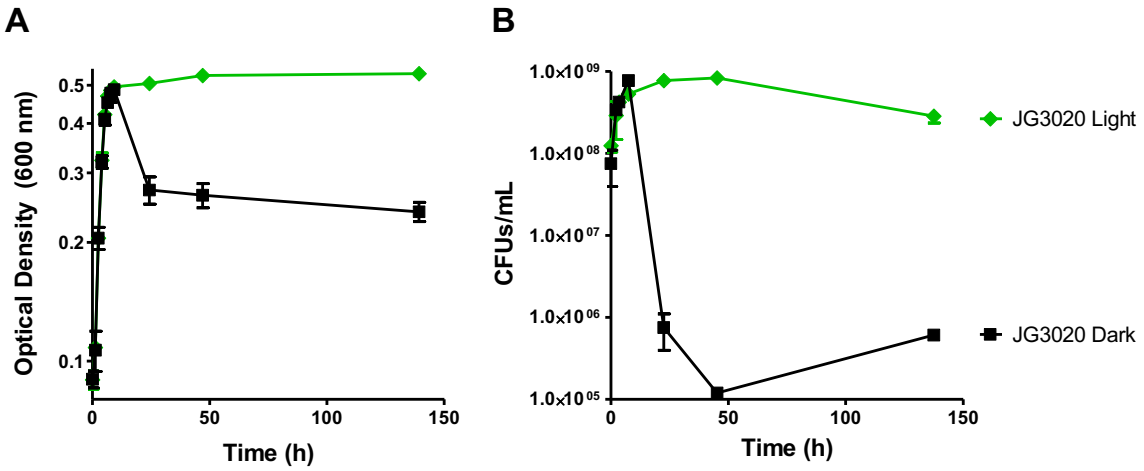

Fig 3.5 Turbidity and viability measurements for high-expression genomic proteorhodopsin strain under green light. *S. oneidensis* JG3020 cultures expressing proteorhodopsin on the genome under phage promoter A1/O4/O7 (were grown either under bright green (525 nm) light (◆) or in the dark (■) in SBM containing 10 mM HEPES, 0.05% casamino acids, 30 mM lactate and 40 mM fumarate. Symbols represent mean optical density at 600 nm, and error bars represent standard error means across three replicates.

While constructing strain JG3020, a strain containing a mutated proteorhodopsin (Lys172 > Thr172) was generated, with a slightly blue-shifted purple hue to cell pellets compared to the reddish hue of other proteorhodopsin strains. This mutated PR strain (JG3019) appeared to survive as well as JG3020 under green light (Fig 3.6), despite having apparently altered light-absorbing properties.

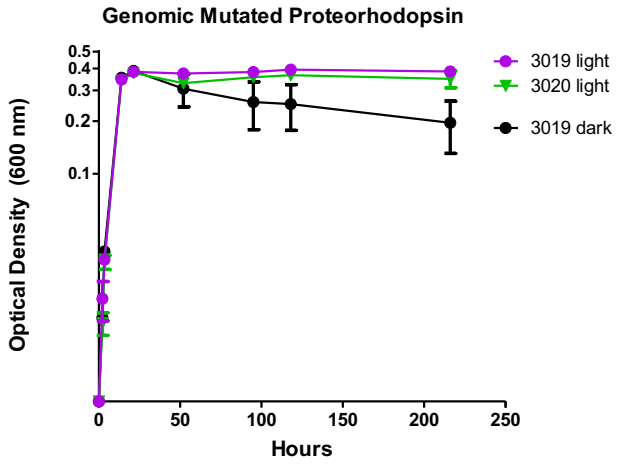

Fig 3.6 Functional analysis of mutated proteorhodopsin under green light. *S. oneidensis* cultures expressing proteorhodopsin on the genome under phage promoter A1/O4/O7 (JG3020; ■), or mutated proteorhodopsin on the genome under phage promoter A1/O4/O7 (JG3019; ▼), were grown either in the light (colored symbols) or dark (black symbols) in SBM containing 10 mM HEPES, 0.05% casamino acids, 20 mM lactate and 40 mM fumarate. Symbols represent mean optical density at 600 nm, and error bars represent standard error means across three replicates

Although loss in both optical density and viability together are highly suggestive of lysis, they do not represent concrete evidence, since a decrease in cell size among starving populations could account for a decrease in culture turbidity. As an alternative measure of lysis, supernatant DNA was quantified in acceptor starved cultures of JG3020 grown in the dark (effectively wild-type) and in the light (as a control for potential eDNA excretion in intact/viable, yet starved cells). After approximately 10 hours of growth and 35 hours of stationary phase, light-grown JG3020 culture supernatants contained 153 ± 27 ng/mL of DNA, while supernatants from dark-grown cultures contained 750 ± 176 ng/mL of DNA. An abiotic control contained 8.5 ng/mL of DNA. Altogether these results are indicative of lysis under respiratory starvation in *S. oneidensis.*

Contribution of prophages to respiratory stress induced lysis in S. oneidensis

The temperate prophage occupying position SO_2939-3013 in the genome of *S. oneidensis* is currently termed LambdaSo (λSo). Lysis by this phage has been shown to be necessary for normal biofilm formation in *S. oneidensis* as evidenced by poor surface coverage and defective development of three-dimensional structures. In comparison with two other known prophages, deletion of λSo has the most pronounced effect on biofilm formation in static conditions, although a deletion of all three prophages is required for total abrogation (Gödeke et al., 2011). The putative holin for λSo (SO_2971) is annotated as a canonical λ-type phage holin S. However, little identity exists between the amino acid sequence encoded by SO_2971 and the canonical λ coliphage holin (identity = 12.8%, similarity = 20.8%). Based on size and topology – predicted by consensus between multiple methods (Bernsel et al., 2009) – the λSo holin is expected to function through SAR-endolysin/pinholin-type mechanism. In accordance with this hypothesis, the putative λSo endolysin R (SO_2973) contains a predicted signal peptide-like N-terminal membrane spanning domain that failed to meet the cutoff for a cleavable signal peptide as determined using SignalP 4.1 (Petersen et al., 2011). Furthermore, the amino acid sequence encoded by SO_2973 shares significant sequence identity with multiple lysozyme-like enzymes annotated as SAR endolysins including SAR endolysins from two *Burkholderia* phages Bcep22I (identity= 51.4%, similarity = 65.5%) and BcepIL02 (identity = 49.7%, similarity = 65.0%) , as well as and KMV45 of *Pseudomonas*

aeruginosa phage ΦKMV (Briers et al., 2011) (identity = 25.8%, similarity = 37.1%). All amino acid sequence alignments were performed using EMBOSS Needle global alignment with BLOSUM62 scoring matrix (Rice et al., 2000).

Unlike with λSo, no genes are annotated as putative holins within either MuSo1 (SO_0641-0683) or MuSo2 (SO_2652-2704). However, bioinformatic analysis identified genes within the lysis operons of both MuSo prophages that encode for proteins with predicted transmembrane domains. Noteworthy among these is SO_2673 which lies in the vicinity of the gene for the putative cytoplasmic MuSo2 endolysin (*lys* – SO_2671) and codes for a protein with two predicted transmembrane domains and three positively charged residues at the C-terminus. These are common attributes used to identify and annotate putative holin genes (Wang et al., 2000). However, SO_2673 codes for an amino acid sequence 202 residues long, slightly larger than the classical cutoff (Wang et al., 2000) but not atypical for some holin families (Reddy and Saier, 2013). Another gene within the lysis operon, SO_2675, encodes a predicted inner-membrane protein containing a conserved domain with an unknown function (Fig 3.7).

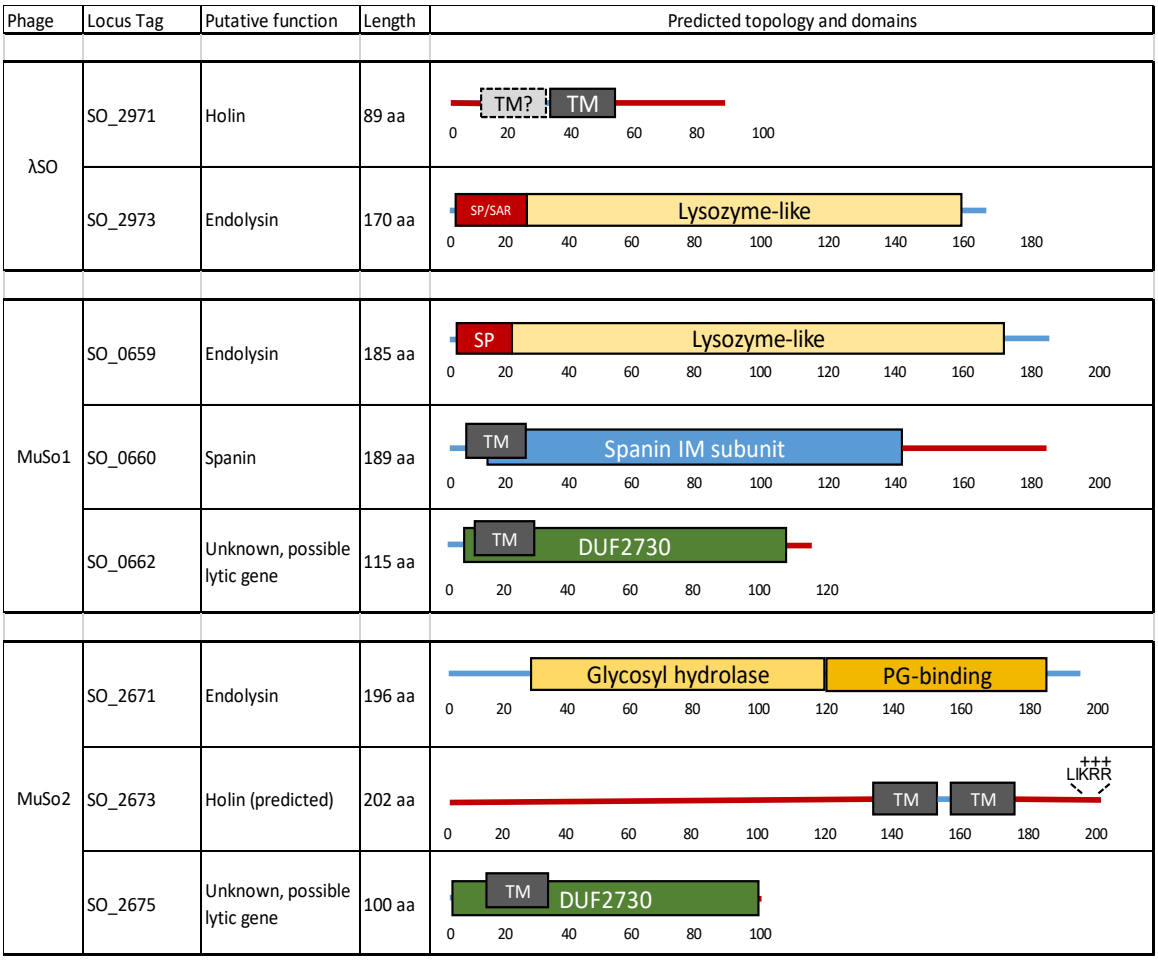

Fig 3.7 Annotated and predicted domains of putative prophage lysis proteins in MR-1. Predicted cytoplasmic-facing segments of amino acid sequence are in red, while periplasmic-facing or extracellular segments are in blue. TM = transmembrane domain, SP = signal peptide, SAR = signal anchor repeat domain, IM = inner-membrane, PG = peptidoglycan, DUF = domain of unknown function.

The MuSo1 gene SO_0659 encodes an endolysin with a topology similar to characterized SAR endolysins (Briers et al., 2011; Xu et al., 2004), but with a predicted cleavable signal peptide (Petersen et al., 2011). BLAST analysis for SO_0659 generated hits for several SAR endolysins, including the well characterized R^{21} (Park et al., 2007) (identity = 33.7%, similarity = 46.4%). No holin gene could be identified for MuSo1. However the locus SO_0660 and SO_0662 are within the putative lysis gene operon, and encode for predicted inner membrane proteins. SO_0660 is annotated as a possible spanin-like protein, while SO_0662 contains a domain of unknown function. BLAST analysis for SO_0662 generated no homologous sequences that have been previously characterized. It is possible that MuSo1 contains an endolysin but does not contain a

holin gene, suggesting that it may rely on the operons of other prophages for optimal lytic function, or that it responds to PMF loss in a holin-independent manner.

Considering that all three prophages in *S. oneidensis* MR-1 are active in lysis, and that they are predicted to be activated by collapse of proton motive force, it was hypothesized that lysis in *S. oneidensis* electron acceptor limited anaerobic cultures occurs as a direct result of bacteriophage activation, and that lytic bacteriophage release in *S. oneidensis* is dependent on PMF loss, allowing for robust temporal control of lysis in *S. oneidensis* strains engineered for biotechnology applications. Each prophage was deleted using the double homologous recombination method described in chapter 2 of this thesis. Single and double mutants, along with a phageless triple deletion mutant were constructed, removing a 50,125 bp region containing 97.2% of prophage λSo, a 35,782 bp region containing 100% of MuSo1, and a 34,857 bp region containing 90.2% of MuSo2. Deletions were confirmed by sequencing across the deletion junction, along with PCR using primers amplifying unique genes within each of the three prophages to ensure reintegration elsewhere in the genome did not occur. Despite predictions, a phageless mutant (JG3456) did not survive better under electron acceptor starvation than WT *S. oneidensis* (Fig 3.8). Therefore, it was concluded that phages are not a major contributor to lysis under electron acceptor starvation in *S. oneidensis* MR-1.

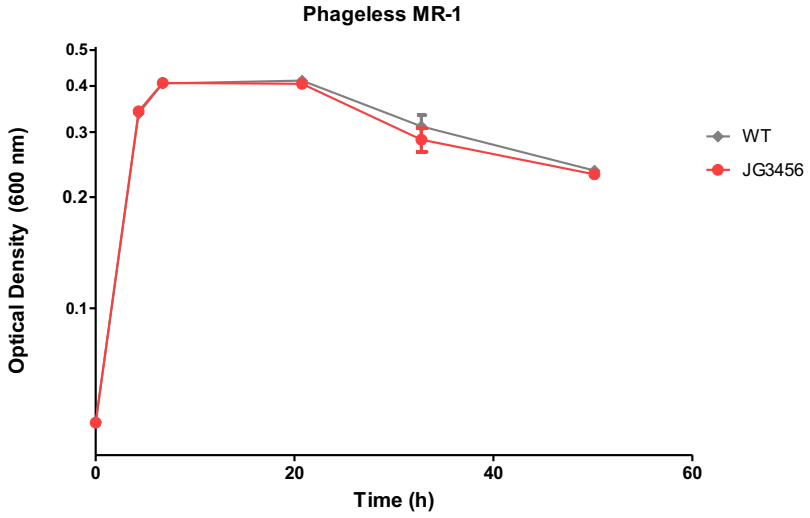

Fig 3.8 Growth/death of phage-cured *S. oneidensis*. Phage-less strain JG3456 (●), and WT (JG274; ■), were grown in SBM containing 10 mM HEPES, 0.05% casamino acids, 30 mM lactate and 40 mM fumarate. Symbols represent mean optical density at 600 nm, and error bars represent standard error means across three replicates.

Death phase Tn-seq: General results

To uncover potential genetic contributors to death and survival of *S. oneidensis* MR-1 under electron acceptor starvation, and to determine whether certain energy metabolism pathways are required for use of proteorhodopsin for survival, a transposon library was constructed in proteorhodopsin-expressing strain, JG3020. For JG3020::Tn library construction, approximately 97,000 colonies were collected from a high-efficiency mating between JG3020 and a donor strain bearing the MiniHimar transposon on a suicide vector, resulting in a library of 52,874 unique transposon mutants for the parent library in the light (t_{0L}) and 51,081 mutants in the dark (t_{0D}). Selection through ~2.2-2.3 generations of growth (Table 3.1) resulted in a loss of 1,368 unique insertions in the light grown population (t_{1L}), and 2,583 insertions in the dark grown population (t_{1D}). Further selection through stationary phase in the light (t_{2L}) eliminated 2,602 insertions, and death phase selection in the dark (t_{2D}), eliminated 2,555 insertions. Finally, regrowth in the light after fresh medium transfer (t_{3L}) eliminated 8,223 unique insertions, resulting in a final pool of 40,681 unique mutants that underwent selection while utilizing proteorhodopsin. Regrowth of t_{2D} in the dark after transfer into fresh medium (t_{3D}), eliminated 7,484 mutants, resulting in a final pool of 38,459 unique mutants that underwent selection without proteorhodopsin utilization (see Fig 3.9 for a visual depiction of library collection points at specific optical densities). Adding the number of population doublings between t_1 and peak density (estimated to be 0.55 for light-grown, and 0.48 for dark grown cultures), yields an estimated total of 6.079 doublings between t_{1L} and t_{3L}, and 6.209 doublings between t_{1D} and t_{3D}.

Table 3.1 Generations of growth and death/lysis per library in Tn-seq

	Doublings			Halvings	
Tn library	t_1/t_0	t_3/t_1	Total	CFU/mL	OD600
JG3020::Tn Light	2.181	6.079	8.259	2.124	-0.037
JG3020::Tn Dark	2.282	6.209	8.491	4.447	0.565

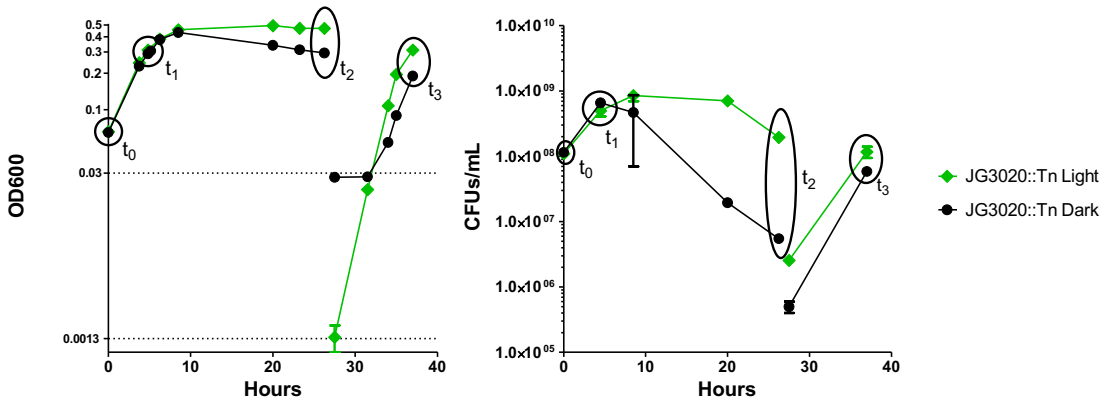

Fig 3.9 Death-phase Tn-seq. A JG3020::tn library was grown in SBM containing 10 mM HEPES, 0.05% casamino acids, 20 mM lactate and 40 mM fumarate under green light exposure (◆) and in the dark (●), allowed to undergo death/stationary phase, then transferred to fresh medium for recovery. Cell pellets were collected from the inoculum (t_0), at 0.31 OD_{600} (t_1), after stationary/death phase (t_2), and following growth in fresh medium (t_3). Symbols represent mean optical density at 600 nm, and error bars represent standard error means across three replicates.

A caveat noted in the interpretation of this data is the carryover of dead unlysed cells in t_{3D}. These cells are useful when assaying for strictly lysis, but are detrimental for analysis of viable cells, as they represent an estimated 15-16% of reads in outgrown dark cultures leading to a high level of inherent noise and possibly masking less prominent death phase fitness effects. Nonetheless, enrichment of many mutants was apparent in t_{3D} over t_{2D}. Generally, transposon mutants with <1000 reads in the parent library were not considered, unless related mutants with >1000 insertions and strong fitness benefits or defects were found. Consistent with results showing no effect of prophage deletion on survival during acceptor starvation, no deletions in genes predicted to code for prophage endolysins nor holins had appreciable effects on fitness in this assay.

Death phase Tn-seq: Shifts in central metabolism

One benefit to Tn-seq is the ability to determine the utilization of metabolic pathways under different growth conditions by measuring fitness defects from associated gene insertions. Surprising effects on central metabolism were able to be measured during death / electron acceptor starvation in this Tn-seq experiment, most notably those suggesting utilization of the Entner-Doudoroff pathway, pyruvate kinase PykA, and an oxaloacetate and glutamine consuming homoserine/threonine synthesis pathway as

reductive metabolic strategy (Fig 3.10 and Table 3.2). Furthermore, insertions in genes coding for TCA cycle enzymes largely yielded neutral effects in light and dark treatments (Table 3.3), suggesting the TCA cycle was not utilized in death / stationary phase. In all cases where significant defects were associated with central metabolism, they were present only in dark grown cultures, with one exception being insertions in *ppc* which also yields fitness defects under aerobic and anaerobic growth conditions (Brutinel and Gralnick, 2012b). This suggests that death-phase shifts in central metabolism are part of an energy-producing/conserving strategy, as they were unnecessary when proton motive force was supplemented.

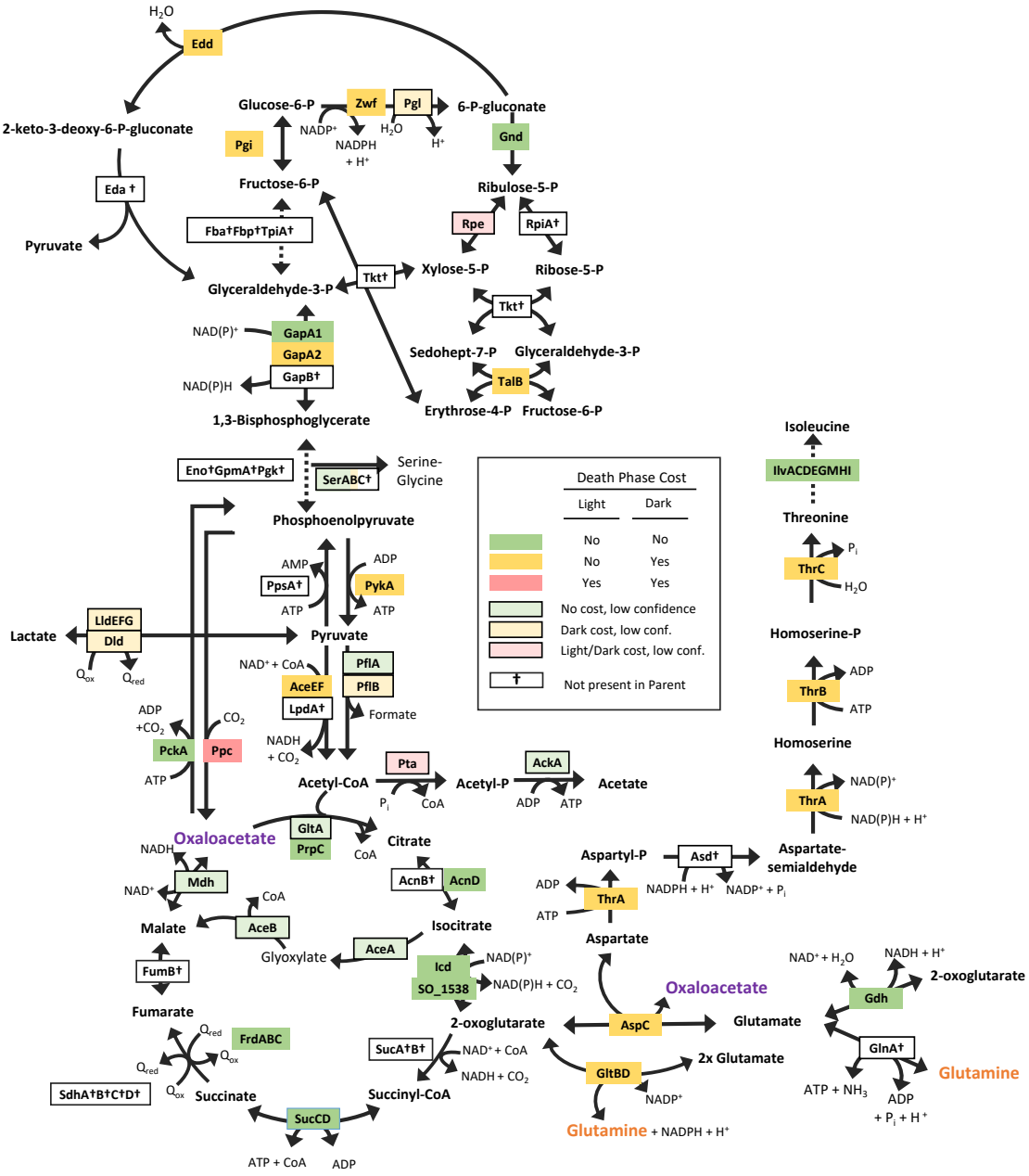

Fig 3.10 Transposon mutant fitness effects under respiratory stress / death phase in central metabolic pathways. Colors shown indicate whether transposon mutants exhibited fitness defects in a JG3020::tn library when incubated under light (proteorhodopsin driven pmf supplementation) and/or in the dark (no pmf supplementation). A thick bounding box around an enzyme name indicates <1000 read abundance mapping to insertions in corresponding gene in the parent JG3020::tn library and/or a high defect during growth in each condition, signifying relatively low confidence in death phase fitness determinations due to likely bottlenecking effects. Symbol † indicates no reads were found mapping to gene in parent library.

Table 3.2 JG3020::tn mutants in central metabolic pathways with negative death phase fitness (w_d)[a] and associated genes

Gene product	Locus	Parent	Light				Dark			
		Reads	Reads			w_d [a]	Reads			w_d [a]
		t_0	t_1	t_2	t_3		t_1	t_2	t_3	
glucose-6-phosphate isomerase Pgi	SO_3547	2708	760	172	92	2.142*	766	167	2	-3.628*
6-phosphogluconate dehydratase Edd	SO_2487	14081	15209	5578	12988	-0.459	14412	9024	2141	-2.846
6-phosphogluconolactonase Pgl	SO_2488	842	805	332	297	-1.179	754	416	26	-4.429
glucose-6-phosphate 1-dehydrogenase Zwf	SO_2489	13500	13820	5896	11508	-0.279	14426	9446	4031	-2.104
transaldolase B TalB	SO_3546	5606	2898	852	1192	1.451	2496	854	80	-1.791
glyceraldehyde-3-phosphate dehydrogenase (NAD+) GapA	SO_2345	1745	1650	722	1189	-0.169	1517	1088	108	-3.266
D-3-phosphoglycerate dehydrogenase SerA	SO_0862	985	339	120	183	3.479*	275	143	350	5.352*
phosphoserine phosphatase SerB	SO_1223	1143	508	119	163	1.700*	415	290	1	-4.724*
pyruvate kinase II PykA	SO_2491	14445	14537	5711	12888	-0.12	14753	8703	312	-5.65
L-lactate dehydrogenase complex protein LldG	SO_1518	1566	1130	447	354	-0.283*	1019	480	72	-2.140*
L-lactate dehydrogenase iron-sulfur cluster-binding protein LldF	SO_1519	2995	1959	644	447	-0.346*	2025	714	59	-3.569*
L-lactate dehydrogenase complex protein LldE	SO_1520	3217	1244	573	275	1.722*	1363	793	99	-0.416*
respiratory FAD-dependent D-lactate dehydrogenase Dld	SO_1521	11117	3236	819	170	0.791*	2628	861	0	< -5.70*
pyruvate formate-lyase PflB	SO_2912	17400	3089	856	146	2.627*	2557	879	1	-3.797*
pyruvate formate-lyase 1 activating enzyme PflA	SO_2913	3148	423	118	43	4.852*	371	152	1	-0.146*
pyruvate dehydrogenase E1 component AceE	SO_0424	18002	15529	6064	10260	0.075	15031	9259	4051	-1.188
dihydrolipoamide acetyltransferase AceF	SO_0425	6267	5751	2044	4084	-0.069	5690	3066	881	-2.316
acetate kinase AckA	SO_2915	2556	251	77	30	6.346*	244	141	0	1.286*
phosphate acetyltransferase Pta	SO_2916	6654	679	182	0	-0.362*	875	200	1	-1.814*
phosphoenolpyruvate carboxylase Ppc	SO_0274	9857	7222	2200	812	-1.823	6595	3260	416	-2.413
NADPH-dependent glutamate synthase small subunit GltD	SO_1324	3178	1898	605	376	-0.184	1754	762	28	-3.64
NADPH-dependent glutamate synthase large subunit GltB	SO_1325	14178	7755	2487	1689	0.306	7144	3187	180	-2.624
aspartate aminotransferase AspC	SO_2350	2006	1337	669	997	1.287	1324	897	114	-1.911
threonine synthase ThrC	SO_3413	4332	3550	998	1929	0.0004	3190	1211	234	-2.5717
homoserine kinase ThrB	SO_3414	1193	651	182	295	1.3728	745	446	86	-1.2706
bifunctional aspartokinase I / homoserine dehydrogenase I ThrA	SO_3415	15126	12472	4305	6965	0.0144	12740	6247	1834	-2.1264
Total sequence reads (millions)		**36.61**	**33.99**	**12.44**	**26.17**		**34.66**	**19.24**	**29.93**	

* low confidence in scores due to low read abundance, severe anaerobic growth defects, or a combination of both

[a] Calculated from equation: $w_d = log_2 \frac{(mutant\ reads/total\ reads)_{t_3}}{(mutant\ reads/total\ reads)_{t_1}} - log_2 \frac{(mutant\ reads/total\ reads)_{t_1}}{(mutant\ reads/total\ reads)_{t_0}} \times \frac{doublings^b{}_{t_3/t_1}}{doublings^b{}_{t_1/t_0}}$

[b] See Table 3.1

Table 3.3 JG3020::tn mutants in central metabolic pathways with positive, neutral, or near-neutral death phase fitness (w_d)[a]

Gene product	Locus	Parent	Light				Dark			
		Reads	Reads			w_d [a]	Reads			w_d [a]
		t_0	t_1	t_2	t_3		t_1	t_2	t_3	
phosphoenolpyruvate carboxykinase PckA	SO_0162	22494	20004	7444	14154	0.052	21613	12204	18834	-0.046
NAD dependent malate dehydrogenase Mdh	SO_0770	545	464	198	441	0.653*	437	295	467	0.959*
quinol:fumarate reductase menaquinol-oxidizing subunit FrdC	SO_0396	17717	19684	5831	13874	-0.849	19378	9648	13606	-0.866
quinol:fumarate reductase menaquinol-oxidizing subunit FrdC	SO_0397	6332	6605	2355	4982	-0.498	7428	3583	5737	-1.003
quinol:fumarate reductase FAD-binding subunit FrdA	SO_0398	10668	10253	3642	8011	-0.117	10755	5230	8475	-0.38
quinol:fumarate reductase FeS subunit FrdB	SO_0399	5151	4555	1685	3468	0.18	4508	2620	3255	0.05
succinyl-CoA synthase beta subunit SucC	SO_1932	2063	1678	655	1003	0.167	1373	994	1884	2.051
succinyl-CoA synthase alpha subunit SucD	SO_1933	5111	3283	1396	3070	1.762	3293	2007	6204	2.635
citrate synthase GltA	SO_1926	1259	1013	356	612	0.226	848	378	394	0.441
2-methylcitrate synthase PrpC	SO_0344	11671	11035	3812	8443	-0.082	11132	5783	9265	-0.083
2-methyl citrate dehydratase Fe-S dependent AcnD	SO_0343	5083	3642	1369	2842	1.062	3665	2007	2542	0.752
isocitrate dehydrogenase NADP-dependent Icd	SO_2629	7694	6389	2596	4591	0.35	6325	3923	7882	1.083
isocitrate dehydrogenase NAD-dependent	SO_1538	3730	3329	1256	2355	0.037	3528	1926	3510	0.207
glutamate dehydrogenase (NAD+) Gdh	SO_2593	34753	31727	13178	24367	0.065	31407	20500	25951	0.118
6-phosphogluconate dehydrogenase decarboxylating Gnd	SO_1902	9277	8936	3935	6545	-0.22	8935	5938	6100	-0.407
glyceraldehyde-3-phosphate dehydrogenase (NAD+) GapA	SO_0538	7421	6659	2137	5119	0.135	6869	3406	6626	0.247
malate synthase A AceB	SO_1483	9176	9919	2947	7702	-0.599	10093	5135	8215	-0.675
isocitrate lyase AceA	SO_1484	4923	5645	1919	4313	-0.86	5635	3079	4045	-1.012
Total sequence reads (millions)		**36.61**	**33.99**	**12.44**	**26.17**		**34.66**	**19.24**	**29.93**	

* Low confidence in score due to low parent library read abundance

[a] Calculated from equation: $w_d = log_2 \frac{(mutant\ reads/total\ reads)_{t_3}}{(mutant\ reads/total\ reads)_{t_1}} - log_2 \frac{(mutant\ reads/total\ reads)_{t_1}}{(mutant\ reads/total\ reads)_{t_0}} \times \frac{doublings^b{}_{t_3/t_1}}{doublings^b{}_{t_1/t_0}}$

[b] See Table 3.1

The finding that insertions in *pykA* (SO_2491) and *edd* (SO_2487) yield mutant fitness defects implies a heavy reliance on upper glycolysis reactions during death phase in *S. oneidensis.* However, the source of carbon entering glycolysis for surviving cells is unclear. Glycogen could serve as a carbon source, but mutants in potential glycogen degradation (*glgP*) and glycogen synthesis pathways did not appear to have death phase fitness defects (data not shown). Similarly, no N-acetylglucosamine degradation or utilization mutants had apparent fitness defects. Residual lactate, or a small amount generated through pyruvate fermentation (Pinchuk et al., 2011), could certainly serve as the carbon source for the small subset of cells that survive, but it would need to be respiration-linked to produce ATP through the PflAB-Pta-AckA route, or it would be net ATP-consuming to drive reductive L-homoserine synthesis via oxaloacetate. Lactate metabolism also cannot explain the apparent reliance on pyruvate kinase (PykA) for survival in dark-treated cultures. Despite indications towards alternative carbon sources, none were evident in this screen.

Death-phase Tn-seq: Formate dehydrogenase mutants survive

A large set of mutants identified by this screen to survive respiratory stress better than the aggregate pool are those containing insertions in genes coding for a set of two formate dehydrogenases, and associated proteins involved in their export and maturation (Table 3.4). These mutants were identified as better survivors by being enriched in dark-treated JG3020::tn libraries at t_3, while having relatively null or negative selection in light-treated JG3020::tn t_3 library. These include an operon occupying loci SO_4503-4515 which include two heterotrimeric formate dehydrogenases (FdhABC, SO_4509-11; Fnr-inducible FdhABC, SO_4513-15) along with predicted accessory proteins. Transposon insertions in another formate dehydrogenase operon in the *S. oneidensis* genome, coding for a nitrate-inducible trimeric protein, FdnGHI (SO_0101-03), were not enriched for survival in this screen, likely because nitrate was not directly provided in the growth medium. The most likely explanation for enrichment of mutants defective in formate dehydrogenase function under conditions of respiratory starvation, is that formate dehydrogenase mutants of *S. oneidensis* are able to utilize pyruvate in the absence of an electron acceptor (Kane et al., 2016).

Table 3.4 Death phase fitness (w_d)[a] for formate dehydrogenase and related genes in JG3020::tn library

Gene annotation	Locus	Parent	Light treatment				Dark treatment			
		Reads	Reads			w_d[a]	Reads			w_d[a]
		t_0	t_1	t_2	t_3		t_1	t_2	t_3	
formate dehydrogenase assembly/maturation protein	SO_4503	4428	3097	1010	1209	0.16	3466	1608	9908	2.47
formate dehydrogenase associated protein of unknown function DUF3505	SO_4504	14602	13303	4716	8882	-0.13	13994	9372	170597	3.77
formate dehydrogenase associated protein of unknown function DUF3506	SO_4505	13780	11925	4041	7213	-0.06	11181	7700	166769	4.72
iron-sulfur cluster-binding protein	SO_4506	15818	12630	4173	6454	0.02	12431	9217	303040	5.55
formate dehydrogenase chaperone FdhT	SO_4507	6736	5273	1806	2985	0.24	5132	3320	125435	5.67
formate dehydrogenase accessory protein FdhX	SO_4508	4448	3573	1493	2595	0.50	3709	2657	18296	3.01
formate dehydrogenase molybdopterin-binding subunit FdhA	SO_4509	29320	30337	9545	26505	-0.25	31167	16351	160315	2.12
formate dehydrogenase FeS subunit FdhB	SO_4510	3973	4153	1190	3146	-0.50	3893	2390	18029	2.29
formate dehydrogenase cytochrome b subunit FdhC	SO_4511	17087	15850	4944	3834	-1.67	16098	7067	893	-3.94
Fnr-inducible formate dehydrogenase accessory protein FdhX	SO_4512	7912	6717	2286	4008	-0.01	6647	3921	10364	1.32
Fnr-inducilble formate dehydrogenase molybdopterin-binding subunit FdhA	SO_4513	24785	23471	8281	14837	-0.36	24565	15170	39268	0.71
Fnr-inducible formate dehydrogenase FeS subunit FdhB	SO_4514	8227	5847	2132	4106	0.94	5871	4057	11272	2.26
Fnr-inducible formate dehydrogenase cytochrome b subunit FdhC	SO_4515	13190	11634	3439	3740	-1.05	11540	5064	1782	-2.17
twin arginine protein translocase system protein TatA	SO_4202	1163	867	365	668	0.88	760	812	7601	4.99
twin arginine protein translocase system protein TatB	SO_4203	242	128	36	84	2.03	125	112	1316	5.99
twin arginine protein translocase system protein TatC	SO_4204	2875	1726	815	1103	1.48	1821	1510	16644	4.98
nitrate-inducible formate dehydrogenase molybdopterin-binding subunit FdnG	SO_0101	42212	44953	15939	32465	-0.64	46464	24935	34838	-0.80
nitrate-inducible formate dehydrogenase iron-sulfur subunit FdnH	SO_0102	5488	6367	2040	5503	-0.73	7034	3077	6418	-1.11
nitrate-inducible formate dehydrogenase cytochrome b subunit FdnI	SO_0103	4582	4174	1621	3312	0.12	4037	2393	3633	0.34
nitrate-inducible formate dehydrogenase chaperone FdhE	SO_0104	11396	12282	3439	10070	-0.51	11730	5150	11116	-0.19
Total sequence reads (millions)		**36.6**	**34.0**	**12.4**	**26.2**		**34.7**	**19.2**	**29.9**	

[a] Calculated from equation: $w_d = log_2 \frac{(mutant\ reads/total\ reads)_{t_3}}{(mutant\ reads/total\ reads)_{t_1}} - log_2 \frac{(mutant\ reads/total\ reads)_{t_1}}{(mutant\ reads/total\ reads)_{t_0}} \times \frac{doublings^b{}_{t_3/t_1}}{doublings^b{}_{t_1/t_0}}$

[b] See Table 3.1

Mutants containing insertions in genes coding for the twin-arginine translocation system, *tatABC* (SO_4203-04), were among the most highly enriched in dark-treated cultures, with near-null selection (a very slight apparent enrichment), in light-treated JG3020::tn. The phenotype exhibited by these mutants is also very likely due to expected effects of *tatABC* knockout on formate dehydrogenase activity, as both FdhA subunits (SO_4509 and SO_4513) are predicted to by translocated through the inner membrane by TatABC. To test this hypothesis, a Δ*tatABC* mutant was created. This mutant exhibits a growth phenotype very similar to a formate dehydrogenase gene deletion mutant (ΔSO_4509-11 ΔSO_4513-15 ΔSO_0101-03, here referred to as Δ*fdh*^{3}), with characteristic growth inhibition by formate supplementation in the medium (Fig 3.11A), along with an ability to ferment pyruvate at rates higher than WT (Fig 3.11B).

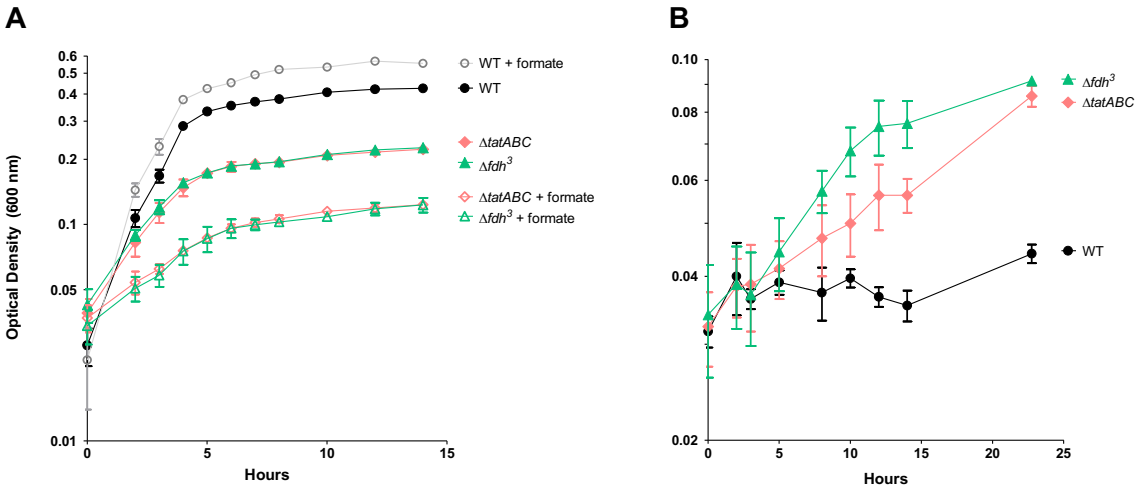

Fig 3.11 Δ*tatABC* and formate dehydrogenase knockout comparisons. WT strain JG274 (●), Δ*tatABC* (■), and Δ*fdh*^{3} (▲) were grown in SBM containing 10 mM HEPES, 0.05% casamino acids, with (A) 20 mM lactate, 60 mM fumarate, and either 20 mM NaCl (closed symbols) or 20 mM sodium formate (open symbols); or (B) 20 mM sodium pyruvate only. Symbols represent mean optical density at 600 nm, and error bars represent standard error means across three replicates.

To test death-phase fitness results derived from Tn-seq, a Δ*tatABC* strain, along with two formate dehydrogenase deletion mutants, strain Δ*fdh*^{2}, with two homologous *fdhABC* clusters (SO_4509-11 and SO_4513-15) deleted, and strain Δ*fdh*^{3} were competed against a *gfpmut3**-expressing strain of *S. oneidensis* (described in Chapter 2 of this thesis and referred to as MR-1+*gfp*). Briefly, cultures inoculated with a 50:50 mix of test mutant and MR-1+*gfp* were taken through a round of growth and death, followed by a secondary round of growth. Competition cultures containing Δ*tatABC,* Δ*fdh*^{2} or

Δ*fdh*^{3} strain all recovered more quickly than cultures containing 50:50 WT JG274 and MR-1+*gfp,* or MR-1+*gfp* alone (data not shown). Flow cytometry was used to determine mutant and MR-1+*gfp* abundance at inoculation (t_0), following ~3.5 generations of growth (t_1), and following death and ~5.6 generations of regrowth in fresh medium (t_3). Flow cytometry readings were taken following death and prior to inoculation in fresh medium, however they were not useful for analysis due to lost GFP fluorescence in acceptor starved cultures. For every timepoint, GFP fluorescence in MR-1+*gfp* pure cultures was measured, and used to correct competition measurements for small percentage (<5%) of MR-1+*gfp* cells without GFP signal.

While Δ*tatABC,* Δ*fdh*^{2} or Δ*fdh*^{3} mutants were selected against during growth (see columns A and B in table 3.5), they were enriched during death phase. By subtracting the effects of growth per doubling (as determined by $\log_2$(%mutant abundance in t1 / % mutant abundance in t0 / # generations in t_0 to t_1), and scaling for the number of doublings in the final regrowth (multiplying by # generations of growth between t_1 and t_3), it was determined that Δ*tatABC,* Δ*fdh*^{2} and Δ*fdh*^{3} strains were significantly enriched (Table 3.5). As a control, JG274 was enriched against MR-1+*gfp* during growth phase (as expected due to the fitness cost associated with GFP-production) but was not found to be enriched during death phase after controlling for the effects of growth on fitness.

Table 3.5 Death phase fitness of gene deletions resulting in formate dehydrogenase activity knockout

	% makeup of strain vs MR-1+*gfp*			log2 ratios		Growth doublings		Death phase fitness (log2)		
	A	B	C	D	E	F	G	H	I	J
genotype	t0	t1	t3	log2(B/A)	log2(C/B)	t1/t0	t3/t1	E-(D/F×G)	Mean (H)	SEM (H)
JG274	46.2%	50.9%	61.1%	0.140	0.263	3.29	8.505	-0.099	-0.024	0.048
	-	52.4%	68.7%	0.180	0.392	3.55	8.512	-0.039		
	-	50.6%	67.2%	0.131	0.409	3.23	8.494	0.065		
Δ*tatABC*	48.7%	32.6%	57.9%	-0.579	0.829	3.59	5.537	1.724	1.350	0.285
	-	34.7%	33.1%	-0.491	-0.065	3.59	6.249	0.791		
	-	34.6%	55.1%	-0.495	0.671	3.58	5.792	1.536		
Δ*fdh3*	50.5%	31.1%	47.0%	-0.698	0.593	3.29	5.781	1.818	1.792	0.026
	-	30.7%	41.5%	-0.717	0.435	3.29	6.113	1.767		
	-	-	48.2%	-	-	-	-	-		
Δ*fdh2*	49.9%	29.7%	29.8%	-0.749	0.005	3.29	5.573	1.273	1.916	0.321
	-	28.3%	48.5%	-0.819	0.777	3.29	5.825	2.226		
	-	29.8%	59.0%	-0.745	0.984	3.61	6.134	2.248		

[a] A positive/negative $\log_2$ ratio indicates positive/negative selection for/against strain, while 0 indicates equal fitness with competitor.

Death-phase fitness benefits for Δ*tatABC* and formate dehydrogenase mutants were statistically less pronounced in this assay than in Tn-seq. Assuming pyruvate fermentation is the primary mechanism for survival of these mutants, the discrepancy in results from these two types of assays is unsurprising. In Tn-seq, the fraction of mutants with enhanced pyruvate fermentation phenotypes is miniscule compared to that in direct competition assays. It would thus be expected that pyruvate released from lysed cells could sustain the entire Fdh-knockout mutant population. However, in head-to-head competition, with a percentage of pyruvate-fermentation-capable mutants near 30-35% of the total population at the beginning of death phase, pyruvate sourced from lysed cells is likely not enough to sustain the mutants. The fact that any measurable fitness benefit is seen in direct competition experiments suggests that pyruvate is metabolically generated in surviving cells of dying acceptor-starved cultures and is better utilized in Fdh-knockout mutants.

Among other survival-enriched mutants potentially related to formate dehydrogenase function, were those with insertions in genes coding for molybdenum and tungsten cofactor biosynthesis proteins (Table 3.6). The α-subunits of the three formate dehydrogenases in *S. oneidensis,* encoded by genes *fdhA1* (SO_0409), *fdhA2* (SO_0413) and *fdnG* (SO_0103) are all annotated as requiring molybdenum cofactors. Insertions in two homologous molybdenum uptake system gene clusters (*modABC*; SO_3372-74 and SO_2948-50), and one molybdenum cofactor biosynthesis protein (MogA; SO_0062) did not yield a positive fitness for acceptor starvation, but every mutant with insertions in genes annotated as belonging to molybdopterin/tungstopterin cofactor biosynthesis or tungstate uptake pathways resulted in a positive effect on fitness. These results suggest that tungsten may be the primary metal cofactor in one or both *S. oneidensis* formate dehydrogenase α-subunits coded by *fdhA* genes. Whether the nitrate-inducible formate dehydrogenase α-subunit FdnG uses tungsten as a cofactor cannot be inferred by this Tn-seq experiment, since no nitrate was supplied in the medium and thus they were not expressed.

Table 3.6 Death phase fitness (w_d)[a] for molybdenum/tungsten uptake and cofactor biosynthesis in JG3020::tn library

Gene product	Locus	Parent	Light treatment				Dark treatment			
		Reads	Reads			w_d[a]	Reads			w_d[a]
		t_0	t_1	t_2	t_3		t_1	t_2	t_3	
tungstate-responsive two component signal transduction system histidine kinase	SO_4717	23778	20592	6965	15225	0.22	21076	13215	157708	3.37
tungstate-responsive two component signal transduction system response regulator	SO_4718	5900	4728	1541	3575	0.57	4859	2810	22555	2.97
ABC-type tungstate uptake system substrate-binding component TupA	SO_4719	6979	5314	2042	3507	0.58	5618	3323	27306	3.13
ABC-type tungstate uptake system permease component TupB	SO_4720	8306	6096	2120	4702	0.95	6484	3557	30742	3.21
ABC-type tungstate uptake system ATPase componet TupC	SO_4721	423	203	63	313	3.66	203	159	1737	5.97
tungstopterin-guanine dinucleotide biosynthesis protein A MobA	SO_4722	5840	4552	1103	2036	-0.08	4551	2131	33810	3.87
bifunctional tungstopterin-guanine dinucleotide biosynthesis protein MobB/MoeA	SO_4723	13841	11060	3702	4517	-0.31	10902	6302	87496	3.94
tungsten cofactor biosynthesis protein MoaA	SO_4724	8690	7582	2563	5777	0.24	8054	4388	9007	0.46
molybdopterin/tungstopterin synthase sulfurylase MoeB	SO_0137	7146	5473	1454	2056	-0.26	5442	2513	40458	3.96
molybdenum cofactor biosynthesis protein MoeA	SO_0138	8918	6964	2298	4605	0.48	6577	4239	34359	3.58
molybdenum cofactor biosynthesis protein MogA	SO_0065	8180	6523	2224	2627	-0.32	6338	3311	3138	-0.02
molydopterin cofactor biosynthesis protein	SO_4502	16602	13589	4543	7265	-0.02	13777	7072	3684	-1.17
transcriptional repressor of molybdate and molybdenium cofactor metabolism ModE	SO_3862	7140	6879	2504	6303	0.10	7521	3826	5804	-0.58
ABC-type molybdate uptake system substrate-binding component ModA	SO_3863	2446	2111	786	1889	0.51	2355	1436	1554	-0.45
ABC-type molybdate uptake system permease component ModB	SO_3864	1616	1259	380	1170	0.98	1289	721	1065	0.61
ABC-type molybdate uptake system ATPase component ModC	SO_3865	11303	9133	3738	6370	0.42	9783	6110	7619	0.20
ABC-type molybdate uptake system ATPase component ModC	SO_4446	7877	7294	2663	5896	0.08	7915	3927	6254	-0.36
ABC-type molybdate uptake system permease component ModB	SO_4447	1569	1369	497	1160	0.39	1403	707	1512	0.54
ABC-type molybdate uptake system substrate-binding component ModA	SO_4448	5681	4966	1813	3377	0.06	4635	3189	3762	0.49
molybdenum cofactor biosynthesis protein E MoaE	SO_4449	27	20	9	0	N/A	0	0	160	N/A
molybdenum cofactor biosynthesis protein D MoaD	SO_4450	1440	1250	478	439	-0.86	1130	673	8262	3.82
molybdenum cofactor biosynthesis protein C MoaC	SO_4451	4237	2681	1199	1146	0.69	2669	2204	26578	5.13
molybdenum cofactor biosynthesis protein A MoaA	SO_4452	11303	9916	3151	6079	-0.10	10014	5207	44521	2.62
Total sequence reads (millions)		**36.6**	**34.0**	**12.4**	**26.2**		**34.7**	**19.2**	**29.9**	

[a] Calculated from equation: $w_d = log_2 \frac{(mutant\ reads/total\ reads)_{t_3}}{(mutant\ reads/total\ reads)_{t_1}} - log_2 \frac{(mutant\ reads/total\ reads)_{t_1}}{(mutant\ reads/total\ reads)_{t_0}} \times \frac{doublings^{b}{}_{t_3/t_1}}{doublings^{b}{}_{t_1/t_0}}$

[b] See Table 3.1

Periplasmic formate dehydrogenases in other bacteria that have been shown to use tungsten as a cofactor, including those found in *Moorella thermoacetica* (Andreesen and Ljungdahl, 1973)*, Desulfovibrio gigas* (Moura et al., 2004; Raaijmakers et al., 2002, 2001), *Eubacterium adiminophilum* (Graentzdoerffer et al., 2003)*, Methylobacterium extorquens* (Laukel et al., 2003)*,* and *Campylobacterium jejuni,* all lack a third heme-containing gamma-subunit and appear to be within a distinct αβ class of formate dehydrogenases (Niks and Hille, 2019). It would thus be unexpected for the two FdhA proteins in *S. oneidensis* – which appear to most closely resemble the Mo-containing FDH-O from *E. coli* (Kane et al., 2016) – to use tungsten as their cofactor. However, it is peculiar that insertions in *tupABC,* which is highly selective for tungsten in other organisms (Andreesen & Makdessi, 2008), leads to fitness benefits during death phase in Tn-seq, and the magnitudes of these effects are very similar to those yielded by formate dehydrogenase and *tatABC* knockout transposon mutants. Although, this is highly suggestive that tungstate is a cofactor for FdhA proteins, molybdenum as a cofactor cannot entirely be ruled out from this data. Since two molybdate uptake gene clusters exist in the genome, single transposon mutant knockouts are likely to be compensated for by an intact homologous cluster. However, in his dissertation work, Davies (2017) found that formate dehydrogenase activity in whole *S. oneidensis* cell extracts was highest when medium was supplemented with tungstate rather than molybdate. Furthermore, *fdhA1* (SO_4509) and *fdhA2* (SO_4513) were upregulated under both tungstate and molybdate supplementation, but *fdhA2* (SO_4513) was most highly upregulated under tungstate supplementation. Interestingly, *fdnG* was upregulated only when neither tungstate nor molybdate were supplemented. Finally, using inductively coupled plasma mass spectrometry (ICP-MS), Davies (2017) found that purified FdhA2 contained tungsten, not molybdenum as a cofactor. Attempts to purify FdhA2 with molybdate supplementation were not fruitful. Although FdhA1 was not chosen for purification and ICP-MS analysis due to a lower effect of tungstate supplementation on *fdhA1* expression induction compared to *fdhA2*, Tn-seq results and the findings by Davies (2017) suggest it too contains a tungsten cofactor. Future experiments testing the differential effects of deletions in the multiple annotated molybdenum and tungsten cofactor biosynthesis gene clusters may have potential to unveil the specific reactions these pathways catalyze. In

particular, the cluster *moaE/D/C/A* (SO_4449-52), annotated as belonging to a putative molybdenum biosynthesis pathway, may instead play a role in tungsten cofactor biosynthesis, since the effect of transposon insertions in these genes points to formate dehydrogenase activity knockout.

Death phase Tn-seq: Cell envelope integrity defects exacerbate death under respiratory stress

Among transposon insertions having the highest deleterious effect on death phase survival in dark grown libraries were those related to outer membrane (OM) phospholipid and lipopolysaccharide maintenance. Transposon insertions in the operon *mlaB-mlaC-mlaD-mlaE-mlaF,* along with those in the related gene *mlaA* elsewhere in the genome, generally resulted in strong death phase fitness defects in this screen (Table 3.7). The *mlaABCDEF* genes encode for an ABC-type transport system with components present in the outer membrane, periplasm, and inner-membrane. Initial genetic experiments in *E. coli* suggested an ATP-dependent mechanism in which the OM lipoprotein MlaA removes phospholipids from the OM outer leaftlet and traffics them to the inner membrane MlaBDEF complex through the periplasmic MlaC (Malinverni and Silhavy, 2009). How the periplasmic-facing MlaA is able to access outer leaflet phospholipids was initially unclear, but associations between MlaA and an OM porins OmpC/F(Chong et al., 2015) suggested these formed a channel for MlaA. Further structural work showed that the α-helical MlaA itself forms a channel that spans the inner leaflet, but not the outer leaflet, and through which phospholipids may travel in a proposed retrograde fashion to MlaC (Abellón-Ruiz et al., 2017). Contrary to the model in which MlaC directs OM phospholipids from MlaA to the IM via MlaBDEF, recent experiments have shown a strongly unidirectional ATP-independent trafficking of phospholipid from MlaD to MlaC (Hughes et al., 2019), calling into question the dominant directional flow of phospholipids in the Mla system. Altogether, the mechanisms driving outer membrane symmetry maintenance by the Mla system, the role of the MlaF ATPase, and the destination of MlaC-bound phospholipids from either membrane remain unclear.

Table 3.7 Death phase fitness (w_d)[a] for outer membrane phospholipid maintenance and lipopolysaccharide biosynthesis pathway, and cell envelope stress response regulation mutants

		JG3020::tn Parent	JG3020::tn Light				JG3020::tn Dark			
Gene product	Locus	Reads	Reads			w_d [a]	Reads			w_d [a]
		t_0	t_1	t_2	t_3		t_1	t_2	t_3	
phospholipid transport-associated protein MlaA	SO_3197	18492	8868	3643	4231	1.903	8508	5241	0	<-10.01
ABC-type phospholipid uptake (salvage) system anti-anti-sigma factor MlaB	SO_3950	2500	2882	1204	2069	-0.950	2714	1863	1763	-0.949
ABC-type phospholipid uptake (salvage) system periplasmic chaperone MlaC	SO_3951	2025	1132	315	479	1.128	1082	470	1	-7.623
ABC-type phospholipid uptake (salvage) system substrate-binding component MlaD	SO_3952	11917	6310	2748	3770	1.839	6489	4002	985	-0.338
ABC-type phospholipid uptake (salvage) system permease component MlaE	SO_3953	3714	1573	540	486	1.764	1226	726	1	-5.913
ABC-type phospholipid uptake (salvage) system ATPase component MlaF	SO_3954	8105	3999	1377	2368	2.103	3637	2099	0	<-8.687
ADP-heptose-LPS heptosyltransferase WaaC	SO_4678	14264	8884	2744	5361	1.216	8412	1562	18	-6.799
bifunctional heptose 7-phosphate kinase/heptose 1-phosphate adenyltransferase RfaE	SO_3745	9329	6954	1990	4344	0.561	6300	1286	137	-3.986
lipid A biosynthesis lauroyl acyltransferase LpxL	SO_3746	4225	1592	503	309	1.552	1546	737	5	-4.330
KDO 2-(lauroyl)-lipid IVA acyltransferase LpxM	SO_2088	4346	2239	1090	1000	1.527	2397	1406	70	-2.766
membrane anchored FtsH modulator component 1 HflK	SO_0605	4195	3151	1107	1677	0.300	2697	1623	0	<-9.667
membrane anchored FtsH modulator component 2 HflC	SO_0606	8651	6769	2505	3455	0.079	6971	3667	28	-7.116
RNA polymerase sigma factor 24 RpoE	SO_1342	1350	1799	427	0	<-11.84	1721	904	137	-4.608
sigma-E factor negative regulatory protein RseA	SO_1343	1459	1447	509	350	-1.929	1334	975	1865	0.831
RseA degrading zinc metalloprotease RseP	SO_1636	7094	8673	1049	60	-7.878	8034	1766	242	-5.545
serine protease DegS	SO_3943	9777	9470	2757	537	-3.929	9237	5209	7537	-0.074
Total sequence reads (millions)		**36.61**	**33.99**	**12.44**	**26.17**		**34.66**	**19.24**	**29.93**	

[a] Calculated from equation: $w_d = log_2 \frac{(mutant\ reads/total\ reads)_{t_3}}{(mutant\ reads/total\ reads)_{t_1}} - log_2 \frac{(mutant\ reads/total\ reads)_{t_1}}{(mutant\ reads/total\ reads)_{t_0}} \times \frac{doublings^{b}{}_{t_3/t_1}}{doublings^{b}{}_{t_1/t_0}}$

[b] See Table 3.1

Irrespective of the underlying mechanisms, disruptions *mlaABCDEF* or homologous genes have been shown in multiple Gram-negative bacteria to promote accumulation of phospholipids in the outer leaflet, manifesting in sensitivity to EDTA/SDS and certain antibiotic treatments (Abellón-Ruiz et al., 2017; Chong et al., 2015; Malinverni and Silhavy, 2009), along with hypervesiculation (Baarda et al., 2019; Davies et al., 2019; Roier et al., 2016).

To test fitness defects observed in death-phase Tn-seq for *mlaABCDEF* mutants, gene deletion mutants Δ*mlaA* (ΔSO_3197) and Δ*mlaC* (ΔSO_3951) were constructed and their growth, death and fitness phenotypes observed. Compared to WT, Δ*mlaA* and Δ*mlaC* mutants did not have apparent differences in growth rate, but exhibited a quicker initial rate of turbidity loss upon entry intro death phase, with a slightly higher final density (Fig 3.12A). A more rapid, but not altogether greater, loss in viability was also observed for Δ*mlaA/C* mutants during death phase (Fig 3.12B). The recovery in viable cells between 30 and 40 hours in pure *mlaA/C* cultures is similar to that seen previously (Fig 3.4B), and suggests the surviving population is able to respond to membrane stress.

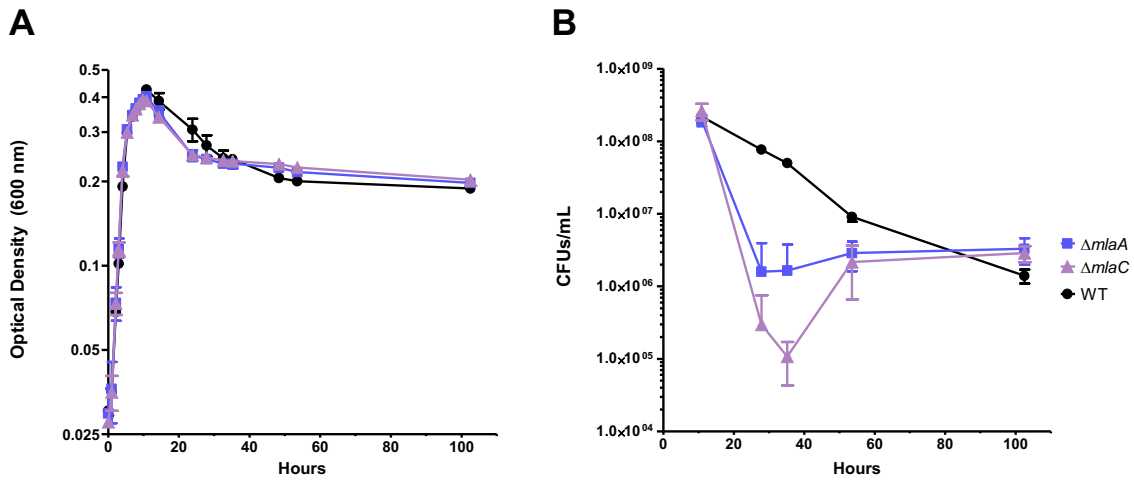

Fig 3.12 Mla system gene deletion mutant growth and death phenotypes. Wild type (●), Δ*mlaA* (■), and Δ*mlaC* (▲) *S. oneidensis* strains were grown in SBM with 20 mM lactate and 40 mM fumarate and assayed for optical density at 600 nm (A) and colony forming units (CFU)(B). Symbols represent mean, and error bars represent standard error means across three replicates.

Competition assays intended to mimic Tn-seq in which Δ*mlaA* or Δ*mlaC* were grown with MR-1+*gfp* at a 50:50 ratio, allowed undergo death phase for approximately 16 hours, then transferred to fresh medium for a recovery, showed a significant fitness

defect for both Δ*mlaA/C* strains (Table 3.8). Considering that 16 hours of death phase results in approximately 2 orders of magnitude loss in viability of Δ*mlaA/C* strains compared to WT (Fig 3.12B), these fitness defects are unsurprising. Altogether, these results point to accelerated death with lysis during respiratory stress in *mla* mutants, but suggest that long term viability following death phase may be no worse than WT while in pure culture.

Table 3.8 Death phase fitness of Mla system gene deletion mutants

	% makeup of strain vs MR-1+*gfp*			Log_2 ratios		Growth doublings		Death phase fitness (Log_2)		
	A	B	C	D	E	F	G	H	I	J
Genotype	t0	t1	t3	Log_2(B/A)	Log_2(C/B)	t1/t0	t3/t1	E - (D/F×G)	Mean (H)	SEM (H)
	47.3%	53.1%	63.8%	0.167	0.266	3.17	7.031	-0.105		
JG274	49.6%	53.3%	54.0%	0.175	0.018	2.77	5.868	-0.352	-0.327	0.121
	50.1%	54.7%	48.3%	0.211	-0.179	3.33	5.423	-0.523		
	61.1%	56.7%	1.5%	-0.108	-5.210	3.21	6.441	-4.993		
Δ*mlaA*	59.2%	55.3%	1.2%	-0.144	-5.556	3.10	6.595	-5.251	-5.407	0.295
	63.8%	56.4%	0.8%	-0.114	-6.205	3.10	6.174	-5.978		
	63.1%	59.0%	1.5%	-0.097	-5.340	3.09	5.659	-5.162		
Δ*mlaC*	64.2%	58.2%	0.7%	-0.118	-6.406	3.02	5.222	-6.202	-6.676	1.038
	63.9%	58.0%	0.1%	-0.123	-8.901	3.19	6.147	-8.663		

Apart from the Mla system, other transposon mutants with gene disruptions known to cause outer membrane instability displayed high fitness defects. Insertions in the gene encoding an ADP-heptose-LPS heptosyltransferase, *waaC,* and a related gene *rfaE*, encoding a heptose-7-phosphate kinase/heptose-1-phosphate adenyltransferase, yielded death-phase fitness defects in dark drown cultures (Table 3.7). The proteins encoded by these genes are highly conserved across Gram-negative bacteria and perform key roles in LPS inner core biosynthesis. RfaE performs an ATP-driven intermediate step in the synthesis of ADP-L-glycero-β-D-manno-heptose, originating from sedoheptulose-7-P (Valvano et al., 2000). WaaC catalyzes the transfer of ADP-L-glycero-β-D-manno-heptose to 3-deoxy-D-manno-oct-2-ulopyranosonic acid (Kdo_2)-LipidA, the first heptose addition to the inner core oligosaccharide (Grizot et al., 2006; Klein and Raina, 2019). Disruptions in these genes in *E. coli* results in typically viable cells displaying a "deep-rough" phenotype with LPS lacking o-specific polysaccharide and characterized by hypersensitivity to hydrophobic antibiotics, detergents and bile salts (Grizot et al., 2006;

Klein and Raina, 2019; Rietschel et al., 1994; Tamaki et al., 1971; Valvano et al., 2000). Other genes related to lipid A biosynthesis, *lpxL* and *lpxM,* encoding enzymes involved in the final two steps of Kdo_2-lipid A biosynthesis (Trent, 2009), were also found to yield fitness defects when disrupted in the dark-grown transposon library. Insertions in genes for FtsH regulator components HflK and HflC produced strong fitness defects in the dark library, likely due to the role of FtsH in regulating LPS biosynthesis components LpxC and KdtA (Katz and Ron, 2008), which are present on the MR-1 genome, but did not have representative transposon mutants in JG3020::tn parent libraries. It may be interesting to note that transposon insertions in both the Mla pathway and Lipid-A core oligosaccharide biosynthesis pathways yield mild apparent fitness benefits in the JG3020 library when utilizing proteorhodopsin under light. In *E. coli*, a Δ*waaC* deletion mutant has a constitutively activated sigma E cell envelope stress response (Klein et al., 2009), while a specific gain of function mutation in *mlaA* has also been noted to induce sigma E (Sutterlin et al., 2016). In light-grown libraries, mutants with the strongest quantifiable defects during stationary phase were those with insertions in *rseP,* encoding a cytoplasmic site-specific protease necessary for degradation of the inner-membrane-spanning anti-sigma E factor RseA. Insertions in the gene for DegS the serine protease that responds to unfolded outer membrane porins and cleaves a periplasmic residue of RseA, activating it for RseP-catalyzed degradation (Li et al., 2009; Sohn et al., 2007; Walsh et al., 2003), also had fitness defects in light-grown libraries but surprisingly not dark-grown cultures. This suggests that cell envelope stress occurs in *S. oneidensis* anaerobic cultures entering stationary phase even with proteorhodopsin utilization, but that PMF supplementation may allow cells to successfully mount a sigma-E-driven envelope stress response while a lack of both electron acceptor and PMF supplementation makes a response unachievable. Gene deletions that cause minor LPS-synthesis or membrane stability defects, may potentially prime light-grown cultures to respond to membrane stress upon entry into stationary phase by prematurely activating the sigma E stress response.

Another set of genes related to cell envelope integrity with fitness defects in corresponding transposon mutants are those coding for penicillin-binding protein 1A (*mrcA)* and its activator LpoA, Braun's lipoprotein Lpp, and genes in the *ybgC-tolQ-tolR-*

tolA-tolB-ybgF operon. Insertions in these genes caused defects in both light- and dark-grown cultures, with more severe effects in the dark (Table 3.9). In *Vibrio cholerae,* deletions in *mrcA* and *lpoA* have been shown to result in increased susceptibility to cell-wall-synthesis-targeting antibiotics and bile salts, along with spherical cell shapes and a competitive disadvantage in stationary phase owing to accumulation of D-amino acids (Dörr et al., 2014). Interestingly, insertions in genes analogous to *mrcA and lpoA, mrcB and lpoB,* did not yield strong death phase fitness defects in dark-grown cultures, which suggest that like *V. cholerae* (Dörr et al., 2014), but unlike *E. coli* (Yousif et al., 1985), the proteins encoded by these genes do not appear to perform overlapping roles in *S. oneidensis*.

The Tol-Pal system is highly-conserved among Gram-negative bacteria and is a multiunit complex spanning the cell envelope, consisting of the IM proton channel TolQR, IM-anchored TolA, periplasmic TolB, and outer membrane peptidoglycan binding lipoprotein, Pal (Petiti et al., 2019). The exact function of the Tol complex is unclear, but it is thought to use proton motive force to constrict the OM during cell division, evidenced in part by PMF-dependent envelope-spanning interaction between TolA and Pal (Cascales et al., 2000), and localization of the entire Tol complex to the septum during cell division (Gerding et al., 2007; Petiti et al., 2019). In addition to Pal, TolB has been shown to interact with Lpp, a major lipoprotein that covalently attaches to peptidoglycan (Braun, 1975; Cascales et al., 2000). Deletion or loss of function mutations in genes encoding the Tol-Pal complex results in OM instability phenotypes marked by detergent and antibiotic hypersensitivity, periplasmic component leakage, and outer membrane vesicle formation (Cascales et al., 2000; Gerding et al., 2007; Petiti et al., 2019)

Table 3.9 Death phase fitness (w_d)[a] for peptidoglycan associated protein/lipoprotein, and Tol-Pal mutants

Gene product	Locus	JG3020::tn Parent	JG3020::tn Light				JG3020::tn Dark			
		Reads	Reads			w_d[a]	Reads			w_d[a]
		t_0	t_1	t_2	t_3		t_1	t_2	t_3	
murein lipoprotein Lpp	SO_1295	273	269	88	129	-0.916	342	5	0	<-9.306
penicillin-binding protein 1A MrcA	SO_0280	2870	1274	316	17	-2.954	1091	40	1	-6.299
penicillin -binding protein activator LpoA	SO_0300	3128	1564	377	56	-1.997	1429	64	3	-5.825
penicillin-binding protein 1B MrcB	SO_0633	19021	19246	7109	13554	-0.466	19242	10949	18550	-0.102
TIGR02722 family lipoprotein - PBP1b activator LpoB	SO_1060	6198	4316	1454	857	-0.826	3813	2065	344	-1.567
TolA energy-transducing system periplasmic component YbgF	SO_2746	3537	3665	1042	679	-2.486	3312	760	288	-3.270
peptidoglycan-associated lipoprotein Pal	SO_2747	1899	1389	279	113	-2.306	1106	255	0	<-7.993
TonB biopolymer transport system periplasmic component TolB	SO_2748	4813	3806	930	282	-2.747	3816	750	22	-6.531
TolA energy-transducing system inner membrane component TolA	SO_2749	603	448	107	28	-2.748	410	55	1	-7.169
TolA energy-transducing system inner membrane component TolR	SO_2750	466	292	88	41	-0.911	295	33	0	<-6.414
TolA energy-transducing system inner membrane component TolQ	SO_2751	710	415	108	8	-3.503	372	76	0	<-6.006
TolA energy-transducing system-associated acyl-CoA thioesterase YbgC	SO_2752	12977	14753	4769	11934	-0.723	15156	6930	9766	-1.247
Total sequence reads (millions)		**36.61**	**33.99**	**12.44**	**26.17**		**34.66**	**19.24**	**29.93**	

[a] Calculated from equation: $w_d = log_2 \frac{(mutant\ reads/total\ reads)_{t_3}}{(mutant\ reads/total\ reads)_{t_1}} - log_2 \frac{(mutant\ reads/total\ reads)_{t_1}}{(mutant\ reads/total\ reads)_{t_0}} \times \frac{doublings^{b}{}_{t_3/t_1}}{doublings^{b}{}_{t_1/t_0}}$

[b] See Table 3.1

A periplasmic regulator, CpoB (YbgF), has been found in *E. coli* to coordinate the activities of PBP1b-LpoB, in response to the energy state of Tol, likely to coordinate peptidoglycan synthesis with outer membrane invagination (Gray et al., 2015). The *ybgC* gene encodes for an Acyl-CoA thioesterase and is found in association with the *tol-pal* cluster, but its functional relationship to the Tol-Pal system is unclear (Zhuang et al., 2002). *S. oneidensis* YbgC has been shown to regulate motility by mediating c-di-GMP homeostasis (Gao et al., 2017).

Death Phase Tn-seq: Na^+-translocation NADH quinone reductase mutant fitness defects and sodium motive force implications

A set of genes with very strong fitness defects in dark grown libraries when disrupted are those on gene locus SO_1103-1107 encoding one of two Na^+ translocating NADH quinone reductases, here referred to as Nqr1. The other sodium pumping NADH dehydrogenase, Nqr2 (SO_0902-07) did not appear to be necessary for surviving death phase, while disruptions in genes encoding Nuo (SO_1009-1021), the proton pumping NADH-dehydrogenase in MR-1, yielded inconsistent effects on fitness (Table 3.10). These results are surprising, as previous work has demonstrated a slight fitness benefit for anaerobic growth on lactate for Δ*nqr1* mutants, a clear fitness benefit for these mutants during anaerobic growth on NAG and a selective disadvantage during aerobic growth on NAG (Beliaev et al., 2005; Duhl et al., 2018), suggesting that this enzyme is primarily used for aerobic growth.

Table 3.10 Death phase fitness (w_d)[a] for NADH-quinone oxidoreductases

Gene product	Locus	JG3020::tn Parent	JG3020::tn Light				JG3020::tn Dark			
		Reads	Reads			w_d [a]	Reads			w_d [a]
		t_0	t_1	t_2	t_3		t_1	t_2	t_3	
Na-translocating NADH-quinone reductase 1 subunit A NqrA1	SO_1103	7381	7469	2918	6202	-0.229	7365	4469	212	-5.114
Na-translocating NADH-quinone reductase 1 subunit B NqrB1	SO_1104	6747	7088	2643	5899	-0.372	6816	4566	297	-4.564
Na-translocating NADH-quinone reductase 1 subunit C NqrC1	SO_1105	4553	4607	1789	4343	-0.045	4723	2839	121	-5.434
Na-translocating NADH-quinone reductase 1 subunit D NqrD1	SO_1106	7830	6461	2736	5406	0.583	6840	4362	283	-4.068
Na-translocating NADH-quinone reductase 1 subunit E NqrE1	SO_1107	6625	7123	2561	5834	-0.486	6843	3895	362	-4.372
Na-translocating NADH-quinone reductase 1 subunit F NqrF1	SO_1108	6995	7397	2598	5430	-0.579	7511	3778	331	-4.787
Na-translocating NADH-quinone reductase 2 subunit A NqrA2	SO_0902	15704	14220	4729	10244	0.003	14814	7698	26300	1.053
Na-translocating NADH-quinone reductase 2 subunit B NqrB2	SO_0903	8726	8636	2737	6944	-0.188	9451	4334	15869	0.430
Na-translocating NADH-quinone reductase 2 subunit C NqrC2	SO_0904	7638	7686	2629	6061	-0.281	7334	4671	11741	0.834
Na-translocating NADH-quinone reductase 2 subunit D NqrD2	SO_0905	9033	9280	3008	6499	-0.534	10535	5521	16142	0.008
Na-translocating NADH-quinone reductase 2 subunit E NqrE2	SO_0906	7102	7055	2420	5048	-0.371	7164	4084	11924	0.697
Na-translocating NADH-quinone reductase 2 subunit F NqrF2	SO_0907	14744	14947	4978	10590	-0.465	15396	8066	2754	-2.657
NADH-ubiquinone oxidoreductase subunit N NuoN	SO_1009	3028	2862	1072	2577	0.156	2993	1687	927	-1.649
NADH-ubiquinone oxidoreductase subunit M NuoM	SO_1010	6724	8183	3157	6251	-1.073	7584	4371	8244	-0.356
NADH-ubiquinone oxidoreductase subunit L NuoL	SO_1011	9042	8157	3188	6654	0.197	8623	5147	7920	0.060
NADH-ubiquinone oxidoreductase subunit K NuoK	SO_1012	89	72	17	76	0.996	45	31	53	2.909
NADH-ubiquinone oxidoreductase subunit J NuoJ	SO_1013	72	52	38	27	0.418	62	55	128	1.629
NADH-ubiquinone oxidoreductase subunit I NuoI	SO_1014	24	38		13	-3.265				N/A
NADH-ubiquinone oxidoreductase subunit H NuoH	SO_1015	365	216	81	141	1.530	199	118	269	2.812
NADH-ubiquinone oxidoreductase subunit G NuoG	SO_1016	16540	16174	6185	12797	-0.164	16824	9681	16220	-0.124
NADH-ubiquinone oxidoreductase subunit F NuoF	SO_1017	2941	2744	959	2157	0.011	2512	1316	2756	0.749
NADH-ubiquinone oxidoreductase subunit E NuoE	SO_1018	1985	2543	584	1508	-1.640	2840	971	1292	-2.546
NADH-ubiquinone oxidoreductase subunit CD NuoCD	SO_1019	4500	4245	1702	3612	0.082	4753	2472	4939	-0.163
NADH-ubiquinone oxidoreductase subunit B NuoB	SO_1020	5666	6097	1805	5067	-0.469	5985	2772	5569	-0.323
NADH-ubiquinone oxidoreductase subunit A NuoA	SO_1021	3233	3459	1136	3055	-0.358	3532	1870	3177	-0.504
Total sequence reads (millions)		**36.61**	**33.99**	**12.44**	**26.17**		**34.66**	**19.24**	**29.93**	

[a] Calculated from equation: $w_d = log_2 \frac{(mutant\ reads/total\ reads)_{t_3}}{(mutant\ reads/total\ reads)_{t_1}} - log_2 \frac{(mutant\ reads/total\ reads)_{t_1}}{(mutant\ reads/total\ reads)_{t_0}} \times \frac{doublings^{b}{}_{t_3/t_1}}{doublings^{b}{}_{t_1/t_0}}$

[b] See Table 3.1

To test whether Nqr1 is important for survival in respiratory stress, a Δ*nqr1* (ΔSO_1109-1108) mutant was constructed. Anaerobic growth of Δ*nqr1* using lactate as the carbon source and fumarate as the electron acceptor was no different than WT, but differences in both turbidity and viability loss were seen (Fig 3.12). Initial rates in optical density loss (Fig 3.13A) were slower than WT until approximately 13h following entry into death phase, at which point cell density quickly declined. A similar trend was seen for Δ*nqr1* when assaying for viability (Fig 3.13B), but a precipitous loss in colony forming units was observed sooner, after approximately 7 hours following entry into death phase.

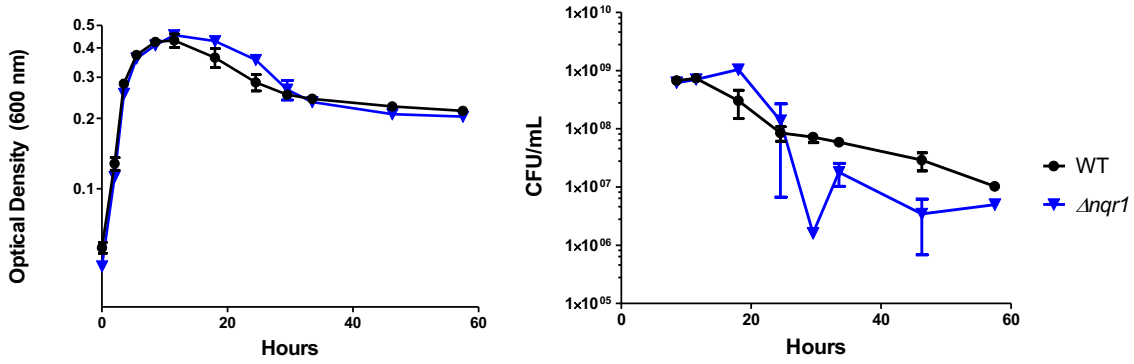

Fig 3.13 Δ*nqr1* deletion mutant growth and death phenotypes. Wild type (●) and Δ*nqr1* (▼) *S. oneidensis* strains were grown in SBM with 20 mM lactate and 40 mM fumarate and assayed for optical density at 600 nm (A) and colony forming units (CFU)(B). Symbols represent mean, and error bars represent standard error means across three replicates.

A competition experiment with Δ*nqr1* and MR-1+*gfp* at a 50:50 starting ratio, showed strong fitness defects for Δ*nqr1* during death phase (Table 3.11), in agreement with Tn-seq fitness scores for individual *nqr1* gene knockouts.

Table 3.11 Death phase fitness of Δ*nqr1*

	% makeup of strain vs MR-1+*gfp*			Log_2 ratios		Growth doublings		Death phase fitness (Log_2)		
	A	B	C	D	E	F	G	H	I	J
Genotype	t0	t1	t3	Log_2(B/A)	Log_2(C/B)	t1/t0	t3/t1	E-(D/F×G)	Mean (H)	SEM (H)
JG274	44.3%	46.3%	64.1%	0.065	0.469	3.94	8.084	0.335		
	48.2%	46.7%	68.4%	0.078	0.549	3.87	7.961	0.388	0.337	0.029
	43.9%	46.5%	61.7%	0.071	0.407	4.09	6.811	0.289		
Δ*nqrABCDEF*	47.2%	48.2%	0.3%	0.031	-7.233	4.07	5.877	-7.278		
	45.9%	49.3%	0.6%	0.063	-6.321	3.77	5.998	-6.421	-6.187	0.707
	47.1%	49.3%	1.8%	0.062	-4.745	3.93	7.436	-4.863		

It is certainly interesting that this enzyme is utilized under electron acceptor starvation, since it is quinone linked, and very likely operates in a forward quinone-reducing direction. As with *pykA* mutants, this suggests the availability of an extracellular electron acceptor, possibly fumarate supplied by lysed cells. Reverse flow of Na^+ with Nqr1 to produce NADH would not only deplete Na^+/H^+ motive force, but it is energetically unfavorable and would require additional SMF/PMF supplementation. Another line of evidence that SMF is not being utilized to oxidize menaquinone and generate NADH during acceptor starvation is that *nqr1A-F* transposon mutants had neutral fitness in light-grown populations. If quinone pool oxidation were a priority in acceptor starvation, light-driven PMF supplementation (and indirect SMF supplementation through antiporters) would have presumably increased reliance on quinone-oxidoreductases such as Nqr1. In acceptor starved cultures, it appears that membrane potential generation, possibly to maintain ATP homeostasis, is the priority in survival, bolstered by the finding that very few fitness defects were found in light-grown transposon mutants. However, without single and combination NADH dehydrogenase operon deletion mutants with proteorhodopsin expression, it is difficult to determine whether PMF/SMF are being used to maintain quinone-pool redox balance and NAD^+/NADH homeostasis, as it is unknown how PMF supplementation affects expression of these operons or utilization of each dehydrogenase. It has been already demonstrated that NADH dehydrogenase can function in reverse electron transport from an electrode in *S. oneidensis,* when engineered to use proteorhodopsin to overcome the energetic barrier in the reaction (Tefft and TerAvest, 2019). It is thus still a possibility that NADH dehydrogenase(s) was/were utilizing light-driven PMF/SMF to run in reverse and empty the quinone pool, but that neutral fitness was seen for individual transposon mutants due to functional complementation.

Fitness defects associated with Nqr1 in dark-grown cultures highlight the potential utility of SMF in *S. oneidensis.* Since the F_oF_1 ATPase in *S. oneidensis* appears to be exclusively proton coupled (Duhl et al., 2018) interconversion between SMF and PMF is likely necessary under these conditions. The *S. oneidensis* genome encodes several Na^+/H^+ antiporters but one, NhaB, was associated with significant fitness defects in death phase Tn-seq when disrupted (Table 3.12). Insertions in this gene also yielded

slight fitness defects with PMF supplementation in light-grown cultures, suggesting a portion of PMF supplied by proteorhodopsin is used to maintain SMF. Insertions in the genes for osmotic stress response activator NhaR and the antiporter it induces NhaA, only yielded mild fitness defects, suggesting that osmotic stress was not a significant factor in these cultures, and possibly hinting that energetic Na^+ gradient maintenance is more important to survival in death phase *S. oneidensis* cultures under these conditions than is sodium homeostasis.

Table 3.12 Na^+/H^+ antiporters and osmotic stress protection activator death phase fitness

		Parent	**Light**			**Dark**		
Gene product	Locus	Reads t_0	Reads t_1	Reads t_3	w_d [a]	Reads t_1	Reads t_3	w_d [a]
sodium:proton antiporter NhaC family	SO_0336	14767	16688	11497	*-0.95*	17251	13094	*-1.01*
sodium:proton antiporter NhaD	SO_0935	16814	15970	11881	*-0.14*	16827	13461	*-0.33*
Na+/H+ antiporter NhaA	SO_1336	16389	17128	12122	-0.60	17921	13032	-0.81
transcr. act. osm. str. prot. NhaR	SO_1338	3297	3395	2601	-0.42	3542	2554	-0.76
sodium:proton antiporter NhaC family	SO_2481	10215	9102	5582	-0.16	8522	6795	0.38
sodium:proton antiporter NhaB	SO_2886	16891	6492	162	-1.40	6144	0	<-8.619
Total sequence reads (millions)		**36.61**	**33.99**	**26.17**		**34.66**	**29.93**	

To further test the contribution of sodium motive force in stationary / death phase cultures of *S. oneidensis,* with and without proton motive force supplementation, a Δ*nhaB* mutant was constructed in the genomic proteorhodopsin strain JG3020 background, resulting in strain Δ*nhaB*+PR. Deleting *nhaB* results in both attenuated growth rate and decreased final yield, with and without proton motive force supplementation (Fig 3.14). Without light-driven PMF supplementation, the Δ*nhaB*+PR mutant lost approximately half of peak turbidity, but with PMF-supplementation, it lost turbidity at a much lower rate (Fig 3.14A). Although Δ*nhaB*+PR cultures survived better with PMF supplementation than without, they were unable to maintain the stability in cell densities seen with JG3020 (Fig 3.14B).

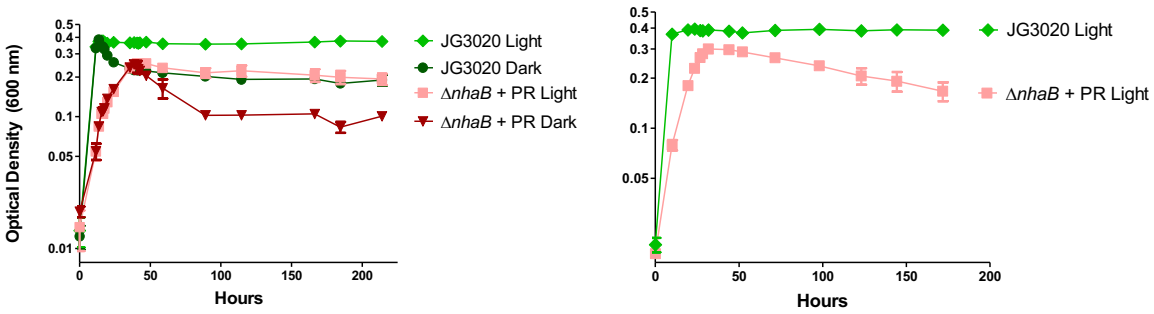

Fig 3.14 Δ*nhaB* deletion mutant growth and death phenotypes with and without PMF-supplementation. *S. oneidensis* Strain Δ*nhaB*+PR and genomic-proteorhodopsin-expressing background strain JG3020 were grown in SBM with 30 mM lactate and 40 mM fumarate under bright green (525 nm) light and assayed for optical density at 600 nm (A) and colony forming units (CFU)(B). Symbols represent mean, and error bars represent standard error means across three replicates.

These results suggest that SMF is a factor in the enhanced survival seen in light-driven PMF-supplemented cultures of *S. oneidensis.* Whether SMF is the dominant factor in survival granted by PMF-supplementation could be tested by deletion of all Na^+/H^+ antiporters in the *S. oneidensis* genome. Additionally, SMF supplementation using a Na^+ pumping rhodopsin such as that found in *Krokinobacter eikastus* (Inoue et al., 2013; Kato et al., 2015; Kovalev et al., 2019), would help tease apart the individual contributions of SMF and PMF to *S. oneidensis* physiology. A puzzling question left from these results is what specific purpose SMF has for survival under electron acceptor limitation. As explained earlier, it is still possible that Nqr1 or Nqr2 are functional under PMF supplementation in driving NADH regeneration and quinone oxidation, but this reaction would be energetically unfavorable in cultures without PMF supplementation. Yet Nqr1 was necessary for survival in this condition, suggesting the primary purpose of Nqr1 was not to supply NADH and oxidize the quinone pool, but rather to generate SMF at the cost of reducing the quinone pool. Nutrient import, toxin efflux, or pH homeostasis regulation seem to be the most likely utilities for SMF in acceptor starved cultures, but they were not explored further.

Concluding remarks

These experiments highlight the adaptation of *S. oneidensis* to utilize a wide variety of electron acceptors, by demonstrating catastrophic effects on viability under electron acceptor starvation. The evolved mechanisms to survive respiratory stress identified in this screen are largely conserved across Gram-negative bacteria, and generally point to

cell envelope stress responses. Regarding energetics, a Na^+-translocating NADH-quinone reductase appeared to be crucial for respiratory stress survival and a Na^+/H^+ antiporter was necessary for full rescue of cell viability in acceptor starvation via PMF supplementation, stressing that sodium motive force is an integral factor in *S. oneidensis* physiology. Finally, the central metabolic pathways *S. oneidensis* utilizes to allow ≤1% of cells to survive under electron acceptor starvation were not necessary when proton motive force was synthetically supplemented by expression of the light-drive proton pump proteorhodopsin, which permits near 100% viability under these conditions. This provides system-wide evidence that proteorhodopsin enables survival under starvation conditions by negating the need for energy-producing central metabolic pathways to achieve homeostasis.

3.4 Materials and Methods

Bacterial strains and culture conditions

Inocula for all experiments were prepared as described in Chapter 2. Minimal growth medium consisted of *Shewanella* basal medium (SBM) prepared as described in Chapter 2. Unless otherwise noted 20 mM D,L-lactate was supplied as the sole carbon source, and 40 mM fumarate was supplied as the sole terminal electron acceptor. For all experiments with proteorhodopsin-expressing strains, 10 μM all-trans retinal was provided to the medium. See Table 3.13 for a list of strains, Table 3.14 for a list of plasmids, and Table 3.15 for a list of primers used in this study.

Proteorhodopsin-expressing transposon library selection during death phase

Existing protocols for transposon sequencing (Brutinel and Gralnick, 2012b), were adapted to develop a genome wide transposon mutant fitness screen for acceptor starvation-induced death phase in *Shewanella.* Briefly, a JG3020::Tn library was grown for approximately 2.7 doublings, allowed to undergo death phase in the dark or stationary phase in the light for 14.75 hours, or until dark cultures reached a turbidity (OD_{600}) of 0.300 from a peak of 0.460, then transferred into fresh anaerobic medium and grown to mid exponential growth phase. Samples were collected for DNA extraction at mid exponential growth (0.31 OD_{600}), following death/stationary phase, and following

regrowth in fresh medium. Three tubes were used for DNA extraction for each treatment at each time point. The primary purpose of collection following death/stationary phase was to identify mutants that undergo lysis to a greater or lesser extent than the overall pool (a corollary for WT in this case), while the primary purpose of collection following regrowth was to identify mutants among the population that did not lyse that remained viable to a greater or lesser extent than the overall pool. Collection at mid exponential growth was intended to subtract relative fitness during growth from final.

An important point to note is following stationary phase, the pelleted light grown library was diluted 1/10 before transfer into fresh medium, while dark-grown dying libraries were pelleted and transferred undiluted into new tubes. The reason for this discrepancy in treatment is stationary phase light cultures were expected to contain 10× the number of viable cells as dying dark cultures. To ensure similar treatment, regrowth cultures were to be incubated for the same number of doublings for viable cells.

Transposon library DNA extraction, sequencing, and mapping

Approximately 30 mL of anaerobic selection cultures (or equivalent amounts of parent transposon library) was pelleted and frozen. Cell pellets were extracted using an epicenter MasterPure Complete DNA and RNA Purification kit (Lucigen), following manufacturer instructions. Extracted DNA was processed as described previously (Brutinel and Gralnick, 2012b). Briefly, approximately 6 μg digested 2 h with MmeI restriction endonuclease, then ligated with barcoded illumina adapters. Ligation products were amplified with adapter, and transposon-specific primers, then normalized for concentration before submission for sequencing on the Illumina HiSeq 2500 platform at the University of Minnesota Genomics Center. Reads were mapped to the *S. oneidensis* MR-1 chromosome (NC_004347.2) and megaplasmid (NC_004349.1), modified to include genomic insertion of the proteorhodopsin gene and promoter at chromosome position 4,951,360.

Competition assay and flow cytometry

Upon inoculation, following a single growth phase, and following regrowth after death phase, samples were collected from anaerobic cocultures via syringe argon-sparged

syringe. Flow cytometry was performed as described in Chapter 2. Inoculation samples were read by flow cytometry undiluted, while samples collected following growth were diluted 1/100. Data analysis was performed in FlowJo software as described in Chapter 2. Pure MR-1+*gfp* cultures were used as a control to assay for GFP expression and used to correct mixed culture data in each timepoint for the small percentage (0.1-5%) of MR-1+*gfp* that did not exhibit fluorescence.

Table 3.13 Strains used in this study

Strain	Parent strain and genotype	Source
JG274	MR-1, wild-type	(Myers and Nealson, 1988)
JG687	JG274 with empty pBBR1-MCS2 (Km^r) broad range expression vector	(Johnson et al., 2010)
JG688	JG274 with proteorhodopsin expressed on pBBR1-MCS2 broad range expression vector	(Johnson et al., 2010)
JG1637	"MR-1+*gfp",* JG274 with genomic insertion of *gfpmut3**	(Kees et al., 2019)
JG2955	"Δ*fdh*^{2}*";* JG274 derivative, Δ*fdhABC1* (ΔSO-4509-4511), Δ*fdhABC2* (ΔSO-4513-4515)	(Kane et al., 2016)
JG2957	"Δ*fdh*^{3}*";* JG274 derivative, Δ*fdhABC1* (ΔSO_4509-11), Δ*fdhABC2* (ΔSO_4513-15), *fdnGHI* (ΔSO_0101-03)	(Kane et al., 2016)
JG2967	JG274 with empty pBBR1-MCS (Cm^r) broad range expression vector	This study
JG2969	JG274 with proteorhodopsin, cloned from JG688 and expressed on pBBR1-MCS (Cm^r) broad range expression vector	This study, Johnson et al., 2010
JG3000	JG274 with genomic proteorhodopsin, P_{lac} and RBS_{II}	
JG3019	JG274 with genomic proteorhodopsin containing a base substitution resulting in Lysine 172 mutation to Threonine, P_{lac} and RBS_{II}	This study
JG3020	JG274 with genomic proteorhodopsin, P_{lac} and RBS_{II}	This study
JG3456	JG274 derivative, prophage-cured (ΔλSo ΔMuSo1 ΔMuSo2)	This study
JG3850	JG274 derivative; Δ*tatABC* (ΔSO_4202-04)	This study
JG4045	JG274 derivative; Δ*mlaA* (ΔSO_3197)	This study
JG4046	JG274 derivative; Δ*mlaC* (ΔSO_3951)	This study
JG4047	JG274 derivative; Δ*nhaB* (ΔSO_2886)	This study
JG4088	JG274 derivative; Δ*nqrABCDEF* (ΔSO_1103-08)	This study

Table 3.14 Plasmids used in this study

Plasmid	Relevant characteristics	Source
pSMV3	Deletion vector, Km^r-only version of pSMV10, *sacB*	(Saltikov and Newman, 2003)
pBBR1-MCS	Broad range expression vector, Chloramphenicol resistance (Cm^r)	(Kovach et al., 1994)
pBBR1-MCS2	Broad range expression vector, Kanamycin resistance (Km^r)	(Kovach et al., 1995)
pGlmS-MCS	pAK1 (pSMV3) derivative for targeted genomic gene insertion. Multiple cloning site with ScaI-BamHI-NheI/BmtI-NotI recognition sequences inserted into SpeI cut site between upstream and downstream fragments.	(This study, Kane, 2016; Teal et al., 2006)
AH-B	Medium strength expression vector with P_{lac} and RBS_{II}	(Harris 2014)
AH-E	Medium strength expression vector with $P_{A1/O4/O5}$ and RBS_{II}	(Harris 2014)
pGlmS-MCS::PR-M	Genomic proteorhodopsin insertion vector with "medium" strength promoter and RBS cloned, via ligation products of AH-B NsiI/NdeI digestion and JG688 plasmid extract NdeI/XhoI digestion, amplified with primers EDK1 and EDK2, then inserted into pGlmS-MCS at BamHI site	This study
pGlmS-MCS::PR-H	Genomic proteorhodopsin insertion vector with "high" strength promoter and RBS, cloned similar to pGlmS-MCS::PR-M but with AH-E plasmid source and EDK2/EDK3 primers	This study

Table 3.15 Primers used in this study

Primer Name	Primer Function	Sequence	Cut site
M13F (-20)	pBBR1-MCS/pSMV3 insert seq.	GTAAAACGACGGCCAGT	
M13R	pBBR1-MCS/pSMV3 insert seq.	CAGGAAACAGCTATGAC	
EDK1	AH-B + PR ligation ampl.	NNNN GGATCC ATGCATGCGCCCAATACGCAA	BamHI
EDK2	PR RBSII ligation ampl. Rev	TCAGTGATGGTGATGGTGATG	
EDK3	AH-E +PR ligation ampl.	NNNN GGATCC ATGCATTCTAGAACTAGTGTTCC	BamHI
EDK 4	pGlmS-MCS constr. OE-PCR UP	NNNN GGGCCC GGCGGCACGTTATTGGTTA	ApaI
EDK 5	pGlmS-MCS constr. OE-PCR UP	TGCAgctagcAGATactagtGTCGggatccACTGGCGGTTTTTTATTGG	
EDK 6	pGlmS-MCS constr OE-PCR DN	CGACactagtATCTgctagcTGCAgcggccgcACCGCCAGTTAGGCGGTTT	
EDK 7	pGlmS-MCS constr. OE-PCR DN	NNNN GAGCTCTCCTGATGTCGCGAGCTTCG	SacI
EDK 8	pGlmS-MCS constr. internal seq.	CCT TGA TTG ACG CCG ATA TG	
EDK9	pGlmS-MCS insert sequencing	TTG CTC TCT TAC CAT GTT GC	
EDK10	pGlmS-MCS insert sequencing	CTTAATAGCCTAAGCCACCAG	
EDK11	pGlmS-MCS cloning adapter 1	AATAactagtATCTggatccCGACgctagcTGCAgcggccgcGTTAactagtGTAC	
EDK12	pGlmS-MCS cloning adapter 2	GTACactagtTAACgcggccgcTGCAgctagcGTCGggatccAGATactagtTATT	
EDK13	genomic attTn7 site insert seq 1F	CACGTACAGATTATTGCTTGTGG	
EDK14	genomic attTn7 site insert seq 2F	CCTACAGTCTATGCCTGCTAAAG	
EDK15	genomic attTn7 site insert seq 2R	CCTCGAGAAACGCGATCAA	
EDK16	genomic attTn7 site insert seq 1R	TGTGGTTTGCGATTTAACCTTAG	
EDK17.1	ΔMuSo1-UP-fw	AAAAAA ACTAGT CTCGGTGCTAAGGTGATTGC	SpeI
EDK18	ΔMuSo1-UP-overlap-rev	AGGTTATAGCTTAGTTAGCTCACAATGTTAATACGA	
EDK19	ΔMuSo1-DWN-overlap-fw	CTAACTAAGCTATAACCTTGCTCCAGCACC	
EDK20.1	ΔMuSo1-DWN-rev	AAAAAA GAGCTC CAGCAATGACGGGCTGATATTTG	SacI
EDK21	ΔMuSo1-check-fw	GCGAAACCGTTTTGATACAC	
EDK22	ΔMuSo1-check-rev	CGAAGACTCTATCTACAGGCCAA	
EDK23.1	ΔMuSo2-up-fw	AAAAAAACTAGTACCCTGCAGTGTTCGGAC	SpeI
EDK24	ΔMuSo2-up-overlap-rev	AAGCTTGCCCGATCCCGTTTACATCCTACA	
EDK25	ΔMuSo2-dwn-overlap-fw	ACGGGATCGGGCAAGCTTATTTCTTCGCTT	
EDK26.1	ΔMuSo2-dwn-rev	AAAAAAGAGCTCATCGAATGTGACCGTTGTGG	SacI
EDK27	ΔMuSo2-check-fw	GCCTGATAACGACAAACAAATTT	
EDK28	ΔMuSo2-check-rev	CCCAGTTTGTGAAGGTTATGAG	

Primer Name	Primer Function	Sequence	Cut site
EDK31	ΔλSo-up--fw	AAAAAAACTAG TAATTGCTTTAGCCGAGGCA	SpeI
EDK32	ΔλSo-up-overlap-rev	AATGAGTGAGGTAAGCTTTCGTTCGTTTGG	
EDK33	ΔλSo-dwn-overlap-fw	AAGCTTACCTCACTCATTAGTATCTTGCTCTTCTGA	
EDK34	ΔλSo-dwn-SacI-rev	AAAAAAGAGCTC GCGGATTTCAGTGTTTCCAG	SacI
EDK35	ΔλSo-check-fw	TGAAAGCGCACATTTCCA	
EDK36	ΔλSo check-rev	GAAACCCTTGTCGGTGAAAA	
EDK49	λSo verification (pos. if present)	ACGGATGATAACCACCATCA	
EDK50	λSo verification (pos. if present)	TTAATGAATGCAAGCCTGGG	
EDK51	MuSo1 verification (pos. if present)	ATCAGTCGCATTCAAAACCG	
EDK52	MuSo1 verification (pos. if present)	CATAAACGACAGGTAAGCCG	
EDK53	MuSo2 verification (pos. if present)	AGAAATGTATCTCGGCCTGT	
EDK54	MuSo2 verification (pos. if present)	GCCAAGGTATCTGGGAAGTA	
EDK55	Δ*tatABC* UP Fw	AAAT GGATCC TCAAGGTCGTTTGTGAACC	BamHI
EDK56	Δ*tatABC* UP Rev	ACAC ACTAGT AATACTAATGCCACCCATGAAG	SpeI
EDK 69	Δ*tatABC* DWN Fw	AATT ACTAGT AACAACTAATGCCTAGAAGGC	SpeI
EDK 70	Δ*tatABC* DWN Rev	ACAC GAGCTC ATTTGCGCTATGTCTGGTTC	SacI
EDK59	Δ*tatABC* check Fwd	ATTGAATCAGGTTGGGTATCG	
EDK 72	Δ*tatABC* check Rev	ATCGCTACCAATAACGATGAG	
EDK 87	Δ*mlaC* UP fw	TTTT ACTAGT CATTAGAATGGGCAGAGCAG	SpeI
EDK 88	Δ*mlaC* Up rev OEPCR	CGCTATGTTT AAAGCAGGGAAGTAAGCG	
EDK 89	Δ*mlaC* DN fw OEPCR	TCCCTGCTTT AAACATAGCGGTAACCCCT	
EDK 90	Δ*mlaC* DN rev		SacI
EDK 91	Δ*mlaC* chk fw	ATACGGATCTTACCTTCGCC	
EDK 92	Δ*mlaC* chk rev	TCTGGTCAATTTTGCAGGC	
EDK 93	Δ*mlaA* UP fw	TTTT ACTAGT CGG CGG GAT AAC TGA TAT TT	SpeI
EDK 94	Δ*mlaA* Up rev OEPCR	GTTGAAATGG GAGTAAGCTCATGCGCTAAC	
EDK 95	Δ*mlaA* DN fw OEPCR	GAGCTTACTC CCATTTCAACTTCATATTGCTCT	
EDK 96	Δ*mlaA* DN rev	ATTA GAGCTC GCAGTAACAATGACATTCGG	SacI
EDK 97	Δ*mlaA* chk fw	AAGTAATCACTCCCCACCAT	
EDK 98	Δ*mlaA* chk rev	TTGCTTGATATTCACCCGAG	

Primer Name	Primer Function	Sequence	Cut site
EDK 99	Δ*nqrA-F* UP fw	AAAA ACTAGT AAACCTTGTCGCTGCTTATC	SpeI
EDK 100	Δ*nqrA-F* UP rev OEPCR	GCCGAAGTC CATATCCACAAGCACTACGTT	
EDK 101	Δ*nqrA-F* DN fw OEPCR	TGTGGATATG GAC TTC GGC GGC TAA TG	
EDK 102	Δ*nqrA-F* DN rev	AAAT GGATCC TGCCTTCGATAGACAGTTCA	BamHI
EDK 103	Δ*nqrA-F* chk fw	TGAATATCAGACGAGCACCT	
EDK 104	Δ*nqrA-F* chk rev	GTAACCCGTTGCTTGATACT	
EDK 105	Δ*nhaB* UP fw	AAAA ACTAGT GCTAAGGTGTGGTGTAACAG	SpeI
EDK 106	Δ*nhaB* UP rev OEPCR	GCCTGTCGC ACTCATTGTCATCGGCATG	
EDK 107	*ΔnhaB* DN fw OEPCR	ACAATGAGT GCG ACA GGC CAC TAA AAC	
EDK 108	*ΔnhaB* UP rev	ATTT GAGCTC GGTAACCACTAAAGGCAACG	SacI
EDK 109	*ΔnhaB* chk Fw	AAGTTGAGTGCTAACTGACG	
EDK 110	*ΔnhaB* chk rev	AATACAATGTCATAGCGCCG	

Chapter 4 – Survival of the first, not the fittest: a biofilm without competition

This chapter is a reprint of a manuscript in review, with minor alterations.

Kees ED, Miller SP, Levar CE, Bond DR, Gralnick JA, Dean AM. Survival of the first, not the fittest: a biofilm without competition

4.1 Summary

For natural selection to operate there must exist heritable variation among individuals that affects their survival and reproduction. All individuals must also eventually die and be replaced by offspring. Now consider a population of immortals whose offspring must all emigrate. The offspring are unable to contribute to the reproductive capacity of the population while the immortals, regardless of reproductive capacity, remain unchanged in frequency. The normal cycle of birth, death, and competitive exclusion is broken. Natural selection has ceased. This scenario is approximated in a stable microbial biofilm where cell death is exceedingly rare and where all offspring emigrate to the planktonic phase. Competitions were conducted between strains of *Shewanella oneidensis* MR-1, a wild-type and a Δ*llpR* mutant that grows half as fast when L-lactate is the carbon source. While the wild-type competitively excludes the mutant in planktonic cultures with a soluble terminal electron acceptor, both strains stably coexist in biofilms grown on graphite anodes as the terminal electron acceptor – even though the mutant still grows at half as fast as the wild-type. Our finding, that natural selection is impeded in a structured microbial community, has broad implications for the fields of evolutionary biology, microbial ecology, biomedicine and industrial fermentation.

4.2 Introduction

Natural selection, the differential survival and reproduction of competing genotypes, is a cornerstone of modern evolutionary theory and the only mechanism known to produce organismal adaptations (Futayama, 2009). Adaptive evolution requires competitive exclusion, the displacement of an inferior competitor by its superior (Hardin, 1960). Although this principle is readily demonstrated in microbial competition experiments (Gause, 1960; Lenski & Travisano, 1994; Zhu et al., 2005), there exist, nevertheless, many exceptions to the rule (Connell, 1978; Hutchinson, 1961; Tilman, 1982). All involve competitors with reduced niche overlap. For example, competitors might be limited by different resources (Lunzer et al., 2002), or favored at different times (Yi and Dean, 2013) or in different places (MacArthur, 1958). Reduced niche overlap promotes a diversity of coexisting types while complete niche overlap excludes all but

the fittest.

The idea that "complete competitors cannot coexist" is firmly rooted in ecology and evolution. After all, for complete competitors to coexist competitive exclusion must be prevented – and that necessitates abolishing natural selection. Here, we explore a means to provide for coexistence of competing organisms with seemingly total niche overlap.

A microbial biofilm provides a practical experimental system with which to decouple reproduction from competitive exclusion (Baltzis and Fredrickson, 1983; Freter et al., 1983). Assume that the biofilm is stable with an actively and outwardly reproducing basal layer, that cell death rates are negligible, and that all progeny must eventually emigrate to the planktonic phase. The normal cycle of birth, death and competitive exclusion is broken. In this theoretical biofilm, natural selection has entirely ceased.

4.3 Experimental Design

To simplify the analysis of surface-attached growth, we designed a system in which planktonic growth is inhibited. Our experimental organism is *Shewanella oneidensis*, a genetically tractable facultative anaerobe capable of growth using a variety of terminal electron acceptors (Myers and Nealson, 1988; Nealson and Scott, 2006), including soluble and insoluble metals as well as graphite electrodes poised at anodic potentials (Hau and Gralnick, 2007; Kitayama et al., 2017). Competitions were conducted in a custom designed anaerobic bioreactor (Fig 4.1A) in which only those cells attached to anodes can grow (Fig 4.1B). Under the strict anaerobic conditions imposed, *Shewanella* forms stable, invasion-resistant biofilms that rarely become multi-layered (Kitayama et al., 2017). Importantly, *S. oneidensis* is incapable of growth without an electron acceptor (Myers and Nealson, 1988; Pinchuk et al., 2011), unless specifically engineered to ferment pyruvate (Kane et al., 2016). Thus, competition on the anodes can be monitored by counting emigrants to the non-growing planktonic population under constant medium feed. Control competitions were conducted in anaerobic planktonic cultures with a soluble terminal electron acceptor present.

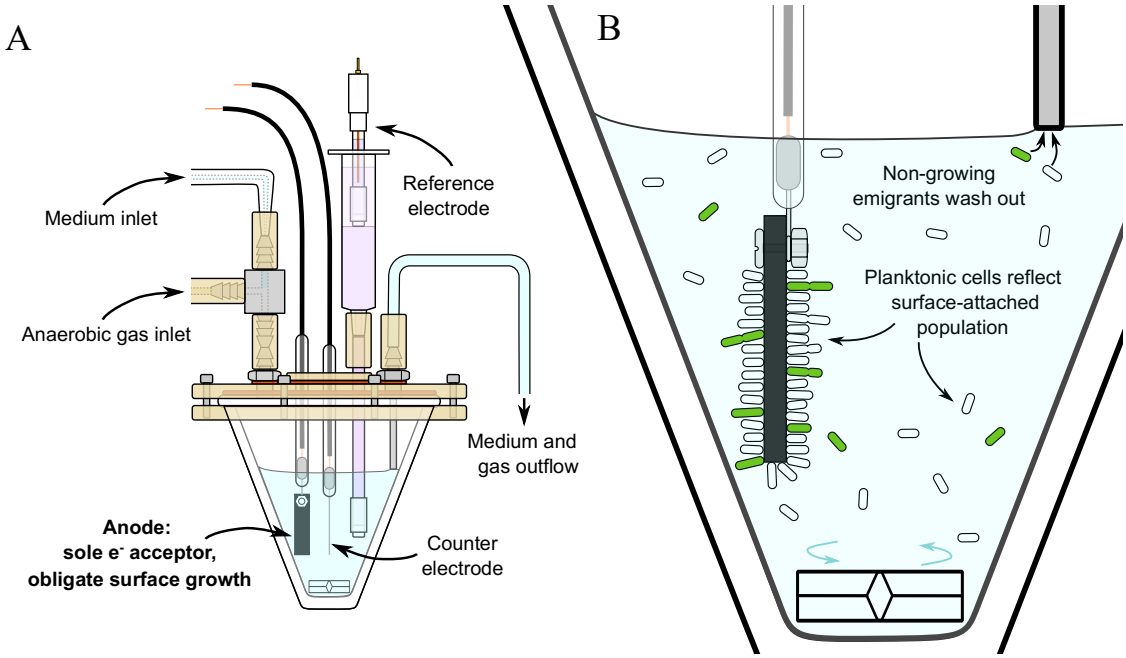

Fig 4.1 Anaerobic three electrode bioreactor. A) Fresh sterile anaerobic medium is pumped at a constant rate into a growth chamber under positive pressure from a flow of sterile humidified argon. Both spent medium and argon exit through an air-locked outlet. Cells are grown on a graphite working electrode poised at anodic potentials with a platinum counter electrode and a Ag/AgCl reference electrode to control the voltage. A magnetic stir bar mixes the planktonic phase. B) Only cells attached to the anode can grow. Hence, the strain ratio in the planktonic phase equals the ratio on the anode times the relative growth rate.

4.4 Results and Discussion

S. oneidensis strain Δ*llpR* has a deletion in the L-lactate positive regulator gene *llpR* which slows growth on L-lactate (Brutinel and Gralnick, 2012c). The wild-type strain, *gfp*$^+$, expresses green fluorescent protein from a genomic copy of *gfpmut3** to allow independent quantitation of mixed surface-attached populations by confocal microscopy and of mixed planktonic populations by flow cytometry. Experiments were conducted in *Shewanella* basal medium (SBM) (Hunt et al., 2010) with L-lactate as the sole carbon source.

Strain Δ*llpR* grows approximately half as fast as *gfp*$^+$ (specific growth rates are 0.329 ± 0.005 hr^{-1} and 0.627 ± 0.009 hr^{-1} respectively) in pure anaerobic planktonic batch-fed cultures with L-lactate as the carbon source and fumarate as the electron acceptor. Under these conditions strain Δ*llpR* is rapidly outcompeted by *gfp*$^+$ (Fig 4.2A). The observed selection coefficient (the slope of the line of the log ratio of strains plotted against time) is s = -0.291 ±0.009 hr^{-1}, which is very similar to the predicted value of 0.329 - 0.627 = -0.298 hr^{-1} obtained as the difference between the growth rate of each

strain in pure culture. The growth rate of Δ*llpR* relative to *gfp*$^+$ (a measure of fitness) is w = 1 - 0.291/0.627 = 0.535 ± 0.011.

Strain Δ*llpR* is also rapidly outcompeted by *gfp*$^+$ when grown planktonically in unpoised three-electrode bioreactors with L-lactate and fumarate (Fig 4.2B). The selection coefficient s = -0.243 ± 0.005 hr^{-1} is smaller than that seen in the batch culture competitions, but both strains grow slower and so the relative growth rate of Δ*llpR*, w = 1 – 0.243/0.520 = 0.533 ± 0.011, is unchanged. These control experiments establish that strains Δ*llpR* and *gfp*$^+$ conform to the competitive exclusion principle during planktonic competition.

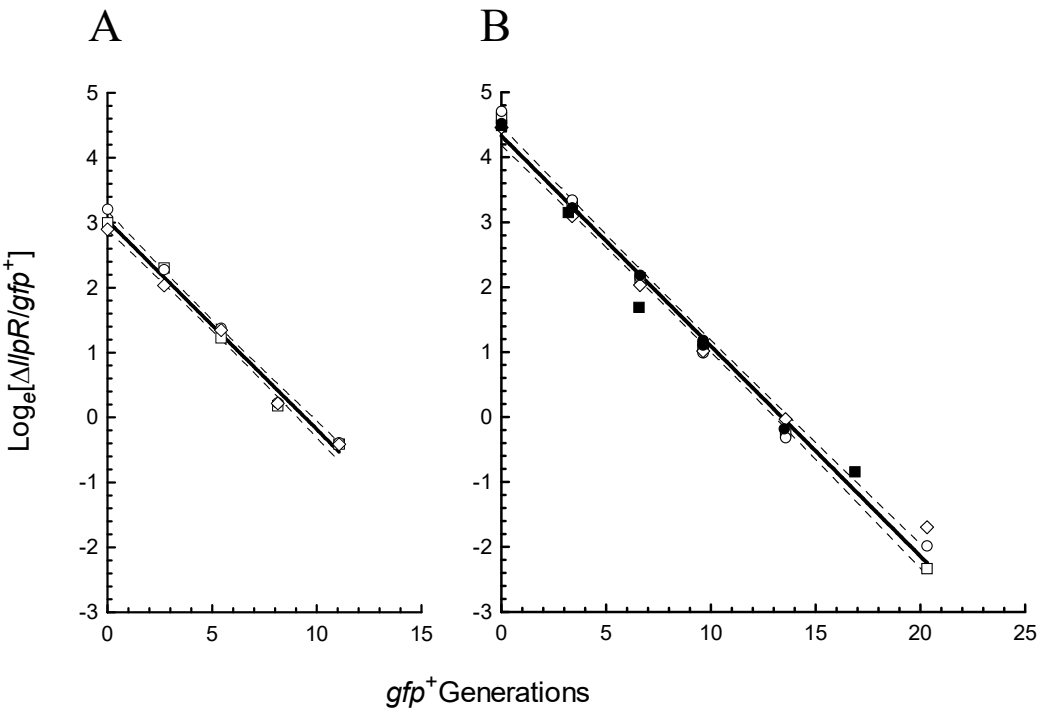

Fig 4.2 Anaerobic competition for lactate with fumarate as the terminal electron acceptor. The slopes of the solid lines (selection coefficients per *gfp*$^+$ generation estimated by linear regression) reveal strong selection against strain Δ*llpR* when placed in competition with strain *gfp*$^+$. A) Three replicate competitions in planktonic batch growth with an overall selection coefficient of -0.321 ± 0.010 gen^{-1}. B) Five replicate competitions across two experiments in bioreactors with electrodes unpoised; overall selection coefficient of -0.324 ± 0.007 gen^{-1}. Dashed lines indicate 95% confidence bands derived from linear regression.

Anodic growth rates can be estimated from the dilution rate and the densities of cells in the planktonic phase and on the electrodes (see Electrode biofilm growth rate determinations in Methods). This calculation assumes that *S. oneidensis* does not grow in the absence of a terminal electron acceptor, as has been repeatedly demonstrated (Kane et al., 2016; Myers and Nealson, 1988; Pinchuk et al., 2011). Growth rate estimates for each

strain were much slower on the anodes than in batch-fed planktonic cultures (0.083 ± 0.005 hr^{-1} and 0.170 ± 0.009 hr^{-1} for Δ*llpR* and *gfp*$^+$ respectively; Fig 4.3A). Nevertheless, the estimated growth rate of Δ*llpR* relative to *gfp*$^+$ on anodes (w = 0.083/0.170 = 0.488 ± 0.054; $p < 0.0001$ by Welch's t-test) is similar to that in planktonic cultures (w = 0.53 ± 0.01). Another measure of the difference in metabolic rates of each strain at anodic surfaces is the respiration rate (measured directly at the anodes via current production) per cell (using protein abundance at the biofilm surface as a proxy). As might be expected of cells that grow at half the wild-type rate, Δ*llpR* cells generate half the current (μA/μg protein) of *gfp*$^+$ cells (0.53 ± 0.05; $p \leq 0.0006$ by paired t-test; n=6; ; Fig 4.3B). We conclude that the relative growth rate is unaffected by attachment, and that it equals the relative respiration rate on the anodes.

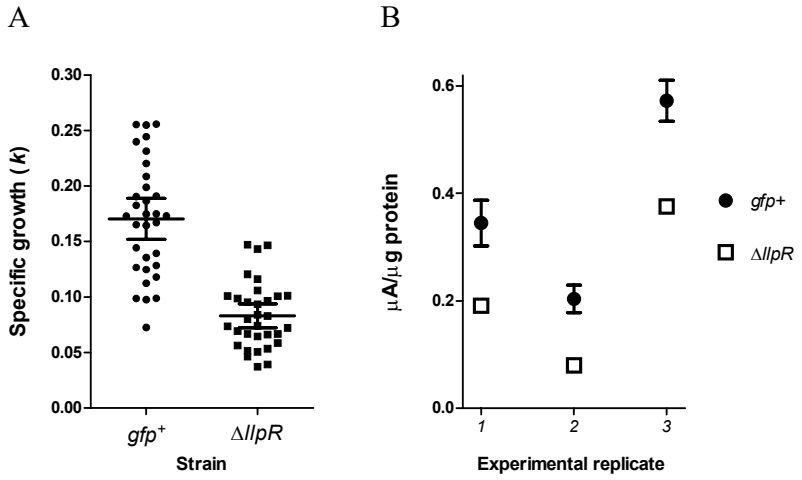

Fig 4.3 Growth rate and respiration rate estimates for electrode-attached cells. A) Specific growth rates calculated by cells/electrode estimates, divided by total cells removed per hour from bioreactors. Each data point represents a specific growth rate calculation per subsampled confocal micrograph for each of two time points used to measure medium flow rates and planktonic cell concentrations. Data are representative of two electrodes per strain, two time points and 8 subsampled images per electrode, for n = 32 replicates. Estimated growth rates are 0.083 ± 0.005 hr-1 and 0.170 ± 0.009 hr-1 for Δ*llpR* and *gfp*$^+$ respectively; p <0.0001 by Welch's t-test. Values are mean and SEM. B) Estimated current to protein ratio (per capita current) for two replicate bioreactors for each strain across three separate experiments. Values are mean and SEM.

In marked contrast with planktonic competitions, the ratio of strains Δ*llpR* and *gfp*$^+$ on poised graphite anodes, as reflected by their planktonic frequencies, remained unchanged over the course of the experiments (Fig 4.4). The strongest estimated selection coefficient among two separate competition experiments was -0.00082 ± 0.00246 gen^{-1} estimated for 671 hours of growth (Fig 4.4A). In this case, a rare mutant at a starting

frequency of 1 cell per 1 million (Log_e x $1/10^6$ = -13.82), with an otherwise strong fitness advantage (equivalent to *gfp*$^+$ against Δ*llpR*), would be expected to cross a threshold of 50% (Log_e x 1/1 = 0) after ~16,815 generations or approximately 7.83 years of continuous culture (1.96 years by the most liberal estimate within the 95% confidence band of the selection coefficient in our bioreactor experiments, -0.00082 – 0.00246 = -0.00328 gen^{-1}). Alternatively, if selection had followed that seen in planktonic growth (Fig 4.2B), after 365 *gfp*$^+$ generations, Δ*llpR* would have been expected to have declined from its initial frequency of ~0.98 to 0.98 x 0.533^{365} = $1.765/10^{100}$ (a frequency smaller than one atom in the known universe, ~$1/10^{80}$). Instead, bioreactors operated for ~365 generations or 1488 hours displayed neutral selection for Δ*llpR* (+0.0001517 ± 0.002633 gen^{-1}) when assayed for colony forming units of each strain by dilution plate counts (Fig 4.4B). Natural selection has been severely constrained on the anodes.

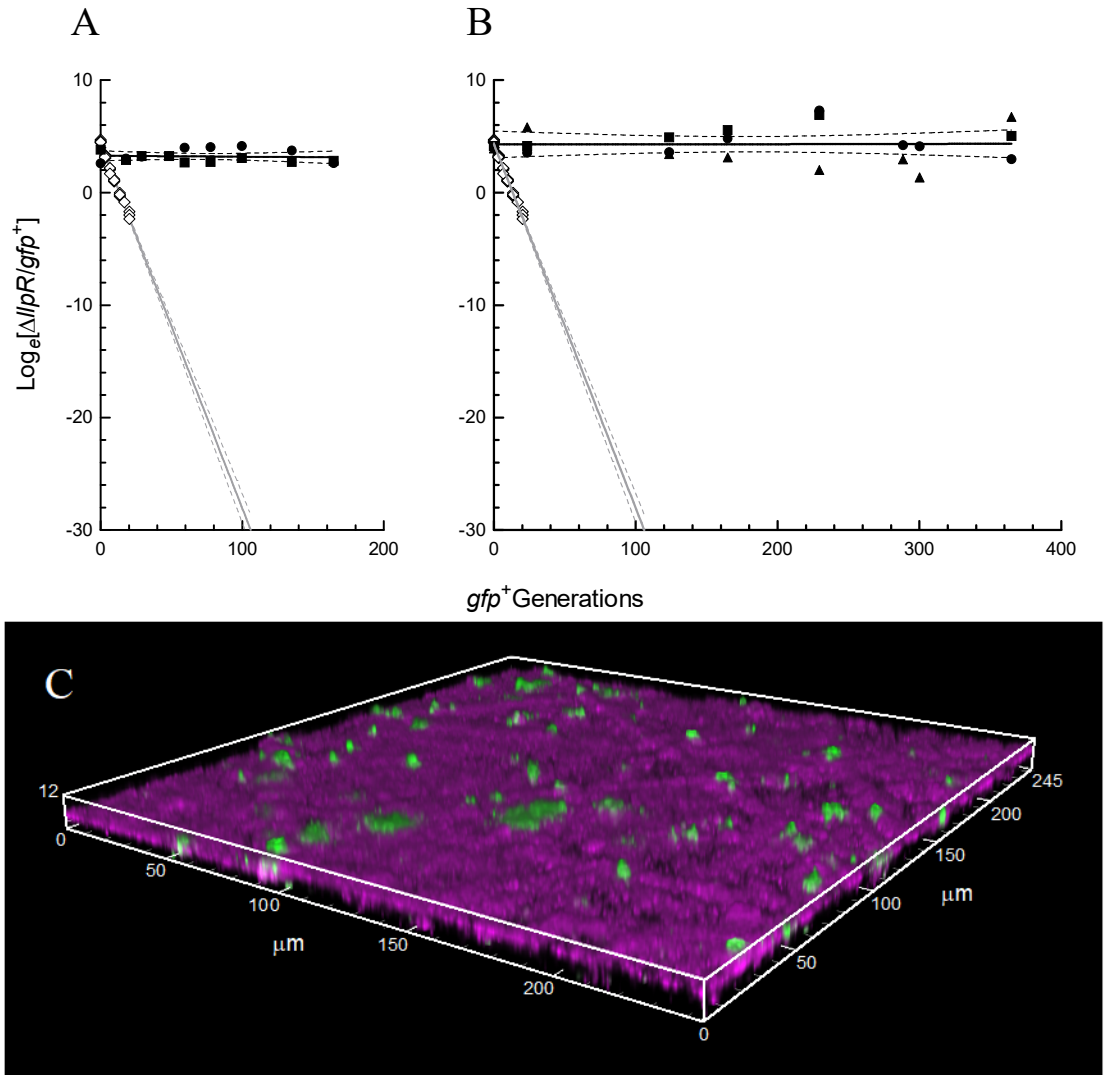

Fig 4.4 Anaerobic competition for lactate in bioreactors with electrodes poised (black lines): A) two replicate competitions conducted over 671 hours (~165 *gfp*$^+$ divisions) with abundances of each strain measured by flow cytometry. B) three replicate competitions conducted for 1488 hours (~365 *gfp*$^+$ divisions) and measured by dilution plate counting. For comparison, grey lines extrapolate the planktonic selection in bioreactors with unpoised electrodes. See Figure 3 – Source Data 1. C) Confocal microscopy volume projection of a mixed Δ*llpR*-*gfp*$^+$ biofilm at 929 hours confirms that *gfp*$^+$ cells (green) still sparsely populate the biofilm which remains dominated by Δ*llpR* cells (magenta). Symbols indicate replicate data points, solid and dashed lines indicate linear regression and associated 95% confidence bands, respectively.

An alternative hypothesis, that neither strain grows in the bioreactors, can be dismissed by the observation of a steady and somewhat increasing abundance of planktonic cells under continuous medium feed. Given a dilution rate of 0.1 hr^{-1}, a non-growing planktonic population should decline by a factor of $e^{-0.1 \times 1488} = 2.4 \times 10^{-65}$. No cells should have remained in the bioreactors. Yet total planktonic populations plateaued

at 100-300 hours and did not significantly change over the remainder of the experiments (Fig 4.5A). Furthermore, upon addition of fumarate to the medium-feed as a soluble terminal electron acceptor, planktonic cell concentrations increase, then decrease when fumarate is removed (Fig 4.5B).

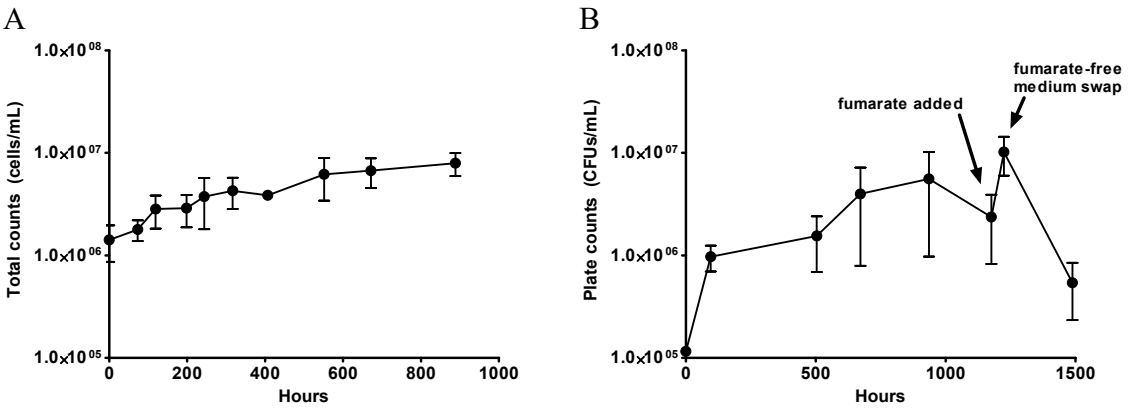

Fig 4.5 Total flow cytometry and CFUs/mL counts through two-month electrode experiment. Non-growing planktonic populations of emigrated anode-grown populations stabilize between 200-400 hours when counting total planktonic cells by flow cytometry across 888 hours(A), or by counting colonies on petri plates across 1488 hours (B). An increase in CFUs/mL can be seen upon addition of 5 mM fumarate at 1176 hours and a corresponding decrease in counts can be seen after reactors are washed out with fumarate-free medium.

Anodic growth rates, instead of being limited by the capacity to metabolize L-lactate, might be limited by anodic respiration rates. This would equalize their growth rates on electrodes, thus inhibiting competitive selection by alternative means than proposed. This hypothesis can be tested by measuring anodic respiration rates upon addition of a carbon source, D-lactate, which *S. oneidensis* preferentially utilizes over L-lactate, and which both strain metabolize equally well (Brutinel and Gralnick, 2012c). Adding D,L-lactate to pure cultures grown on anodes with L-lactate as the carbon source causes an immediate increase in current from strain Δ*llpR*, but not from strain *gfp*$^+$ (Fig 4.6A). The increased current from strain Δ*llpR* demonstrates that, relative to strain *gfp*$^+$, its metabolism on anodes is limited by its capacity to metabolize L-lactate

Another alternative hypothesis posits that strain frequencies are stabilized by availability of an electron acceptor to planktonic cells at a concentration or rate sufficient to support growth but small enough to force both strains to grow at equal rates. This might occur in our bioreactors due to O_2 diffusion in the medium lines or due to electron shuttling to and from the anode via soluble intermediates (Brutinel and Gralnick, 2012a; Mevers et al., 2019). If this indeed were the case, introducing excess electron acceptor to

support maximal growth rates of each strain would generate competitive exclusion, and the resulting change in strain frequencies, would be stabilized upon removal of the perturbation. When air (and thus oxygen) was introduced to bioreactors, the planktonic frequency of strain Δ*llpR* declined due to competitive selection among the growing planktonic population (Fig 4.6B). Once the air was shut off, and an anaerobic environment was restored, strain Δ*llpR* returned to its initial frequency (~98%). Had the medium contained sufficient electron acceptor to support planktonic growth but at equal rates, strain Δ*llpR* would have remained at the lower frequency (~68%) following removal of O_2. That strain Δ*llpR* returned to its original frequency demonstrates that emigrants grown on the anodes replenish cells washed from the bioreactor. A similar outcome occurs when bioreactors are spiked with fumarate (Fig 4.7).

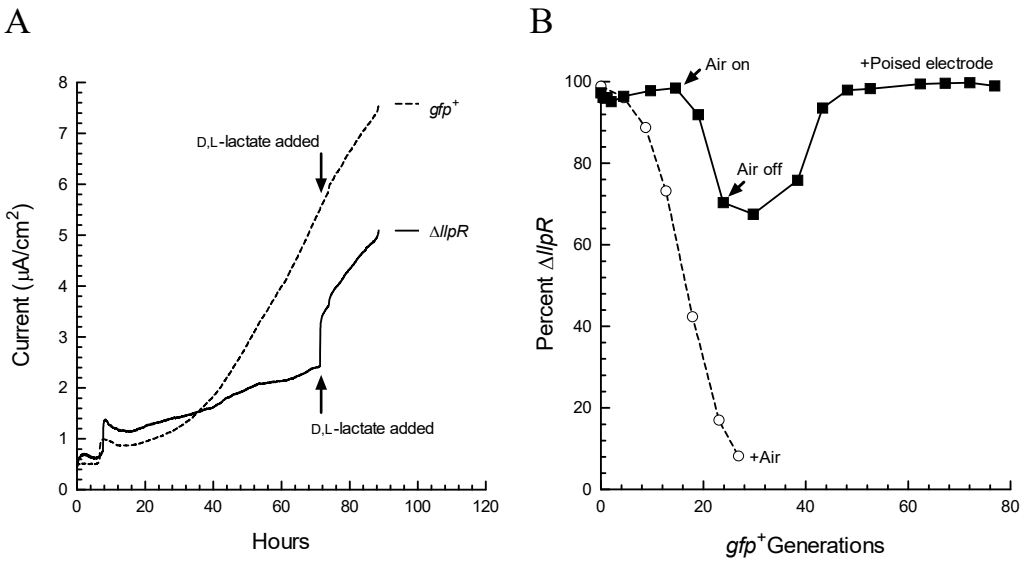

Fig 4.6 Metabolic rate determination of Δ*llpR* and MR-1+*gfp*, and planktonic competitive selection confirmation in bioreactors. A) The carbon source determines the metabolic rate of strain Δ*llpR*. Adding D,L-lactate provides a second carbon source, D-lactate, that is utilized preferentially and equally by both strains. The immediate increase in current from strain Δ*llpR* (but not from strain *gfp*$^+$) demonstrates that it is limited by its capacity to metabolize L-lactate during growth on electrodes. B) Letting air into an anaerobic bioreactor (solid line) provides planktonic cells with O_2 as a terminal electron acceptor. The ensuing competition causes a decline in the frequency of strain Δ*llpR*. Once anaerobic conditions have been re-established, strain Δ*llpR* returns to its original frequency, reflecting migration from a biofilm that is resilient to such perturbations. For comparison, strain Δ*llpR* is at a strong disadvantage during competition in an aerobic planktonic culture (dashed line).

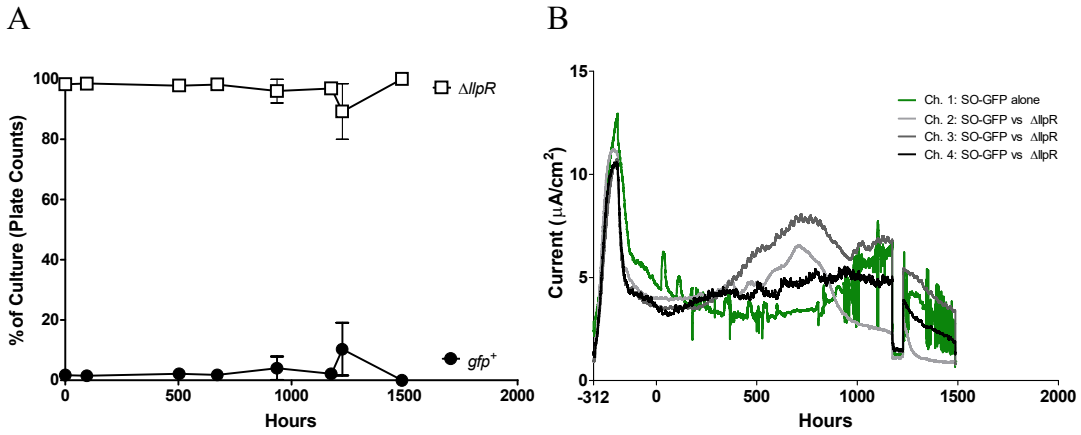

Fig 4.7 Anaerobic planktonic competition begins upon addition of fumarate into bioreactors. A) Percent abundance of competing 2-month old surface-attached biofilms measured by plating planktonic cells. The frequencies of *gfp*$^+$ (open squares) and Δ*llpR* (black circles) were stable during anodic competition. Strain *gfp*$^+$ began to outcompete strain Δ*llpR* at 1176 hours when 5 mM fumarate was added to the medium. Upon switching back to fumarate-free medium, strain *gfp*$^+$ returned to its original planktonic frequency as cells grown on the anodes repopulated the planktonic population washed from the bioreactor. B) Chronoamperometry traces from the same experiment show a decrease in the anodic current at 1176 hours as cells preferentially used the added fumarate as a terminal electron acceptor, and corresponding current restoration when the fumarate was removed

How long can anodic populations persist? Appreciable cell death on the anodes would cause the planktonic population densities to decline, yet they remain high over the course of our experiments. We conclude that *S. oneidensis* MR-1 death rates were sufficiently small not to have affected our results. Intriguingly, laboratory grown *Escherichia coli* (Chao, 2010; Proenca et al., 2018) and *Saccharomyces pombe* (Coelho et al., 2013) cells are also effectively immortal unless exposed to extrinsic stresses. This suggests that microbial cells might generally have very low intrinsic death rates under benign laboratory conditions.

Like natural selection, random genetic drift (accumulated random changes in competitor frequencies and a key force in the neutral theory of molecular evolution) has ceased or slowed to a crawl– and for the same reason. Emigrating progeny do not replace immortal cells on the anodes. Of the three evolutionary forces at play, only mutation is left. But mutation is too weak to be an effective evolutionary force (Hartl, 2000). Assuming a loss of function mutation rate of 10^{-6} per gene per generation it would take 4.6×10^6 generations (or 4.6×10^6 / 0.170/24/365 = 3089 years) for an allele to mutate from a frequency of 0.99 to 0.01. Evolution has, for all practical intents and purposes, ceased on the anodes.

4.5 Concluding remarks

Four conclusions can be drawn from our results. First, natural selection is an immensely powerful force and the conditions needed to negate its impact are particular: a population of immortals whose offspring must all emigrate. Second, conditions approaching this ideal may arise naturally in biofilms. While faster growing types may overgrow slower competitors, they will be unable to sweep the community if surface-attached basal cells remain viable and actively growing. Though each strain uses the same resources, those resources are effectively infinite except for physical space. Once they attach, basal cells no longer interact. This scenario provides a less fit individual an opportunity to stake a claim and grow uninhibited. Thus, as far as basal progenitor cells are concerned, this condition may in fact produce a variety of niche differentiation.

Third, under these circumstances, where competitive exclusion is prevented despite differential reproductive rates, genetic and ecological diversity can be preserved. Selective sweeps are possible only if faster growing populations actively invade or repeatedly re-colonize freshly exposed surfaces. The more stable the basal layer, the less evolvable, invasible, or prone to cheaters the biofilm becomes.

Third, biofilms have potential beneficial applications in medicine and industrial fermentation. Our results show that when conditions are provided for basal surface growth – in our case the surface is a metabolic substrate – the first colonizers persist regardless of their competitive ability. Coating medical devices with stable biofilms of hypothetical nonpathogenic nonimmunogenic microbes might prevent colonization by better-adapted pathogens. New fermenter designs, with large surface area to volume ratios, would maximize immigration from surface-attached cells, yet minimize planktonic growth. Such designs, by preventing strain degeneration and genetic instability, might replace large industrial batch fermenters with smaller, more economical, continuous culture bioreactors.

4.6 Materials and Methods

Strains and growth conditions.

Both experimental strains are derived from wild-type *S. oneidensis* MR-1 (Myers and Nealson, 1988; Nealson and Scott, 2006), and strain Δ*llpR* is described previously (Brutinel and Gralnick, 2012c). Strain *gfp*$^+$ was constructed by insertion of *gfpmut3*,* under control of the constitutive promoter A1/04/03 (Lanzer and Bujard, 1988), into the neutral attTn7 insertion site downstream of gene *glmS* in MR-1 (Lambertsen et al., 2004; Teal et al., 2006). A modified double homologous recombination method (Coursolle et al., 2010) was used to target the gene insertion. *Shewanella* Basal Medium (SBM) consisted of 0.225 g K_2HPO_4, 0.225 g KH_2PO_4, 0.46 g NaCl, 0.225 g $(NH_4)SO_4$, and 0.117 g $MgSO_4 \cdot 7H_2O$ per liter, adjusted to pH 7.2 (using NaOH) with 10 mM HEPES, 0.05% casamino acids (Fisher), and 5 mL/L each of vitamins and mineral mix described previously (Hau et al., 2008). In anaerobic cultures, lactate and fumarate were used, respectively, as carbon source and terminal electron acceptor, and their concentrations are described where noted.

Unless otherwise noted, inocula for all cultures were routinely prepared by growing and isolating colonies on lysogeny broth (LB) 1.5% agar plates, transferring single colonies into LB and growing for 8 hours with aeration, then transferring 10 μL into SBM containing 20 mM Lactate and growing aerobically overnight. Media reservoirs for all continuous-flow experiments were supplemented with 250 nM riboflavin to correct for washout of flavin electron shuttles (Marsili et al., 2008).

Anaerobic Planktonic competitions

Strains *gfp*$^+$ and Δ*llpR* were grown together in sealed, nitrogen-flushed anaerobic tubes containing SBM supplemented with 20 mM L-lactate and 40 mM fumarate. Initial inocula were set at a ratio of 97:3 Δ*llpR*: *gfp*$^+$, and tubes were inoculated at a starting density of 0.010 OD_{600}. Exponential-phase (OD_{600} = 0.200) cultures were transferred to fresh anaerobic medium via syringe to maintain exponential growth. For direct cell counting, samples taken at each time point were exposed to air for 10-20 minutes to facilitate GFP folding and diluted to 10^5-10^6 cells/mL in 0.2 μm-filtered SBM to

determine percent GFP and non-GFP expressing cell abundance by flow cytometry. For dilution plate counts, samples were diluted in SBM, 100 µL was spread on two separate LB-1.5% agar plates, which were incubated first for colony growth at 30 °C for 18 hours, then to enhance GFP fluorescence at 4 °C for 4-24 hours. Colonies formed by strains *gfp*$^+$ and Δ*llpR* were differentiated and counted under UV light.

Three-electrode bioreactors

The three-electrode chambers consist of a 3 cm^2 polished graphite electrode, an Ag/AgCl reference electrode and a Pt counter electrode within a polyether ether ketone (PEEK) topped 35 mL glass cone chamber, with inlet, outlet and sampling ports. At the inlet port, media was fed by peristaltic pump (Ismatec IPC) through Pharmed 0.25 mm ID BPT tubing (Cole Parmer), and the headspace was continuously flushed with argon. At the outlet port a small custom stainless-steel pickup tube was fitted to set the medium volume at 13.3 ± 0.3 mL. To minimize oxygen permeation into medium feed lines, stainless steel or glass fittings were used where possible. Redox potential was set at 240 mV vs SHE using a Bio-Logic SAS model MPG2 potentiostat, and EC-Lab software. Electrode respiration rate was monitored as an average taken over 2 min and expressed as the current (µA) per cm^2 of electrode surface.

Planktonic competition in bioreactors

Filtered SBM medium containing 2 mM L-lactate and 4 mM fumarate was fed through unpoised three-electrode chambers at a dilution rate of 0.185±0.005 h-1. Chambers were inoculated with 200 µL of a 95:5 mix of Δ*llpR*: *gfp*$^+$. One mL samples were taken at routine time points and diluted 4-fold in filtered SBM for flow cytometry measurements.

Competition in anode-attached biofilms

To establish mixed-culture biofilms, 100 µL overnight LB monoculture of each strain was added to individual anaerobic tubes containing 10 mL SBM (30 mM D,L-Lactate and 40 mM fumarate) and grown at 30°C until mid-exponential phase. 1.1 mL of anaerobic mid-exponential *gfp*$^+$ was added to 10 mL anaerobic Δ*llpR* to make a 90:10

mix for inoculation. 1 mL of the inoculum was then added to each of three bioreactor chambers containing filtered SBM with 30 mM D,L-lactate and 40 mM fumarate. A control bioreactor containing *gfp*$^+$ alone was prepared similarly. Working electrodes were poised at 242 mV vs SHE and respiration rate was measured by chronoamperometry. When the respiration rate plateaued at 147 hours, filtered SBM containing 2 mM L-lactate was fed into the chambers by peristaltic pump at a rate of 1.35 mL/hr. Beginning 42 hours after starting continuous media feed, 1-2 mL samples were taken at regular time points and measured undiluted by flow cytometry.

Flow cytometry

All measurements were conducted on a FACSCalibur flow cytometer (Becton Dickson), equipped with 488 nm and 640 nm lasers, using the FL1 green detection channel through a 530/30 filter. Flow rates were set to 35 μL/min and samples were taken in 53 second passes. GFP and non-GFP expressing populations were gated based on control cultures containing 100% *gfp*$^+$, using commercial FlowJo software.

Confocal microscopy

Graphite electrodes containing biofilms were harvested from bioreactor chambers and stained with 5 μM SYTO® dye 41 (ThermoFisher) in filtered SBM. Following 30 min staining, biofilms were imaged on a Nikon A1 confocal microscope.

Electrode biofilm growth rate determinations

Three-electrode chambers containing filtered SBM with 30 mM D,L-lactate and 40mM fumarate were inoculated separately with mid-exponential anaerobic *gfp*$^+$ or Δ*llpR.* Two bioreactors were used for each strain. After 180 hours when respiration rate had plateaued, filtered SBM containing 2 mM L-lactate and 250 nM riboflavin was fed at an average rate of 1.34±0.08 mL/hr. Flow cytometry measurements on planktonic samples were taken at 279 and 300 hours post-inoculation. Electrodes were harvested for staining and imaging at 301 hours post-inoculation. Randomly subsampled regions of 100x images (examples in Fig 4.8) from each electrode were used to count cells within FIJI software (Schindelin et al., 2012) using the Cell Counter plugin. Cell division rates

were calculated from planktonic cell concentrations (derived from flow cytometry counts), medium flow rates, and total number of attached cells per electrode (extrapolated from cell counts on confocal micrographs). Since no measurable planktonic division was occurring, dilution rate did not determine growth rate as in a chemostat. Thus, the total number of cells produced per hour from the electrode and lost to the planktonic phase must match the rate of cells lost from the planktonic phase at steady state due to continuous flow.

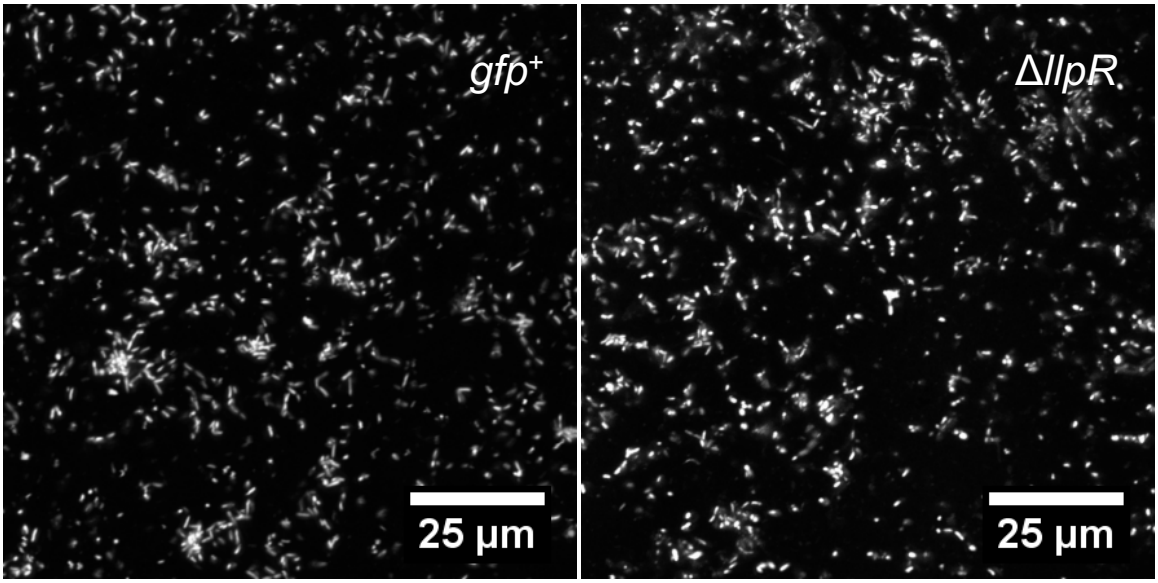

Fig 4.8 Representative confocal microscopy maximum intensity projections of anodic biofilms. *gfp*$^+$ (left) and Δ*llpR* (right) after 301 hours growth under strict anaerobic conditions.

Per capita current measurements

Per capita current production for each strain was determined by dividing the total current produced by the total protein attached to the working electrode surface within a given bioreactor. Briefly, the carbon electrodes were carefully removed from bioreactors and placed in 2 ml microcentrifuge tubes containing SBM medium with no donor or acceptor. Tubes were inverted once to remove loosely attached cells from the electrode surface before electrodes were moved to a microcentrifuge tube containing 1 ml of 0.2 N NaOH. Cells still attached to the electrode surface were lysed by boiling the washed electrodes in 1 ml of 0.5 N NaOH for ten minutes, agitating once after five minutes. The total protein attached to the electrodes was measured using the Pierce bicinchoninic acid

protein assay kit (Thermo Scientific, Rockford, IL) after an appropriate dilution of the cell lysate.

Three separate experiments with duplicates for each strain were performed for a total of 6 replicates each. There was significant batch-to-batch variation for both strains among experimental replicates, with per capita currents ranges of 0.06-0.38 μA/μg for Δ*llpR* and 0.19-0.60 μA/μg for gfp^+. However, the ratios of the per capita currents of Δ*llpR* to gfp^+ were consistent between batches. Therefore, the final per capita current ratio (0.53 ± 0.05) is an average of pairwise comparisons for all replicates with standard error mean. Two separate paired t-tests were conducted accounting for each possible pairing of replicates, and the highest resulting p-value is reported.

4.7 Acknowledgements

We thank Aunica Kane and Evan Brutinel for the strain constructs, and Komal Joshi and Geoff Harms for the design and construction of the batch-fed bioreactors. **Funding:** We thank the BioTechnology Institute and Biocatalysis Initiative at the University of Minnesota for initial funding for this project. This work was funded in part by the Office of Naval Research (Awards N00014-12-1-0309 and N00014-13-1-0552 to JAG). **Author contributions:** A.M.D., J. A. G. and D. R. B. conceived of the project. S. P. M. and C. E. L. developed the experimental system. E. D. K. and C. E. L. modified the bioreactor for continuous flow and E. D. K. completed the final long-term experiments. E. D. K and A. M. D wrote the manuscript and all authors help edited it.

Chapter 5 – Conclusions and Future Directions

This thesis on *Shewanella* is a collection of three variations on the theme of respiration, which is the defining feature that drives research into this organism. Through these approaches, we have come to three very different sets of questions and findings.

Chapter 2 was an interrogation into a specific support pathway in respiration, that of flavin secretion and utilization by redox-active flavoproteins. This chapter demonstrates that flavin secretion not only has an unexpectedly small metabolic cost for *Shewanella* but is essential for full periplasmic flavoprotein function. This possibly reframes our understanding of the utility of secreted flavin electron shuttles as a happy accident; a useful outcome from an otherwise necessary task. Additionally, it is very interesting that no growth defects were seen during fumarate or urocanate respiration in Δ*ushA* mutants, as it was assumed UshA-driven hydrolysis of secreted FAD to FMN and AMP allows for adenosine recovery. It is possible a defect is indeed present in the Δ*ushA* strain, but that it is too small to be seen by simple growth curves. Competition experiments between Δ*ushA* and WT could be conducted to tease out any possible fitness defects, but these might be complicated by a potential community benefit of UshA-driven FAD hydrolysis in the WT strain. Another puzzling result was that despite being unable to acquire exogenous flavins, Δ*bfe* mutants did not have a severe growth defect on fumarate, suggesting the presence of a supplementary or nonspecific mechanism for flavin secretion that also avoids hydrolysis by UshA before allowing for acquisition by periplasmic flavoproteins. Evidently, much work is needed to fully characterize mechanisms behind periplasmic flavin cofactor acquisition in *Shewanella.* A potential chaperone to target is ApbE, as it is a known flavinylation factor and binds FAD with high affinity, potentially acting to sequester and target secreted flavins toward flavoproteins. However, no link has been made or even suggested between ApbE and noncovalent FAD acquisition by flavoproteins. While we have recently generated a Δ*apbE* strain, and preliminary results show a defect under fumarate respiration, these cannot be separated from possible effects of *apbE* deletion on maturation of other flavoproteins such as NADH-dehydrogenases. Enzyme level work such as methyl viologen experiments or in vitro assays with purified FccA and ApbE will better discern whether FAD chaperone activity exists for ApbE.

Chapter 3 is much more broad, and is concerned with the question of what happens when respiration stops for *Shewanella.* How does this organism cope with respiratory stress? Using a tested, but still poorly understood, mechanism for artificially maintaining life for *Shewanella* – a light-driven proton pump – we provided a comparative control to explore at genome scale, the physiological factors that define death and survival under respiratory stress. General findings from this high-throughput screen suggest that severe cell envelope stress is experienced by all cells during electron acceptor limitation, that death in this condition is likely to be predominantly stochastic in nature, and that cells that happen to survive have shifts in central metabolism indicating an energy conserving strategy. Although no genetic elements were found that would suggest programmed cell death was occurring in this condition (e.g. prophage-encoded, or innate cell lysis machinery), it is nonetheless interesting that lysis of the population potentially set up conditions in which surviving cells maintained prolonged viability or even grew. However, whether it was specifically lysis, shifts in central metabolism, or both that enabled survival after electron acceptor depletion is unclear. Survival assays in which *S. oneidensis* is placed spent medium from light-grown or dark-grown cultures, would be effective in determining whether lysis is altruistic. In another case where lysis has been noted for *S. oneidensis,* that occurring during biofilm development, it is indeed an altruistic behavior as it appears to set up a surface matrix of eDNA to which cells can more effectively adhere (Binnenkade et al., 2014; Gödeke et al., 2011). However, in this case the behavior is also programmed, as the lysis is driven by prophages.

A survival benefit afforded to mutants with formate dehydrogenase activity knockout was expected as it facilitates pyruvate fermentation, which was further validated experimentally. However, fitness benefits in mutants with tungstate uptake systems was unexpected and points to tungsten, rather than molybdenum, as the metal cofactor in at least one formate dehydogenase alpha subunit in *S. oneidensis.* Previous protein work in another lab also strongly suggested this to be the case, but further physiological study on the contribution of tungsten to formate metabolism is warranted, particularly comparative formate utilization and fitness assays in constructed mutants containing tungstate and molybdate uptake system defects. Another set of findings suggest that sodium pumping is important for survival under acceptor limitation even for

PMF-supplemented cells, either via SMF generation with unknown utility specific to this condition, or by regulating pH homeostasis through sodium/proton antiporters. How SMF is utilized under this condition is unanswered, and future steps to be taken in this regard are outlined in Chapter 3. Finally, one big question that remains is whether potentially useful information was missed in this screen due to mutant loss during library outgrowth. The design of this high-throughput screen yielded valuable results, but rare mutants, those with strong growth defects but potentially high survival benefits, and those with real-but-mild survival defects/benefits may have easily been masked in the data, due to inherent flaws present in transferring a culture made up of majority dead cells, then sequencing the outgrowth. A new JG3020:tn library containing 50-100k unique mutants was recently generated and different variation on the death-phase Tn-seq was carried out. Rather than transferring death-phase cultures to new liquid medium for outgrowth, they were spread on large trays with minimal agar medium and allowed to grow as colonies. By growing ~1 million colonies per library and repeating the experiment, hopefully higher-quality data will be generated with minimal bottlenecking effects. Three libraries were generated per experiment: (1) grown JG3020:tn cultures at peak density, (2) JG3020::tn incubated in the light from inoculation through death phase and plated at OD = 0.3, and (3) the same cultures incubated in the dark with the same treatment. DNA preparation for high-throughput sequencing is underway.

Chapter 4 leverages what is known about respiration and lactate metabolism in *S. oneidensis* to design a set of experiments asking whether competitive selection based on reproductive rate can be halted when cells grow attached to a surface. The basic premise behind this question is the expectation that when cells grow attached to a substrate in a manner that precludes daughtered cells from overtaking parents (e.g. in a manner similar to an epithelium in which progenitor cells constantly generate daughtered and eventually sloughed off epithelial cells), faster reproductive rates will not render any single cell more fit than another. We found that while two strains of *S. oneidensis* with very different growth rates conform to the competitive exclusion principle when grown planktonically, they remain at stable frequencies when grown as a thin biofilm using an electrode surface as the sole terminal electron acceptor (thus limiting growth strictly to the biofilm for simplified analysis). We confirmed that growth was indeed happening in

biofilms and inferred through multiple lines of evidence that each strain had growth rate differences in biofilms equivalent to those seen planktonically. This study has strong implications for biofilm growth as a natural driver for genetic diversity, along with applications in areas such as industrial fermentation, where a fermenter design incentivizing surface-attached growth could prevent strain degeneration and minimize the effects of microbial contamination. However more questions remain, particularly whether this type of growth could indeed prevent or moderate natural selection in a microbial community. Careful video microscopy of mixed mutant biofilms could provide a first line basis for a deeper understanding of the selective dynamics in this type of system. These types of experiments in organisms other than *Shewanella* or in biofilms that show strong surface attachment but are not reliant on the surface as a metabolic substrate, could be instrumental in determining the broader applications of our findings.

Bibliography

Abbas, C.A., Sibirny, A.A., 2011. Genetic Control of Biosynthesis and Transport of Riboflavin and Flavin Nucleotides and Construction of Robust Biotechnological Producers. *Microbiology and Molecular Biology Reviews* 75(2):321–60. https://doi.org/10.1128/mmbr.00030-10

Abellón-Ruiz, J., Kaptan, S.S., Baslé, A., Claudi, B., Bumann, D., Kleinekathöfer, U., Van Den Berg, B., 2017. Structural basis for maintenance of bacterial outer membrane lipid asymmetry. *Nature Microbiology* 2(12):1616–1623. https://doi.org/10.1038/s41564-017-0046-x

Aigle, A., Bonin, P., Iobbi-Nivol, C., Méjean, V., Michotey, V., 2017. Physiological and transcriptional approaches reveal connection between nitrogen and manganese cycles in *Shewanella algae* C6G3. *Scientific Reports* 7:44725. https://doi.org/10.1038/srep44725

Alves, M.N., Neto, S.E., Alves, A.S., Fonseca, B.M., Carrêlo, A., Pacheco, I., Paquete, C.M., Soares, C.M., Louro, R.O., 2015. Characterization of the periplasmic redox network that sustains the versatile anaerobic metabolism of *Shewanella oneidensis* MR-1. *Frontiers in Microbiology* 6:665. https://doi.org/10.3389/fmicb.2015.00665

Andersen, J.B., Sternberg, C., Poulsen, L.K., Bjørn, S.P., Givskov, M., Molin, S., 1998. New unstable variants of green fluorescent protein for studies of transient gene expression in bacteria. *Applied and Environmental Microbiology* 64(6):2240–2246.

Andreesen, J., Ljungdahl, L., 1973. Formate dehydrogenase of *Clostridium thermoaceticum*: incorporation of selenium 75, and the effects of selenite, molybdate, and tungstate on the enzyme. *Journal of Bacteriology* 116(2):867–873.

Andreesen, J., Makdessi, K., 2008. Tungsten, the surprisingly positively acting heavy metal element for prokaryotes. *Annals of the New York Academy of Sciences* 1125:215–229. https://doi.org/10.1196/annals.1419.003

Arkhipova, O. V., Meer, M. V., Mikoulinskaia, G. V., Zakharova, M. V., Galushko, A.S., Akimenko, V.K., Kondrashov, F.A., 2015. Recent origin of the methacrylate redox system in *Geobacter sulfurreducens* AM-1 through horizontal gene transfer. *PLoS ONE* 10(5):e0125888. https://doi.org/10.1371/journal.pone.0125888

Baarda, B.I., Zielke, R.A., Van, A. Le, Jerse, A.E., Sikora, A.E., 2019. *Neisseria gonorrhoeae* MlaA influences gonococcal virulence and membrane vesicle production. *PLoS Pathogens* 15(3):e1007385. https://doi.org/10.1371/journal.ppat.1007385

Balch, W.E., Fox, G.E., Magrum, L.J., Woese, C.R., Wolfe, R.S., 1979. Methanogens: reevaluation of a unique biological group. *Microbiological reviews* 43(2):260–296.

Baltzis, B.C., Fredrickson, A.G., 1983. Competition of two microbial populations for a single resource in a chemostat when one of them exhibits wall attachment. *Biotechnology and Bioengineering* 25(10):2419–2439. https://doi.org/10.1002/bit.260251012

Bamann, C., Bamberg, E., Wachtveitl, J., Glaubitz, C., 2014. Proteorhodopsin. *Biochimica et Biophysica Acta* 1837:614–625. https://doi.org/10.1016/j.bbabio.2013.09.010

Barchinger, S.E., Pirbadian, S., Sambles, C., Baker, C.S., Leung, K.M., Burroughs, N.J., El-Naggar, M.Y., Golbeck, J.H., 2016. Regulation of gene expression in *Shewanella oneidensis* MR-1 during electron acceptor limitation and bacterial nanowire

formation. *Applied and Environmental Microbiology* 82(17):5428–43. https://doi.org/10.1128/AEM.01615-16

Baron, D., LaBelle, E., Coursolle, D., Gralnick, J.A., Bond, D.R., 2009. Electrochemical measurement of electron transfer kinetics by *Shewanella oneidensis* MR-1. *Journal of Biological Chemistry* 284(42):28865–28873. https://doi.org/10.1074/jbc.M109.043455

Beck, B.J., Downs, D.M., 1998. The apbE gene encodes a lipoprotein involved in thiamine synthesis in *Salmonella typhimurium*. *Journal of Bacteriology* 180(4):885–91.

Belchik, S.M., Kennedy, D.W., Dohnalkova, A.C., Wang, Y., Sevinc, P.C., Wu, H., Lin, Y., Lu, H.P., Fredrickson, J.K., Shi, L., 2011. Extracellular reduction of hexavalent chromium by cytochromes MtrC and OmcA of *Shewanella oneidensis* MR-1. *Applied and Environmental Microbiology* 77(12):4035–41. https://doi.org/10.1128/AEM.02463-10

Beliaev, A.S., Klingeman, D.M., Klappenbach, J.A., Wu, L., Romine, M.F., Tiedje, J.M., Nealson, K.H., Fredrickson, J.K., Zhou, J., 2005. Global transcriptome analysis of *Shewanella oneidensis* MR-1 exposed to different terminal electron acceptors. *Journal of Bacteriology* 187:7138–7145. https://doi.org/10.1128/JB.187.20.7138-7145.2005

Bennett, B.D., Brutinel, E.D., Gralnick, J.A., 2015. A ferrous iron exporter mediates iron resistance in *Shewanella oneidensis* MR-1. *Applied and Environmental Microbiology* 81(22):7938–7944. https://doi.org/10.1128/AEM.02835-15

Bennett, B.D., Redford, K.E., Gralnick, J.A., 2018a. Survival of anaerobic Fe^{2+} stress requires the ClpXP protease. *Journal of Bacteriology* 200(8):e00671-17. https://doi.org/10.1128/JB.00671-17

Bennett, B.D., Redford, K.E., Gralnick, J.A., 2018b. MgtE homolog FicI acts as a secondary ferrous iron importer in *Shewanella oneidensis* strain MR-1. *Applied and Environmental Microbiology* 84(6):e01245-17. https://doi.org/10.1128/AEM.01245-17

Bernsel, A., Viklund, H., Hennerdal, A., Elofsson, A., 2009. TOPCONS: Consensus prediction of membrane protein topology. *Nucleic Acids Research* 37(suppl. 2):W465–W468. https://doi.org/10.1093/nar/gkp363

Bertsova, Y. V., Fadeeva, M.S., Kostyrko, V.A., Serebryakova, M. V., Baykov, A.A., Bogachev, A. V., 2013. Alternative pyrimidine biosynthesis protein ApbE is a flavin transferase catalyzing covalent attachment of FMN to a threonine residue in bacterial flavoproteins. *Journal of Biological Chemistry* 288(20):14276–14286. https://doi.org/10.1074/jbc.M113.455402

Binnenkade, L., Teichmann, L., Thormanna, K.M., 2014. Iron triggers λSo prophage induction and release of extracellular DNA in *Shewanella oneidensis* MR-1 biofilms. *Applied and Environmental Microbiology* 80(17):5304–5316. https://doi.org/10.1128/AEM.01480-14

Bogachev, A. V., Bertsova, Y. V., Bloch, D.A., Verkhovsky, M.I., 2012. Urocanate reductase: Identification of a novel anaerobic respiratory pathway in *Shewanella oneidensis* MR-1. *Molecular Microbiology* 86(6):1452–1463. https://doi.org/10.1111/mmi.12067

Bogachev, A. V, Baykov, A.A., Bertsova, Y. V, 2018. Flavin transferase: the maturation

factor of flavin-containing oxidoreductases. *Biochemical Society transactions* 46(5):1161–1169. https://doi.org/10.1042/BST20180524
Braun, V., 1975. Covalent lipoprotein from the outer membrane of *Escherichia coli*. *BBA - Reviews on Biomembranes* 415(3):335–77. https://doi.org/10.1016/0304-4157(75)90013-1
Briers, Y., Peeters, L.M., Volckaert, G., Lavigne, R., 2011. The lysis cassette of bacteriophage ϕKMV encodes a signal-arrest-release endolysin and a pinholin. *Bacteriophage* 1(1):25–30. https://doi.org/10.4161/bact.1.1.14868
Brock, T.D., 1961. Christian Gram - The differential staining of Schizomyctes in tissue sections and in dried preparations. In: Milestones in Microbiology. Prentice-Hall International, Inc., Englewood Cliffs, N.J., pp. 215–218.
Brutinel, E.D., Gralnick, J.A., 2012a. Shuttling happens: Soluble flavin mediators of extracellular electron transfer in *Shewanella*. *Applied Microbiology and Biotechnology* 93(1):41–48. https://doi.org/10.1007/s00253-011-3653-0
Brutinel, E.D., Gralnick, J.A., 2012b. Anomalies of the anaerobic tricarboxylic acid cycle in *Shewanella oneidensis* revealed by Tn-seq. *Molecular Microbiology* 86(2):273–283. https://doi.org/10.1111/j.1365-2958.2012.08196.x
Brutinel, E.D., Gralnick, J.A., 2012c. Preferential utilization of D-lactate by *Shewanella oneidensis*. *Applied and Environmental Microbiology* 78(23):8474–8476. https://doi.org/10.1128/AEM.02183-12
Bursac, T., Gralnick, J.A., Gescher, J., 2017. Acetoin production via unbalanced fermentation in *Shewanella oneidensis*. *Biotechnology and Bioengineering* 114(6):1283–1289. https://doi.org/10.1002/bit.26243
Cascales, E., Gavioli, M., Sturgis, J.N., Lloubes, R., 2000. Proton motive force drives the interaction of the inner membrane TolA and outer membrane Pal proteins in *Escherichia coli*. *Molecular Microbiology* 38(4):904–15. https://doi.org/10.1046/j.1365-2958.2000.02190.x
Catalão, M.J., Gil, F., Moniz-Pereira, J., São-José, C., Pimentel, M., 2013. Diversity in bacterial lysis systems: Bacteriophages Show the way. *FEMS Microbiology Reviews* 37:554–571. https://doi.org/10.1111/1574-6976.12006
Chao, L., 2010. A model for damage load and its implications for the evolution of bacterial aging. *PLoS Genetics* 6(8):e1001076. https://doi.org/10.1371/journal.pgen.1001076
Chen, Y., Wang, F., 2015. Insights on nitrate respiration by *Shewanella*. *Frontiers in Marine Science* 1:80. https://doi.org/10.3389/fmars.2014.00080
Chong, Z.S., Woo, W.F., Chng, S.S., 2015. Osmoporin OmpC forms a complex with MlaA to maintain outer membrane lipid asymmetry in *Escherichia coli*. *Molecular Microbiology* 98(6):1133–46. https://doi.org/10.1111/mmi.13202
Coelho, M., Dereli, A., Haese, A., Kühn, S., Malinovska, L., Desantis, M.E., Shorter, J., Alberti, S., Gross, T., Tolić-Nørrelykke, I.M., 2013. Fission yeast does not age under favorable conditions, but does so after stress. *Current Biology* 23(19):1844–52. https://doi.org/10.1016/j.cub.2013.07.084
Connell, J.H., 1978. Diversity in tropical rain forests and coral reefs. *Science* 199(4335):1302–10. https://doi.org/10.1126/science.199.4335.1302
Coursolle, D., Baron, D.B., Bond, D.R., Gralnick, J.A., 2010. The Mtr respiratory pathway is essential for reducing flavins and electrodes in *Shewanella oneidensis*.

Journal of Bacteriology 192(2):467–474. https://doi.org/10.1128/JB.00925-09
Coursolle, D., Gralnick, J.A., 2010. Modularity of the Mtr respiratory pathway of *Shewanella oneidensis* strain MR-1. *Molecular Microbiology* 77(4):995–1008. https://doi.org/10.1111/j.1365-2958.2010.07266.x
Covington, E.D., Gelbmann, C.B., Kotloski, N.J., Gralnick, J.A., 2010. An essential role for UshA in processing of extracellular flavin electron shuttles by *Shewanella oneidensis*. *Molecular Microbiology* 78(2):519–532. https://doi.org/10.1111/j.1365-2958.2010.07353.x
Davies, C., Taylor, A.J., Elmi, A., Winter, J., Liaw, J., Grabowska, A.D., Gundogdu, O., Wren, B.W., Kelly, D.J., Dorrell, N., 2019. Sodium Taurocholate Stimulates Campylobacter jejuni Outer Membrane Vesicle Production via Down-Regulation of the Maintenance of Lipid Asymmetry Pathway. *Frontiers in cellular and infection microbiology* 9:177. https://doi.org/10.3389/fcimb.2019.00177
Davies, J.A., 2017. Characterisation of the reversible formate dehydrogenases of *Shewanella*. University of East Anglia.
Davison, B.H., Stephanopoulos, G., 1986. Coexistence of *S. cerevisiae* and *E. coli* in chemostat under substrate competition and product inhibition. *Biotechnology and Bioengineering* 28(11):1742–1752. https://doi.org/10.1002/bit.260281119
Derby, H.A., Hammer, B.W., 1931. Bacteriology of butter IV. Bacteriological studies on surface taint butter. *Research Bulletin (Iowa Agriculture and Home Economics Experiment Station* 11(145):1.
Dioumaev, A.K., Brown, L.S., Shih, J., Spudich, E.N., Spudich, J.L., Lanyi, J.K., 2002. Proton transfers in the photochemical reaction cycle of proteorhodopsin. *Biochemistry* 41:5348–5358. https://doi.org/10.1021/bi025563x
Dörr, T., Möll, A., Chao, M.C., Cava, F., Lam, H., Davis, B.M., Waldor, M.K., 2014. Differential Requirement for PBP1a and PBP1b in In Vivo and In Vitro Fitness of *Vibrio cholerae*. *Infection and Immunity* 82(5):2115–24. https://doi.org/10.1128/iai.00012-14
Duhl, K.L., Tefft, N.M., TerAvest, M.A., 2018. *Shewanella oneidensis* MR-1 utilizes both sodium- and proton-pumping NADH dehydrogenases during aerobic growth. *Applied and Environmental Microbiology* 84(12):e00415-18. https://doi.org/10.1128/AEM.00415-18
Dykhuizen, D.E., Hartl, D.L., 1983. Selection in Chemostats. *Microbiology Reviews* 47(2):150–168.
Edwards, M.J., Baiden, N.A., Johs, A., Tomanicek, S.J., Liang, L., Shi, L., Fredrickson, J.K., Zachara, J.M., Gates, A.J., Butt, J.N., Richardson, D.J., Clarke, T.A., 2014. The X-ray crystal structure of *Shewanella oneidensis* OmcA reveals new insight at the microbe-mineral interface. *FEBS Letters* 588(10):1886–90. https://doi.org/10.1016/j.febslet.2014.04.013
Edwards, M.J., White, G.F., Norman, M., Tome-Fernandez, A., Ainsworth, E., Shi, L., Fredrickson, J.K., Zachara, J.M., Butt, J.N., Richardson, D.J., Clarke, T.A., 2015. Redox Linked Flavin Sites in Extracellular Decaheme Proteins Involved in Microbe-Mineral Electron Transfer. *Scientific Reports* 5:11677. https://doi.org/10.1038/srep11677
Flynn, J.M., Ross, D.E., Hunt, K.A., Bond, D.R., Gralnick, J.A., 2010. Enabling unbalanced fermentations by using engineered electrode-interfaced bacteria. *mBio*

1(5):e00190-10. https://doi.org/10.1128/mBio.00190-10
Fonseca, B.M., Paquete, C.M., Neto, S.E., Pacheco, I., Soares, C.M., Louro, R.O., 2013. Mind the gap: cytochrome interactions reveal electron pathways across the periplasm of *Shewanella oneidensis* MR-1. *Biochemical Journal* 449(1):101 LP – 108. https://doi.org/10.1042/BJ20121467
Fredrickson, J.K., Romine, M.F., Beliaev, A.S., Auchtung, J.M., Driscoll, M.E., Gardner, T.S., Nealson, K.H., Osterman, A.L., Pinchuk, G., Reed, J.L., Rodionov, D. a, Rodrigues, J.L.M., Saffarini, D. a, Serres, M.H., Spormann, A.M., Zhulin, I.B., Tiedje, J.M., 2008. Towards environmental systems biology of *Shewanella*. *Nat. Rev. Microbiol.* 6:592–603. https://doi.org/10.1038/nrmicro1947
Freter, R., Stauffer, E., Cleven, D., Holdeman, L. V., Moore, W.E., 1983. Continuous-flow cultures as in vitro models of the ecology of large intestinal flora. *Infection and Immunity* 39(2):666–675.
Fuhrman, J.A., Schwalbach, M.S., Stingl, U., 2008. Proteorhodopsins: an array of physiological roles? *Nature reviews. Microbiology* 6(6):488–494. https://doi.org/10.1038/nrmicro1893
Futayama, D.J., 2009. Evolution, 2nd ed. Sinauer Associates, Sunderland, MA.
Gao, T., Meng, Q., Gao, H., 2017. Thioesterase YbgC affects motility by modulating c-di-GMP levels in *Shewanella oneidensis*. *Scientific Reports* 7(1):3932. https://doi.org/10.1038/s41598-017-04285-5
Gause, G., 1932. Experimental studies on the struggle for existence I. Mixed population of two species of yeast. *Journal of Experimental Biology* 9:389–402. https://doi.org/10.1097/00010694-193602000-00018
Gause, G.F., 1960. The Struggle for Existence. Williams and Wilkins, Baltimore, MD.
Gerding, M.A., Ogata, Y., Pecora, N.D., Niki, H., De Boer, P.A.J., 2007. The trans-envelope Tol-Pal complex is part of the cell division machinery and required for proper outer-membrane invagination during cell constriction in *E. coli*. *Molecular Microbiology* 63(4):1008–25. https://doi.org/10.1111/j.1365-2958.2006.05571.x
Gödeke, J., Paul, K., Lassak, J., Thormann, K.M., 2011. Phage-induced lysis enhances biofilm formation in *Shewanella oneidensis* MR-1. *The ISME journal* 5:613–626. https://doi.org/10.1038/ismej.2010.153
Gómez-Consarnau, L., Akram, N., Lindell, K., Pedersen, A., Neutze, R., Milton, D.L., González, J.M., Pinhassi, J., 2010. Proteorhodopsin phototrophy promotes survival of marine bacteria during starvation. *PLoS Biology* 8(4):e1000358. https://doi.org/10.1371/journal.pbio.1000358
Gómez-Consarnau, L., González, J.M., Coll-Lladó, M., Gourdon, P., Pascher, T., Neutze, R., Pedrós-Alió, C., Pinhassi, J., 2007. Light stimulates growth of proteorhodopsin-containing marine Flavobacteria. *Nature* 445:210–213. https://doi.org/10.1038/nature05381
Graentzdoerffer, A., Rauh, D., Pich, A., Andreesen, J.R., 2003. Molecular and biochemical characterization of two tungsten- and selenium-containing formate dehydrogenases from *Eubacterium acidaminophilum* that are associated with components of an iron-only hydrogenase. *Archives of microbiology* 179(2):116–130. https://doi.org/10.1007/s00203-002-0508-1
Gram, H.C., 1884. Über die isolierte Färbung der Schizomyceten in Schnitt- und Trockenpräparaten. *Fortschritte der Medizin*.

Gray, A.N., Egan, A.J.F., van't Veer, I.L., Verheul, J., Colavin, A., Koumoutsi, A., Biboy, J., Altelaar, M.A.F., Damen, M.J., Huang, K.C., Simorre, J.P., Breukink, E., den Blaauwen, T., Typas, A., Gross, C.A., Vollmer, W., 2015. Coordination of peptidoglycan synthesis and outer membrane constriction during *Escherichia coli* cell division. *eLife* 4:e07118. https://doi.org/10.7554/eLife.07118

Grizot, S., Salem, M., Vongsouthi, V., Durand, L., Moreau, F., Dohi, H., Vincent, S., Escaich, S., Ducruix, A., 2006. Structure of the *Escherichia coli* Heptosyltransferase WaaC: Binary Complexes with ADP AND ADP-2-deoxy-2-fluoro Heptose. *Journal of Molecular Biology* 363(2):383–94. https://doi.org/10.1016/j.jmb.2006.07.057

Gründling, A., Manson, M.D., Young, R., 2001. Holins kill without warning. *Proceedings of the National Academy of Sciences of the United States of America* 98:9348–9352. https://doi.org/10.1073/pnas.151247598

Hardin, G., 1960. The competitive exclusion principle. *Science (New York, N.Y.)* 131:1292–1297. https://doi.org/10.1126/science.131.3409.1292

Harris, A.J., 2014. Development and application of variable strength expression vectors in Shewanella oneidensis MR-1. University of Minnesota.

Hartl, D.L., 2000. A Primer of Population Genetics, 3rd ed. Sinauer Associates, Sunderland, MA.

Hau, H.H., Gilbert, A., Coursolle, D., Gralnick, J.A., 2008. Mechanism and consequences of anaerobic respiration of cobalt by *Shewanella oneidensis strain* MR-1. *Applied and Environmental Microbiology* 74:6880–6886. https://doi.org/10.1128/AEM.00840-08

Hau, H.H., Gralnick, J.A., 2007. Ecology and biotechnology of the genus *Shewanella*. *Annual review of microbiology* 61:237–258. https://doi.org/10.1146/annurev.micro.61.080706.093257

Herbert, D., Elsworth, R., Telling, R.C., 1956. The Continuous Culture of Bacteria; a Theoretical and Experimental Study. *Journal of General Microbiology* 14:601–622. https://doi.org/10.1099/00221287-14-3-601

Hobot, J.A., Carlemalm, E., Villiger, W., Kellenberger, E., 1984. Periplasmic gel: New concept resulting from the reinvestigation of bacterial cell envelope ultrastructure by new methods. *Journal of Bacteriology* 160(1):143–52.

Hughes, G.W., Hall, S.C.L., Laxton, C.S., Sridhar, P., Mahadi, A.H., Hatton, C., Piggot, T.J., Wotherspoon, P.J., Leney, A.C., Ward, D.G., Jamshad, M., Spana, V., Cadby, I.T., Harding, C., Isom, G.L., Bryant, J.A., Parr, R.J., Yakub, Y., Jeeves, M., Huber, D., Henderson, I.R., Clifton, L.A., Lovering, A.L., Knowles, T.J., 2019. Evidence for phospholipid export from the bacterial inner membrane by the Mla ABC transport system. *Nature microbiology*. https://doi.org/10.1038/s41564-019-0481-y

Hunt, K.A., Flynn, J.M., Naranjo, B., Shikhare, I.D., Gralnick, J.A., 2010. Substrate-level phosphorylation is the primary source of energy conservation during anaerobic respiration of *Shewanella oneidensis* strain MR-1. *Journal of Bacteriology* 192:3345–3351. https://doi.org/10.1128/JB.00090-10

Hutchinson, G.E., 1961. The Paradox of the Plankton. *The American Naturalist* 95(882):137–45. https://doi.org/10.1086/282171

Inoue, K., Ono, H., Abe-Yoshizumi, R., Yoshizawa, S., Ito, H., Kogure, K., Kandori, H., 2013. A light-driven sodium ion pump in marine bacteria. *Nature Communications* 4:1678. https://doi.org/10.1038/ncomms2689

Jiang, S., Hur, H.-G., 2013. Effects of the anaerobic respiration of *Shewanella oneidensis* MR-1 on the stability of extracellular U(VI) nanofibers. *Microbes and environments / JSME* 28:312–315. https://doi.org/10.1264/jsme2.ME12149

Johnson, E.T., Baron, D.B., Naranjo, B., Boad, D.R., Schmidt-Dannert, C., Gralnick, J.A., 2010. Enhancement of survival and electricity production in an engineered bacterium by light-driven proton pumping. *Applied and Environmental Microbiology* 76:4123–4129. https://doi.org/10.1128/AEM.02425-09

Juárez, O., Nilges, M.J., Gillespie, P., Cotton, J., Barquera, B., 2008. Riboflavin is an active redox cofactor in the Na^+-pumping NADH:quinone oxidoreductase (Na^+-NQR) from *Vibrio cholerae*. *Journal of Biological Chemistry* 283(48):33162–7. https://doi.org/10.1074/jbc.M806913200

Kane, A.L., 2016. Microbial Interactions: From Microbes to Minerals. University of Minnesota.

Kane, A.L., Brutinel, E.D., Joo, H., Maysonet, R., VanDrisse, C.M., Kotloski, N.J., Gralnick, J.A., 2016. Formate metabolism in *Shewanella oneidensis* generates proton motive force and prevents growth without an electron acceptor. *Journal of Bacteriology* 198(8):1337–1346. https://doi.org/10.1128/JB.00927-15

Kato, Y., Inoue, K., Kandori, H., 2015. Kinetic Analysis of H^+-Na^+ Selectivity in a Light-Driven Na^+-Pumping Rhodopsin. *Journal of Physical Chemistry Letters* 6(24):5111–5. https://doi.org/10.1021/acs.jpclett.5b02371

Katz, C., Ron, E.Z., 2008. Dual role of FtsH in regulating lipopolysaccharide biosynthesis in *Escherichia coli*. *Journal of Bacteriology* 190(21):7117–22. https://doi.org/10.1128/JB.00871-08

Kees, E.D., Pendleton, A.R., Paquete, C.M., Arriola, M.B., Kane, A.L., Kotloski, N.J., Intile, P.J., Gralnick, J.A., 2019. Secreted flavin cofactors for anaerobic respiration of fumarate and urocanate by *Shewanella oneidensis*: cost and role. *Applied and Environmental Microbiology* 85(16):e00852-19. https://doi.org/10.1128/aem.00852-19

Kim, H.J., Hyun, M.S., Chang, I.S., Kim, B.H., 1999. A microbial fuel cell type lactate biosensor using a metal-reducing bacterium, *Shewanella putrefaciens*. *Journal of Microbiology and Biotechnology* 9(3):365–7.

Kitayama, M., Koga, R., Kasai, T., Kouzuma, A., Watanabe, K., 2017. Structures, compositions, and activities of live *Shewanella* biofilms formed on graphite electrodes in electrochemical flow cells. *Applied and Environmental Microbiology* 83(17):e00903-17. https://doi.org/10.1128/AEM.00903-17

Klein, G., Lindner, B., Brabetz, W., Brade, H., Raina, S., 2009. *Escherichia coli* K-12 suppressor-free mutants lacking early glycosyltransferases and late acyltransferases. Minimal lipopolysaccharide structure and induction of envelope stress response. *Journal of Biological Chemistry* 284(23):15369–89. https://doi.org/10.1074/jbc.M900490200

Klein, G., Raina, S., 2019. Regulated Assembly of LPS, Its Structural Alterations and Cellular Response to LPS Defects. *International Journal of Molecular Sciences* 20(2):E356. https://doi.org/10.3390/ijms20020356

Koronakis, V., Sharff, A., Koronakis, E., Luisi, B., Hughes, C., 2000. Crystal structure of the bacterial membrane protein TolC central to multidrug efflux and protein export. *Nature* 405(6789):914–9. https://doi.org/10.1038/35016007

Kotloski, N.J., Gralnick, J.A., 2013. Flavin electron shuttles dominate extracellular electron transfer by *Shewanella oneidensis*. *mBio* 4(1):e00553-12. https://doi.org/10.1128/mBio.00553-12

Kovach, M.E., Elzer, P.H., Steven Hill, D., Robertson, G.T., Farris, M.A., Roop, R.M., Peterson, K.M., 1995. Four new derivatives of the broad-host-range cloning vector pBBR1MCS, carrying different antibiotic-resistance cassettes. *Gene* 166(1):175–6. https://doi.org/10.1016/0378-1119(95)00584-1

Kovach, M.E., Phillips, R.W., Elzer, P.H., Roop, R.M., Peterson, K.M., 1994. pBBR1MCS: A broad-host-range cloning vector. *BioTechniques* 16(5):800–2.

Kovalev, K., Polovinkin, V., Gushchin, I., Alekseev, A., Shevchenko, V., Borshchevskiy, V., Astashkin, R., Balandin, T., Bratanov, D., Vaganova, S., Popov, A., Chupin, V., Büldt, G., Bamberg, E., Gordeliy, V., 2019. Structure and mechanisms of sodium-pumping KR2 rhodopsin. *Science Advances* 5(4):eaav2671. https://doi.org/10.1126/sciadv.aav2671

Lambertsen, L., Sternberg, C., Molin, S., 2004. Mini-Tn7 transposons for site-specific tagging of bacteria with fluorescent proteins. *Environmental Microbiology* 6(7):726–32. https://doi.org/10.1111/j.1462-2920.2004.00605.x

Lanzer, M., Bujard, H., 1988. Promoters largely determine the efficiency of repressor action. *Proceedings of the National Academy of Sciences of the United States of America* 85(23):8973–8977. https://doi.org/10.1073/pnas.85.23.8973

Laukel, M., Chistoserdova, L., Lidstrom, M.E., Vorholt, J.A., 2003. The tungsten-containing formate dehydrogenase from *Methylobacterium extorquens* AM1: Purification and properties. *European Journal of Biochemistry* 270(2):325–33. https://doi.org/10.1046/j.1432-1033.2003.03391.x

Lenski, R.E., Hattingh, S.E., 1986. Coexistence of two competitors on one resource and one inhibitor: A chemostat model based on bacteria and antibiotics. *Journal of Theoretical Biology* 122(1):83–93. https://doi.org/10.1016/S0022-5193(86)80226-0

Lenski, R.E., Rose, M.R., Simpson, S.C., Tadler, S.C., 1991. Long-Term Experimental Evolution in *Escherichia coli* . I . Adaptation and Divergence During. *The American Naturalist* 138(November):1315–1341. https://doi.org/10.1086/285289

Lenski, R.E., Travisano, M., 1994. Dynamics of adaptation and diversification: a 10,000-generation experiment with bacterial populations. *Proceedings of the National Academy of Sciences* 91(15):6808–14. https://doi.org/10.1073/pnas.91.15.6808

Levin, B.R., Stewart, F.M., Chao, L., 1977. Resource-Limited Growth, Competition, and Predation: A Model and Experimental Studies with Bacteria and Bacteriophage. *The American Naturalist* 111(977):3–24. https://doi.org/10.1086/283134

Leys, D., Tsapin, A.S., Nealson, K.H., Meyer, T.E., Cusanovich, M.A., Van Beeumen, J.J., 1999. Structure and mechanism of the flavocytochrome c fumarate reductase of *Shewanella putrefaciens* MR-1. *Nature Structural Biology* 6(12):1113–1117. https://doi.org/10.1038/70051

Li, X., Wang, B., Feng, L., Kang, H., Qi, Y., Wang, J., Shi, Y., 2009. Cleavage of RseA by RseP requires a carboxyl-terminal hydrophobic amino acid following DegS cleavage. *Proceedings of the National Academy of Sciences* 106(35):14837–42. https://doi.org/10.1073/pnas.0903289106

Light, S.H., Su, L., Rivera-Lugo, R., Cornejo, J.A., Louie, A., Iavarone, A.T., Ajo-Franklin, C.M., Portnoy, D.A., 2018. A flavin-based extracellular electron transfer

mechanism in diverse Gram-positive bacteria. *Nature* 562(7725):140–144. https://doi.org/10.1038/s41586-018-0498-z
Lovley, D.R., Holmes, D.E., Nevin, K.P., 2004. Dissimilatory Fe(III) and Mn(IV) reduction. *Advances in Microbial Physiology* 49:219–286. https://doi.org/10.1016/S0065-2911(04)49005-5
Lunzer, M., Natarajan, A., Dykhuizen, D.E., Dean, A.M., 2002. Enzyme kinetics, substitutable resources and competition: From biochemistry to frequency-dependent selection in *lac*. *Genetics* 162(1):485–99.
MacArthur, R.H., 1958. Population Ecology of Some Warblers of Northeastern Coniferous Forests. *Ecology* 178(1):30–43. https://doi.org/10.2307/1931600
MacHeroux, P., Kappes, B., Ealick, S.E., 2011. Flavogenomics - A genomic and structural view of flavin-dependent proteins. *FEBS Journal* 278(15):2625–34. https://doi.org/10.1111/j.1742-4658.2011.08202.x
Maier, T.M., Myers, J.M., Myers, C.R., 2003. Identification of the gene encoding the sole physiological fumarate reductase in *Shewanella oneidensis* MR-1. *Journal of Basic Microbiology* 43(4):312–327. https://doi.org/10.1002/jobm.200390034
Malinverni, J.C., Silhavy, T.J., 2009. An ABC transport system that maintains lipid asymmetry in the Gram-negative outer membrane. *Proceedings of the National Academy of Sciences* 106(19):8009–14. https://doi.org/10.1073/pnas.0903229106
Marsili, E., Baron, D.B., Shikhare, I.D., Coursolle, D., Gralnick, J.A., Bond, D.R., 2008. *Shewanella* secretes flavins that mediate extracellular electron transfer. *Proceedings of the National Academy of Sciences of the United States of America* 105(10):3968–3973. https://doi.org/10.1073/pnas.0710525105
Masiá Canuto, M., Gutiérrez Rodero, F., 2002. Antifungal drug resistance to azoles and polyenes. *The Lancet infectious diseases* 2:550–563. https://doi.org/10.1016/S1473-3099(02)00371-7
McLean, J.S., Pinchuk, G.E., Geydebrekht, O. V., Bilskis, C.L., Zakrajsek, B.A., Hill, E.A., Saffarini, D.A., Romine, M.F., Gorby, Y.A., Fredrickson, J.K., Beliaev, A.S., 2008. Oxygen-dependent autoaggregation in *Shewanella oneidensis* MR-1. *Environmental Microbiology* 10(7):1861–76. https://doi.org/10.1111/j.1462-2920.2008.01608.x
Mevers, E., Su, L., Pishchany, G., Baruch, M., Cornejo, J., Hobert, E., Dimise, E., Ajo-Franklin, C.M., Clardy, J., 2019. An elusive electron shuttle from a facultative anaerobe. *eLife* 8:e48054. https://doi.org/10.7554/eLife.48054
Mitchell, A.C., Peterson, L., Reardon, C.L., Reed, S.B., Culley, D.E., Romine, M.R., Geesey, G.G., 2012. Role of outer membrane c-type cytochromes MtrC and OmcA in *Shewanella oneidensis* MR-1 cell production, accumulation, and detachment during respiration on hematite. *Geobiology* 10(4):355–70. https://doi.org/10.1111/j.1472-4669.2012.00321.x
Mitchell, P., 1961. Coupling of Phosphorylation to Electron and Hydrogen Transfer by a Chemi-Osmotic type of Mechanism. *Nature* 191(4784):144–148. https://doi.org/10.1038/191144a0
Moura, J.J.G., Brondino, C.D., Trincao, J., Romao, M.J., 2004. Mo and W bis-MGD enzymes: nitrate reductases and formate dehydrogenases. *Journal of biological inorganic chemistry* 9(7):791–799. https://doi.org/10.1007/s00775-004-0573-9
Myers, C.R., Nealson, K.H., 1988. Bacterial manganese reduction and growth with

manganese oxide as the sole electron acceptor. *Science* 240(4857):1319–1321. https://doi.org/10.1126/science.240.4857.1319
Nealson, K.H., Scott, J., 2006. Ecophysiology of the Genus *Shewanella*. In: Dworkin, M. (Ed.), The Prokaryotes. Springer Science, New York, pp. 1133–1151.
Nikaido, H., 2003. Molecular basis of bacterial outer membrane permeability revisited. *Microbiology and molecular biology reviews : MMBR*.
Niks, D., Hille, R., 2019. Molybdenum- and tungsten-containing formate dehydrogenases and formylmethanofuran dehydrogenases: Structure, mechanism, and cofactor insertion. *Protein Science* 28(1):111–22. https://doi.org/10.1002/pro.3498
Okamoto, A., Hashimoto, K., Nealson, K.H., Nakamura, R., 2013. Rate enhancement of bacterial extracellular electron transport involves bound flavin semiquinones. *Proceedings of the National Academy of Sciences* 110(19):7856–7861. https://doi.org/10.1073/pnas.1220823110
Okamoto, A., Kalathil, S., Deng, X., Hashimoto, K., Nakamura, R., Nealson, K.H., 2014. Cell-secreted flavins bound to membrane cytochromes dictate electron transfer reactions to surfaces with diverse charge and pH. *Scientific Reports* 4:5628. https://doi.org/10.1038/srep05628
Palovaara, J., Akram, N., Baltar, F., Bunse, C., Forsberg, J., Pedrós-Alió, C., González, J.M., Pinhassi, J., 2014. Stimulation of growth by proteorhodopsin phototrophy involves regulation of central metabolic pathways in marine planktonic bacteria. *Proceedings of the National Academy of Sciences of the United States of America* 111(35):E3650-8. https://doi.org/10.1073/pnas.1402617111
Park, T., Struck, D.K., Dankenbring, C.A., Young, R., 2007. The pinholin of lambdoid phage 21: Control of lysis by membrane depolarization. *Journal of Bacteriology* 189:9135–9139. https://doi.org/10.1128/JB.00847-07
Paulick, A., Koerdt, A., Lassak, J., Huntley, S., Wilms, I., Narberhaus, F., Thormann, K.M., 2009. Two different stator systems drive a single polar flagellum in *Shewanella oneidensis* MR-1. *Molecular Microbiology* 71:836–850. https://doi.org/10.1111/j.1365-2958.2008.06570.x
Pealing, S.L., Black, A.C., Manson, F.D.C., Ward, F.B., Reid, G.A., Chapman, S.K., 1992. Sequence of the Gene Encoding Flavocytochrome c from *Shewanella putrefaciens*: A Tetraheme Flavoenzyme That Is a Soluble Fumarate Reductase Related to the Membrane-Bound Enzymes from Other Bacteria. *Biochemistry* 31(48):12132–12140. https://doi.org/10.1021/bi00163a023
Petersen, T.N., Brunak, S., von Heijne, G., Nielsen, H., 2011. SignalP 4.0: discriminating signal peptides from transmembrane regions. *Nature Methods* 8:785–786. https://doi.org/10.1038/nmeth.1701
Petiti, M., Serrano, B., Faure, L., Lloubes, R., Mignot, T., Duché, D., 2019. Tol Energy-Driven Localization of Pal and Anchoring to the Peptidoglycan Promote Outer-Membrane Constriction. *Journal of Molecular Biology*. https://doi.org/10.1016/J.JMB.2019.05.039
Pham, T.H., Boon, N., Aelterman, P., Clauwaert, P., De Schamphelaire, L., Vanhaecke, L., De Maeyer, K., Höfte, M., Verstraete, W., Rabaey, K., 2008. Metabolites produced by *Pseudomonas* sp. enable a Gram-positive bacterium to achieve extracellular electron transfer. *Applied Microbiology and Biotechnology* 77(5):1119–29. https://doi.org/10.1007/s00253-007-1248-6

Pilyugin, S.S., Waltman, P., 1999. The Simple Chemostat with Wall Growth. *SIAM Journal on Applied Mathematics* 59(5):1552–1572. https://doi.org/10.1137/S0036139997326181

Pinchuk, G.E., Geydebrekht, O. V., Hill, E.A., Reed, J.L., Konopka, A.E., Beliaev, A.S., Fredrickson, J.K., 2011. Pyruvate and lactate metabolism by *Shewanella oneidensis* MR-1 under fermentation, oxygen limitation, and fumarate respiration conditions. *Applied and Environmental Microbiology* 77(23):8234–40. https://doi.org/10.1128/AEM.05382-11

Pirbadian, S., Barchinger, S.E., Leung, K.M., Byun, H.S., Jangir, Y., Bouhenni, R.A., Reed, S.B., Romine, M.F., Saffarini, D.A., Shi, L., Gorby, Y.A., Golbeck, J.H., El-Naggar, M.Y., 2014. *Shewanella oneidensis* MR-1 nanowires are outer membrane and periplasmic extensions of the extracellular electron transport components. *Proceedings of the National Academy of Sciences* 111(35):12883–12888. https://doi.org/10.1073/pnas.1410551111

Proenca, A.M., Rang, C.U., Buetz, C., Shi, C., Chao, L., 2018. Age structure landscapes emerge from the equilibrium between aging and rejuvenation in bacterial populations. *Nature Communications* 9(1):3722. https://doi.org/10.1038/s41467-018-06154-9

Raaijmakers, H., Macieira, S., Dias, J.M., Teixeira, S., Bursakov, S., Huber, R., Moura, J.J.G., Moura, I., Romão, M.J., 2002. Gene Sequence and the 1.8 Å Crystal Structure of the Tungsten-Containing Formate Dehydrogenase from *Desulfovibrio gigas*. *Structure* 10(9):1261–1272. https://doi.org/https://doi.org/10.1016/S0969-2126(02)00826-2

Raaijmakers, H., Teixeira, S., Dias, J.M., Almendra, M.J., Brondino, C.D., Moura, I., Moura, J.J.G., Romão, M.J., 2001. Tungsten-containing formate dehydrogenase from *Desulfovibrio gigas*: metal identification and preliminary structural data by multi-wavelength crystallography. *JBIC Journal of Biological Inorganic Chemistry* 6(4):398–404. https://doi.org/10.1007/s007750100215

Reddy, B.L., Saier, M.H., 2013. Topological and phylogenetic analyses of bacterial holin families and superfamilies. *Biochimica et Biophysica Acta - Biomembranes* 1828:2654–2671. https://doi.org/10.1016/j.bbamem.2013.07.004

Rice, K., Bayles, K., 2008. Molecular control of bacterial death and lysis. *Microbiology and molecular biology reviews : MMBR* 72:85–109. https://doi.org/10.1128/MMBR.00030-07

Rice, P., Longden, I., Bleasby, A., 2000. EMBOSS: the European Molecular Biology Open Software Suite. *Trends in genetics : TIG* 16:276–277. https://doi.org/10.1016/S0168-9525(00)02024-2

Rietschel, E.T., Kirikae, T., Schade, F.U., Mamat, U., Schmidt, G., Loppnow, H., Ulmer, A.J., Zähringer, U., Seydel, U., Di Padova, F., 1994. Bacterial endotoxin: molecular relationships of structure to activity and function. *FASEB journal* 8(2):217–25.

Roier, S., Zingl, F.G., Cakar, F., Durakovic, S., Kohl, P., Eichmann, T.O., Klug, L., Gadermaier, B., Weinzerl, K., Prassl, R., Lass, A., Daum, G., Reidl, J., Feldman, M.F., Schild, S., 2016. A novel mechanism for the biogenesis of outer membrane vesicles in Gram-negative bacteria. *Nature Communications* 7:10515. https://doi.org/10.1038/ncomms10515

Ross, D.E., Brantley, S.L., Tien, M., 2009. Kinetic characterization of OmcA and MtrC,

terminal reductases involved in respiratory electron transfer for dissimilatory iron reduction in *Shewanella oneidensis* MR-1. *Applied and Environmental Microbiology* 75(15):5218–26. https://doi.org/10.1128/AEM.00544-09

Ross, D.E., Flynn, J.M., Baron, D.B., Gralnick, J.A., Bond, D.R., 2011. Towards electrosynthesis in *Shewanella*: Energetics of reversing the Mtr pathway for reductive metabolism. *PLoS ONE* 6(2):e16649. https://doi.org/10.1371/journal.pone.0016649

Saltikov, C.W., Newman, D.K., 2003. Genetic identification of a respiratory arsenate reductase. *Proceedings of the National Academy of Sciences of the United States of America* 100:10983–10988. https://doi.org/10.1073/pnas.1834303100

Sani, R.K., Peyton, B.M., Dohnalkova, A., 2008. Comparison of uranium(VI) removal by *Shewanella oneidensis* MR-1 in flow and batch reactors. *Water Research* 42:2993–3002. https://doi.org/10.1016/j.watres.2008.04.003

Schicklberger, M., Sturm, G., Gescher, J., 2013. Genomic Plasticity Enables a secondary electron transport pathway in *Shewanella oneidensis*. *Applied and Environmental Microbiology* 79(4):1150–1159. https://doi.org/10.1128/AEM.03556-12

Schindelin, J., Arganda-Carreras, I., Frise, E., Kaynig, V., Longair, M., Pietzsch, T., Preibisch, S., Rueden, C., Saalfeld, S., Schmid, B., Tinevez, J.Y., White, D.J., Hartenstein, V., Eliceiri, K., Tomancak, P., Cardona, A., 2012. Fiji: An open-source platform for biological-image analysis. *Nature Methods* 9(7):676–682. https://doi.org/10.1038/nmeth.2019

Schuetz, B., Schicklberger, M., Kuermann, J., Spormann, A.M., Gescher, J., 2009. Periplasmic electron transfer via the c-type cytochromes MtrA and FccA of *Shewanella oneidensis* MR-1. *Applied and Environmental Microbiology* 75(24):7789–7796. https://doi.org/10.1128/AEM.01834-09

Sheng, L., Fein, J.B., 2014. Uranium reduction by *Shewanella oneidensis* MR-1 as a function of $NaHCO_3$ concentration: Surface complexation control of reduction kinetics. *Environmental Science & Technology* 48:3768–75. https://doi.org/10.1021/es5003692

Silhavy, T.J., Kahne, D., Walker, S., 2010. The bacterial cell envelope. *Cold Spring Harbor perspectives in biology* 2(5):a000414. https://doi.org/10.1101/cshperspect.a000414

Sohn, J., Grant, R.A., Sauer, R.T., 2007. Allosteric Activation of DegS, a Stress Sensor PDZ Protease. *Cell* 131(3):572–83. https://doi.org/10.1016/j.cell.2007.08.044

Steindler, L., Schwalbach, M.S., Smith, D.P., Chan, F., Giovannoni, S.J., 2011. Energy starved *Candidatus Pelagibacter ubique* substitutes light-mediated ATP production for endogenous carbon respiration. *PLoS ONE* 6:e19725. https://doi.org/10.1371/journal.pone.0019725

Stewart, F.M., Levin, B.R., 1973. Partitioning of resources and the outcome of interspecific competition: a model and some general considerations. *American Naturalist* 107(954):171–198.

Sturm, G., Richter, K., Doetsch, A., Heide, H., Louro, R.O., Gescher, J., 2015. A dynamic periplasmic electron transfer network enables respiratory flexibility beyond a thermodynamic regulatory regime. *ISME Journal* 9(8):1802–1811. https://doi.org/10.1038/ismej.2014.264

Sutterlin, H.A., Shi, H., May, K.L., Miguel, A., Khare, S., Huang, K.C., Silhavy, T.J.,

2016. Disruption of lipid homeostasis in the Gram-negative cell envelope activates a novel cell death pathway. *Proceedings of the National Academy of Sciences* 113(11):E1565-74. https://doi.org/10.1073/pnas.1601375113
Tamaki, S., Sato, T., Matsuhashi, M., 1971. Role of lipopolysaccharides in antibiotic resistance and bacteriophage adsorption of *Escherichia coli* K-12. *Journal of Bacteriology* 105(3):968–75.
Taylor, P., Pealing, S.L., Reid, G.A., Chapman, S.K., Walkinshaw, M.D., 1999. Structural and mechanistic mapping of a unique fumarate reductase. *Nature Structural Biology* 6(12):1108–1112. https://doi.org/10.1038/70045
Teal, T.K., Lies, D.P., Wold, B.J., Newman, D.K., 2006. Spatiometabolic stratification of *Shewanella oneidensis* biofilms. *Applied and Environmental Microbiology* 72(11):7324–7330. https://doi.org/10.1128/AEM.01163-06
Tefft, N.M., TerAvest, M.A., 2019. Reversing an Extracellular Electron Transfer Pathway for Electrode-Driven Acetoin Reduction. *ACS Synthetic Biology* 8(7):1590–1600. https://doi.org/10.1021/acssynbio.8b00498
Thöny-Meyer, 2002. Cytochrome c maturation: a complex pathway for a simple task? *Biochem Soc Trans* 30(4):633–638. https://doi.org/10.1042/BST0300633
Tilman, D., 1982. Resource Competition and Community Structure. Princeton University Press, NJ.
Trent, M.S., 2009. Biosynthesis and Membrane Assembly of Lipid A. In: Microbial Glycobiology - Structures, Relevance and Applications. Elsevier, pp. 1–5.
Valvano, M.A., Marolda, C.L., Bittner, M., Glaskin-Clay, M., Simon, T.L., Klena, J.D., 2000. The rfaE gene from *Escherichia coli* encodes a bifunctional protein involved in biosynthesis of the lipopolysaccharide core precursor ADP-L- glycero-D-manno-heptose. *Journal of Bacteriology* 182(2):488–97. https://doi.org/10.1128/JB.182.2.488-497.2000
van Opijnen, T., Bodi, K.L., Camilli, A., 2009. Tn-seq: high-throughput parallel sequencing for fitness and genetic interaction studies in microorganisms. *Nature methods* 6:767–772. https://doi.org/10.1038/nmeth.1377
von Canstein, H., Ogawa, J., Shimizu, S., Lloyd, J.R., 2008. Secretion of flavins by *Shewanella* species and their role in extracellular electron transfer. *Applied and environmental microbiology* 74(3):615–23. https://doi.org/10.1128/AEM.01387-07
Walsh, N.P., Alba, B.M., Bose, B., Gross, C.A., Sauer, R.T., 2003. OMP peptide signals initiate the envelope-stress response by activating DegS protease via relief of inhibition mediated by its PDZ domain. *Cell* 113(1):61–71. https://doi.org/10.1016/S0092-8674(03)00203-4
Walter, J.M., Greenfield, D., Bustamante, C., Liphardt, J., 2007. Light-powering *Escherichia coli* with proteorhodopsin. *Proceedings of the National Academy of Sciences of the United States of America* 104:2408–2412. https://doi.org/10.1073/pnas.0611035104
Wang, Q., Jones, A.A.D., Gralnick, J.A., Lin, L., Buie, C.R., 2019. Microfluidic dielectrophoresis illuminates the relationship between microbial cell envelope polarizability and electrochemical activity. *Historia da Historiografia* 5(1):eaat5564. https://doi.org/10.1126/sciadv.aat5664
Wang, Smith, Young, 2000. Holins: the protein clocks of bacteriophage infections. *Annual review of microbiology* 54:799–825.

https://doi.org/10.1146/annurev.micro.54.1.799
Wang, Z., Shi, Z., Shi, L., White, G.F., Richardson, D.J., Clarke, T.A., Fredrickson, J.K., Zachara, J.M., 2015. Effects of soluble flavin on heterogeneous electron transfer between surface-exposed bacterial cytochromes and iron oxides. *Geochimica et Cosmochimica Acta* 163:299–310. https://doi.org/10.1016/j.gca.2015.03.039
Webster, D.P., TerAvest, M.A., Doud, D.F.R., Chakravorty, A., Holmes, E.C., Radens, C.M., Sureka, S., Gralnick, J.A., Angenent, L.T., 2014. An arsenic-specific biosensor with genetically engineered *Shewanella oneidensis* in a bioelectrochemical system. *Biosensors and Bioelectronics* 62:320–324. https://doi.org/10.1016/j.bios.2014.07.003
White, G.F., Edwards, M.J., Gomez-Perez, L., Richardson, D.J., Butt, J.N., Clarke, T.A., 2016. Mechanisms of Bacterial Extracellular Electron Exchange. *Advances in Microbial Physiology* 68:87–138. https://doi.org/10.1016/bs.ampbs.2016.02.002
Wiser, M.J., Lenski, R.E., 2015. A comparison of methods to measure fitness in *Escherichia coli*. *PLoS ONE* 10(5). https://doi.org/10.1371/journal.pone.0126210
Xu, M., Struck, D.K., Deaton, J., Wang, I.-N., Young, R., 2004. A signal-arrest-release sequence mediates export and control of the phage P1 endolysin. *Proceedings of the National Academy of Sciences of the United States of America* 101:6415–6420. https://doi.org/10.1073/pnas.0400957101
Yi, X., Dean, A.M., 2013. Bounded population sizes, fluctuating selection and the tempo and mode of coexistence. *Proceedings of the National Academy of Sciences* 110(42):16945–50. https://doi.org/10.1073/pnas.1309830110
Young, R., 2014. Phage lysis: Three steps, three choices, one outcome. *Journal of Microbiology* 52(3):243–258. https://doi.org/10.1007/s12275-014-4087-z
Young, R., Wang, I.N., Roof, W.D., 2000. Phages will out: Strategies of host cell lysis. *Trends in Microbiology* 8(3):120–128. https://doi.org/10.1016/S0966-842X(00)01705-4
Yousif, S.Y., Broome-Smith, J.K., Spratt, B.G., Beveridge, T., Tropini, C., Salick, M., Crone, W.C., Gopinathan, A., Huang, K.C., Weibel, D.B., Al., E., 1985. Lysis of *Escherichia coli* by beta-lactam antibiotics: deletion analysis of the role of penicillin-binding proteins 1A and 1B. *J. Gen. Microbiol.* 131(10):2839–45. https://doi.org/doi:10.1016/j.cels.2016.05.006
Zhu, G., Golding, G.B., Dean, A.M., 2005. The selective cause of an ancient adaptation. *Science* 307(5713):1279–82. https://doi.org/10.1126/science.1106974
Zhuang, Z., Song, F., Martin, B.M., Dunaway-Mariano, D., 2002. The YbgC protein encoded by the ybgC gene of the tol-pal gene cluster of *Haemophilus influenzae* catalyzes acyl-coenzyme A thioester hydrolysis. *FEBS Letters* 516(1–3):161–3. https://doi.org/10.1016/S0014-5793(02)02533-4